Development of Novel High-Entropy Alloys for Biomedical Applications

by

Şeyma Gürel Saydam

A Dissertation Submitted to the
Graduate School of Sciences and Engineering
in Partial Fulfillment of the Requirements for
the Degree of

Master of Science

in

Mechanical Engineering

February 14, 2020

Development of Novel High-Entropy Alloys for Biomedical Applications

Koç University

Graduate School of Sciences and Engineering

This is to certify that I have examined this copy of a master's thesis by

Şeyma Gürel Saydam

and have found that it is complete and satisfactory in all respects,
and that any and all revisions required by the final
examining committee have been made.

Committee Members:

_____

Prof. Dr. Demircan Canadinç

_____

Assoc. Prof. Alper Uzun

_____

Assoc. Prof. Haluk Çabuk

Date: 14.02.2020

To my family…

ABSTRACT

Development of Novel High-Entropy Alloys for Biomedical Applications

Şeyma Gürel Saydam

Master of Science in Mechanical Engineering

February 14, 2020

High entropy alloys are solid solution alloys that contain multi-principal elements in nearly equi-atomic percent. This unique concept introduces a superior combination of enhanced mechanical properties that cannot be exhibited by conventional alloys consisting of one or two principal elements. The superior properties such as high strength, high fracture toughness, excellent wear and corrosion resistance have led to the investigation of whether the novel materials could be included in the field of medicine as biomaterials. Microstructural properties, mechanical properties and bioactivities of the high entropy alloys $Ti_{25}Ta_{25}Hf_{25}Nb_{25}$, $Ti_{20}Ta_{20}Hf_{20}Nb_{20}Zr_{20}$, $Ti_{20}Ta_{20}Hf_{20}Mo_{20}Zr_{20}$, and the medium entropy alloy CoCrMo have been evaluated to observe the potential for fruitful use of these materials in the biomedical field.

ÖZETÇE

Biyomedikal Uygulamalar için Özgün Yüksek Entropi Alaşımlarının Geliştirilmesi

Şeyma Gürel Saydam

Makine Mühendisliği, Yüksek Lisans

14 Şubat 2020

Yüksek entropili alaşımlar yaklaşık olarak eşit atomik yüzdede çoklu esas elementler içeren katı çözelti alaşımlarıdır. Özgün konsept, bir veya iki esas element içeren geleneksel alaşımlarla elde edilemeyen gelişmiş mekanik özellikler sunar. Yüksek mukavemet, yüksek kırılma tokluğu, mükemmel aşınma ve korozyon direnci gibi üstün özellikler, bu yeni malzemelerin tıp alanında biyomalzemeler olarak dahil edilip edilemeyeceğinin araştırılmasını gerektirmiştir. Yüksek entropi alaşımlarının $Ti_{25}Ta_{25}Hf_{25}Nb_{25}$, $Ti_{20}Ta_{20}Hf_{20}Nb_{20}Zr_{20}$, $Ti_{20}Ta_{20}Hf_{20}Mo_{20}Zr_{20}$ ve orta entropi alaşımı CoCrMo'nun mikro yapısal özellikleri, mekanik özellikleri ve biyoaktiviteleri, bu malzemelerin biyomedikal alanda verimli kullanım potansiyelini gözlemlemek üzere değerlendirilmiştir.

ACKNOWLEDGMENTS

First of all, I would like to extend my deepest gratitude to my advisor Prof. Dr. Demircan Canadinç for his support, leadership, patience, motivation and deep knowledge. I consider myself a lucky person to have the chance to work with Prof. Canadinç, his supportive manner has always taken me forward.

Besides my advisor, I would also like to thank my thesis committee members Assoc. Prof. Alper Uzun and Assoc. Prof. Haluk Çabuk for their encouragement.

I am genuinely thankful to Dr. Barış Yağcı and Dr. Burak Bal for their contribution to my knowledge and thesis.

Thanks for the BAGEP Award of the Science Academy for their financial support.

I am very appreciative of working with the Advanced Materials Group members Elif, İbrahim and Ali Reza. Their support and friendship were invaluable. I am particularly grateful to Ali Reza for his endless support.

Finally, my special thanks to my beloved family, my dear friend Ruhat, and my husband Gürkan. Thank you for your love, trust and support.

TABLE OF CONTENTS

LIST OF TABLES

LIST OF FIGURES

ABBREVIATIONS

at.%	Atomic Percentage
AS	Artificial Saliva
BCC	Body-Centered Cubic
CVN	Charpy V-Notch
EDM	Electrical Discharge Machining (EDM)
EDX	Energy Dispersive X-Ray
FCC	Face-Centered Cubic
HCP	Hexagonal Closed Packed
HEA	High Entropy Alloy
ICP-MS	Inductively Coupled Plasma Mass Spectrometry
MEA	Medium Entropy Alloy
PBS	Phosphate Buffer Solution
SBF	Simulated Body Fluid
SEM	Scanning Electron Microscopy
SS	Stainless Steel
wt.%	Weight Percentage
XPS	X-Ray Photoelectron Spectrometry
XRD	X-Ray Diffraction

Chapter 1:
INTRODUCTION

Metallic materials are extensively used in biomedical applications owing to their satisfactory mechanical properties and biocompatibility. Stainless steel, Co-based alloys, and Ti-based traditional alloys have been popularly utilized as implants, however, the traditionally used implants have been associated with some concerns such as toxicity and elastic modulus mismatch which have effects on implant durability and human health [1–9]. Many studies aiming to increase the efficiency of an implant and the quality of life of the patient by producing an alternative implant material to traditional medical materials are continuing with developments of metallic materials [1,10–15]. As a result of the search for new generation materials, high-entropy alloys have attracted attention with their applications in the biomedical field [2,16–19]. Thanks to their superior properties such as high strength, excellent corrosion resistance, and fracture resistance, these materials can adapt to the human body environment to provide long-lasting use of an implant [20–26]. This study investigates biocompatibility and mechanical properties of three Ti-based high entropy alloys and CoCrMo medium entropy alloys to evaluate their performance as implant materials.

In this section, high entropy alloys as a novel material concept have been discussed within the relative context of this study.

1.1 Background

1.1.1 Biocompatibility

The definition of biocompatibility has been extended as a concept in itself with increasing human needs. The first definition of biocompatibility concerns the chemical activity of an implant that can cause adverse tissue reactions, and biocompatibility became a more considerable topic with the utilization of an implant in the human body for a long period of time. The implant materials in the body can lead to unfavorable biological activities as locally or systemically, therefore implant materials should be non-toxic and non-allergenic to eliminate any harm to human health. Moreover, a host response is important such that an implant material should be appropriate for a specific

application purpose and a site [27]. Host response for the desired application can vary from one to another situation, in the manner that orthopedic implants of knee joints and hip replacements are exposed to biochemical degradation and static/dynamic loadings, and the implants should be designed with considering these biological environment and physiological conditions [28]. Therefore, an implant should support damaged or repaired tissue, and withstand the human body environment and dynamic loadings without causing health risks.

1.1.2 Metallic Biomedical Materials and Their Limitations

Medical metallic materials have been widely preferred in hard tissue replacements and dental implants prior to their superior mechanical properties. Stainless steel, titanium and titanium alloys, cobalt chromium-based alloys are common metallic materials that are of great importance in providing long-term stability in the human body due to their reliable mechanical strength, long-bearing capacity and corrosion resistance [14]. However, some limitations have been observed that harm the biological and mechanical compatibility during the use of common metallic materials in the human body [1,14].

Among the metallic materials, titanium and titanium alloys are one of the most promising biomaterials with excellent biocompatibility and good mechanical properties such as high strength and toughness [14,31]. Commercially pure titanium and Ti-6Al-4V are the main titanium implants that have been developed to use in dental and orthopedic applications [1]. Nevertheless, the biocompatibility of titanium alloys is still a debatable subject due to the high elastic modulus of an implant and the release of toxic ions such as Al and V for the human body [14,15,32]. Therefore, low-modulus and non-toxic Ti alloys have been developing to eliminate potential health risks [33].

In addition, stainless steel has practical applications in orthopedics with good mechanical properties. However, the elemental composition of stainless steel deteriorates biocompatibility by releasing toxic ions from an implant into a body environment. Particularly, Ni ion release from 316L SS into surrounding tissues can lead to adverse reactions such as Ni hypersensitivity [1,32–35]. In order to eliminate cytotoxic issues of stainless steel, high-N Ni-free stainless steel has been proposed [1,36,37]. However, Ni-free stainless steel has limited utilization purposes such as for

thin-walled products [38]. Moreover, high density and higher Young's modulus of stainless steel than bones create elastic modulus mismatch and lead to deterioration of the material integrity of an implant with the bone [36]. The mechanical incompatibility can lead to stress shielding effect [39], prosthesis failure, implant loosening, and bone resorption and so on in long term applications [40,41].

Besides, CoCrMo alloys are the most used Co-based biomedical materials in orthopedic and dental applications. Their high strength and wear resistance provide advantages as well as with their high corrosion resistance in biomedical applications. Spontaneously forming a passive oxide layer on CoCrMo alloys is a key to establish the biocompatibility of CoCrMo [42,43]. While the passive layer facilitates the osseointegration process, it reduces ion release from CoCrMo alloys and eliminates high toxicity [44–46].

On the other hand, titanium alloys show better biocompatibility due to excellent corrosion resistance as Compared with cobalt-based alloys and stainless steel. Pure Ti and Ti-6Al-4V have been mainly used materials as implants, however, some concerns exist due to the strength of Ti and toxicity of Ti-6Al-4V owing to its V and Al content that can damage the neurological system[1,47,48]. In order to eliminate the toxic effects of Ti-6Al-4V, some alloys without V have been developed such that Ti-6Al-7Nb and Ti-5Al-2.5Fe [14,38]. In addition to biological biocompatibility, mechanical compatibility of implant materials has been improved by low modulus alloys. Therefore, nontoxic and low modulus alloys such as Ti-13Nb-13Zr, Ti–12Mo–6Zr–2Fe (TMZF), Ti–15Mo, Ti–16Nb–10Hf, Ti–13Nb–13Zr, Ti–12Mo–6Zr–2Fe (TMZF), and Ti–29Nb–13Ta–4.6Zr (TNZT) have been developed [32,38,57–59,49–56]. The studies showed promising results, such that TNTZ alloys have attracted great attention owing to their low Young's modulus of approximately 60 GPa that is close to that of bone (approximately 30 GPa) with addition to their high corrosion resistance [57].

1.1.3 High Entropy Alloys

The new material concept, based on multi-principal elements different from traditional alloys, was first published in 2004 [60,61]. While traditional alloy design mostly consists of one or two principal elements, high entropy alloys have five or more principal elements with a concentration of 5 and 35 at.% [61–63]. The multicomponent

structure in traditional alloys may create complex and brittle microstructure, however, the higher mixing entropy in HEAs reduces the number of random solid solution phases to create a single solid phase such as face-centered cubic (FCC), body-centered cubic (BCC), and hexagonal close packing (HCP) structures [64–66]. Therefore, the alloys called “high entropy” due to the effects of high configurational entropy on their microstructure such that unique properties exist in HEAs. The superior properties include high strength and hardness [25,26,75,76,67–74], excellent corrosion resistance [22–25,75,77,78], high thermal stability [26,64,79] , good wear resistance , and high fracture resistance [20,21]. The combination of such unique properties with easy production process with available technologies [65] makes HEAs desirable to engineering applications such as in structural applications that can withstand to extreme conditions as in aerospace industry and energy generation fields [80–83], also their high capacity of resistance to harsh conditions with satisfactory strength and toughness makes them substantial candidates in biomedical field.

1.1.4 High Entropy Alloys as Biomedical Materials

Some studies have been investigated to the biocompatibility of high entropy alloys with respect to their corrosion behavior and mechanical properties under different conditions. The popularity of titanium-based alloys owing to their extremely good properties contributed to developments in high entropy alloys since Ti-based alloys indicate promising results for further investigations. Advanced properties have been observed in Ti-based high entropy alloys compared to traditional biomedical materials. Such that, newly developed TiZrNbTaFe showed better corrosion resistance in simulated body fluids than Ti-6Al-4V with improved mechanical biocompatibility [19,84]. Moreover, another Ti-Nb-Ta-Zr based HEA which is TiZrNbTaMo have excellent corrosion resistance that was tested in Phosphate buffer solution (PBS) [18]. In addition to the corrosion resistance of HEAs, some studies have been focused on their mechanical features, such that high strength and good deformability of TiNbTaZrMo has been observed with excellent biocompatibility [17,85]. Moreover, a study showed that TiZrTaHfNb HEA has promising properties such as high wear resistance and corrosion resistance that make TiZrTaHfNb a possible biomedical material [86]. On the other hand, although some studies have investigated the fracture

behavior of HEAs in extreme conditions [87–89], there is a lack of information on the fracture behavior of HEAs for biomedical purposes.

In this study, biological and mechanical compatibility of three HEAs of TiTaHfNb, TiTaHfNbZr, TiTaHfMoZr, and a medium entropy alloy of CoCrMo alloy have been investigated with respect to their corrosion behavior, biocompatibility, and fracture mechanism in order to evaluate their potential to use as implant materials.

1.2 References

[1] M. Niinomi, M. Nakai, J. Hieda, Development of new metallic alloys for biomedical applications, Acta Biomater. 8 (2012) 3888–3903. doi:10.1016/j.actbio.2012.06.037.

[2] Y. Yuan, Y. Wu, Z. Yang, X. Liang, Z. Lei, H. Huang, H. Wang, X. Liu, K. An, W. Wu, Z. Lu, Formation, structure and properties of biocompatible TiZrHfNbTa high-entropy alloys, Mater. Res. Lett. 7 (2019) 225–231. doi:10.1080/21663831.2019.1584592.

[3] C. Oldani, A. Dominguez, Titanium as a Biomaterial for Implants, in: Recent Adv. Arthroplast., InTech, 2012. doi:10.5772/27413.

[4] S. Rajendran, J. Paulraj, P. Rengan, J. Jeyasundari, M. Manivannan, Corrosion behaviour of metals in artificial saliva in presence of spirulina powder, J. Dent. (2009).

[5] S. Rao, T. Ushida, T. Tateishi, Y. Okazaki, S. Asao, Effect of Ti, Al, and V ions on the relative growth rate of fibroblasts (L929) and osteoblasts (MC3T3-E1) cells., Biomed. Mater. Eng. 6 (1996) 79–86. http://www.ncbi.nlm.nih.gov/pubmed/8761518.

[6] S.G. Steinemann, Metal implants and surface reactions, Injury. 27 (1996) S/C16-S/C22. doi:10.1016/0020-1383(96)89027-9.

[7] R. Van Noort, Titanium: The implant material of today, J. Mater. Sci. 22 (1987) 3801–3811. doi:10.1007/BF01133326.

[8] M.P. Staiger, A.M. Pietak, J. Huadmai, G. Dias, Magnesium and its alloys as orthopedic biomaterials: A review, Biomaterials. 27 (2006) 1728–1734. doi:10.1016/j.biomaterials.2005.10.003.

[9] L.N. Miotto, L.M.G. Fais, A.L.R. Ribeiro, L.G. Vaz, Surface properties of Ti-35Nb-7Zr-5Ta, J. Prosthet. Dent. 116 (2016) 102–111. doi:10.1016/j.prosdent.2015.10.024.

[10] T.C. Niemeyer, C.R. Grandini, L.M.C. Pinto, A.C.D. Angelo, S.G. Schneider, Corrosion behavior of Ti–13Nb–13Zr alloy used as a biomaterial, J. Alloys Compd. 476 (2009) 172–175. doi:10.1016/j.jallcom.2008.09.026.

[11] Y. Li, C. Yang, H. Zhao, S. Qu, X. Li, Y. Li, New Developments of Ti-Based Alloys for Biomedical Applications, Materials (Basel). 7 (2014) 1709–1800. doi:10.3390/ma7031709.

[12] T. Akahori, M. Niinomi, Fracture characteristics of fatigued Ti–6Al–4V ELI as an implant material, Mater. Sci. Eng. A. 243 (1998) 237–243. doi:10.1016/S0921-5093(97)00807-1.

[13] E. Chicardi, C.F. Gutiérrez-González, M.J. Sayagués, C. García-Garrido, Development of a novel TiNbTa material potentially suitable for bone replacement implants, Mater. Des. 145 (2018) 88–96. doi:10.1016/j.matdes.2018.02.042.

[14] M. Niinomi, Recent metallic materials for biomedical applications, Metall. Mater. Trans. A. 33 (2002) 477–486. doi:10.1007/s11661-002-0109-2.

[15] C.N. Elias, J.H.C. Lima, R. Valiev, M.A. Meyers, Biomedical applications of titanium and its alloys Biological Materials Science 46-49, Biol. Mater. Sci. (2008) 1–4. www.tms.org/jom.html.

[16] Y.L. Chou, J.W. Yeh, H.C. Shih, The effect of molybdenum on the corrosion behaviour of the high-entropy alloys Co1.5CrFeNi1.5Ti0.5Mox in aqueous environments, Corros. Sci. 52 (2010) 2571–2581. doi:10.1016/j.corsci.2010.04.004.

[17] M. Todai, T. Nagase, T. Hori, A. Matsugaki, A. Sekita, T. Nakano, Novel TiNbTaZrMo high-entropy alloys for metallic biomaterials, Scr. Mater. 129 (2017) 65–68. doi:10.1016/j.scriptamat.2016.10.028.

[18] S.-P. Wang, J. Xu, TiZrNbTaMo high-entropy alloy designed for orthopedic implants: As-cast microstructure and mechanical properties, Mater. Sci. Eng. C. 73 (2017) 80–89. doi:10.1016/j.msec.2016.12.057.

[19] G. Popescu, B. Ghiban, C.A. Popescu, L. Rosu, R. Truscă, I. Carcea, V. Soare, D. Dumitrescu, I. Constantin, M.T. Olaru, B.A. Carlan, New TiZrNbTaFe high entropy alloy used for medical applications, IOP Conf. Ser. Mater. Sci. Eng. 400 (2018) 022049. doi:10.1088/1757-899X/400/2/022049.

[20] B. Gludovatz, A. Hohenwarter, D. Catoor, E.H. Chang, E.P. George, R.O. Ritchie, ChemInform Abstract: A Fracture-Resistant High-Entropy Alloy for Cryogenic Applications., ChemInform. 45 (2014) no-no. doi:10.1002/chin.201447007.

[21] Z. Zhang, M.M. Mao, J. Wang, B. Gludovatz, Z. Zhang, S.X. Mao, E.P. George, Q. Yu, R.O. Ritchie, Nanoscale origins of the damage tolerance of the high-entropy alloy CrMnFeCoNi, Nat. Commun. 6 (2015) 10143. doi:10.1038/ncomms10143.

[22] Y. Shi, B. Yang, P. Liaw, Corrosion-Resistant High-Entropy Alloys: A Review, Metals (Basel). 7 (2017) 43. doi:10.3390/met7020043.

[23] Z. Tang, L. Huang, W. He, P. Liaw, Alloying and Processing Effects on the Aqueous Corrosion Behavior of High-Entropy Alloys, Entropy. 16 (2014) 895–911. doi:10.3390/e16020895.

[24] Y.-J. Hsu, W.-C. Chiang, J.-K. Wu, Corrosion behavior of FeCoNiCrCux high-entropy alloys in 3.5% sodium chloride solution, Mater. Chem. Phys. 92 (2005) 112–117. doi:10.1016/j.matchemphys.2005.01.001.

[25] Y. Qiu, M.A. Gibson, H.L. Fraser, N. Birbilis, Corrosion characteristics of high entropy alloys, Mater. Sci. Technol. 31 (2015) 1235–1243. doi:10.1179/1743284715Y.0000000026.

[26] Z.D. Han, H.W. Luan, X. Liu, N. Chen, X.Y. Li, Y. Shao, K.F. Yao, Microstructures and mechanical properties of Ti NbMoTaW refractory high-entropy alloys, Mater. Sci. Eng. A. 712 (2018) 380–385. doi:10.1016/j.msea.2017.12.004.

[27] D.F. Williams, On the mechanisms of biocompatibility, Biomaterials. 29 (2008) 2941–2953. doi:10.1016/j.biomaterials.2008.04.023.

[28] U. Kamachimudali, T.M. Sridhar, B. Raj, Corrosion of bio implants, Sadhana. 28 (2003) 601–637. doi:10.1007/BF02706450.

[29] F. Toumelin-Chemla, F. Rouelle, G. Burdairon, Corrosive properties of fluoride-containing odontologic gels against titanium, J. Dent. 24 (1996) 109–115. doi:10.1016/0300-5712(95)00033-X.

[30] S. Tamilselvi, V. Raman, N. Rajendran, Corrosion behaviour of Ti–6Al–7Nb and Ti–6Al–4V ELI alloys in the simulated body fluid solution by electrochemical impedance spectroscopy, Electrochim. Acta. 52 (2006) 839–846. doi:10.1016/j.electacta.2006.06.018.

[31] V.S. de Viteri, E. Fuentes, Titanium and Titanium Alloys as Biomaterials, in: Tribol. - Fundam. Adv., 2013. doi:10.5772/55860.

[32] M. V. Popa, E. Vasilescu, P. Drob, C. Vasilescu, S.I. Drob, D. Mareci, J.C.M. Rosca, Corrosion resistance improvement of titanium base alloys, Quim. Nova. 33 (2010) 1892–1896. doi:10.1590/S0100-40422010000900014.

[33] M. Niinomi, Metallic biomaterials, J. Artif. Organs. 11 (2008) 105–110. doi:10.1007/s10047-008-0422-7.

[34] Q. Chen, G.A. Thouas, Metallic implant biomaterials, Mater. Sci. Eng. R Reports. 87 (2015) 1–57. doi:10.1016/j.mser.2014.10.001.

[35] P.J. Uggowitzer, W.-F. Bähre, H. Wohlfromm, M.O. Speidel, Nickel-Free High Nitrogen Austenitic Stainless Steels Produced by Metal Injection Moulding, Mater. Sci. Forum. 318–320 (1999) 663–672. doi:10.4028/www.scientific.net/MSF.318-320.663.

[36] S.J. Stohs, D. Bagchi, Oxidative mechanisms in the toxicity of metal ions, Free Radic. Biol. Med. (1995). doi:10.1016/0891-5849(94)00159-H.

[37] D.A. Basketter, G. Briatico-Vangosa, W. Kaestner, C. Lally, W.J. Bontinck, Nickel, cobalt and chromium in consumer products: a role in allergic contact dermatitis?, Contact Dermatitis. (1993). doi:10.1111/j.1600-0536.1993.tb03318.x.

[38] K. Yang, Y. Ren, Nickel-free austenitic stainless steels for medical applications, Sci. Technol. Adv. Mater. 11 (2010) 014105. doi:10.1088/1468-6996/11/1/014105.

[39] P.J. Uggowitzer, W.-F. Bähre, H. Wohlfromm, M.O. Speidel, Nickel-Free High Nitrogen Austenitic Stainless Steels Produced by Metal Injection Moulding, Mater. Sci. Forum. 318–320 (1999) 663–672. doi:10.4028/www.scientific.net/MSF.318-320.663.

[40] M. Bahraminasab, B.B. Sahari, K.L. Edwards, F. Farahmand, M. Arumugam, Aseptic loosening of femoral components - Materials engineering and design considerations, Mater. Des. 44 (2013) 155–163. doi:10.1016/j.matdes.2012.07.066.

[41] K. Shemtov-Yona, D. Rittel, On the mechanical integrity of retrieved dental implants, J. Mech. Behav. Biomed. Mater. (2015). doi:10.1016/j.jmbbm.2015.05.014.

[42] N. Tagger Green, E.E. Machtei, J. Horwitz, M. Peled, Fracture of Dental Implants: Literature Review and Report of a Case, Implant Dent. 11 (2002) 137–143. doi:10.1097/00008505-200204000-00014.

[43] C. LIU, Z. ZHOU, K.Y. LI, Improved corrosion resistance of CoCrMo alloy with self-passivation ability facilitated by carbon ion implantation, Electrochim. Acta. 241 (2017) 331–340. doi:10.1016/j.electacta.2017.04.127.

[44] A.W.E. Hodgson, S. Kurz, S. Virtanen, V. Fervel, C.-O.A. Olsson, S. Mischler, Passive and transpassive behaviour of CoCrMo in simulated biological solutions, Electrochim. Acta. 49 (2004) 2167–2178. doi:10.1016/j.electacta.2003.12.043.

[45] I. Peter, M. Rosso, Study of Ti-Enriched CoCrMo Alloy for Dental Application, IEEE Access. 3 (2015) 73–80. doi:10.1109/ACCESS.2015.2398312.

[46] A. Łukaszczyk, J. Augustyn-Pieniązek, Corrosion resistance of Co-Cr-Mo alloy used in dentistry, Arch. Metall. Mater. 60 (2015) 523–528. doi:10.1515/amm-2015-0084.

[47] D.A. Puleo, W.W. Huh, Acute toxicity of metal ions in cultures of osteogenic cells derived from bone marrow stromal cells, J. Appl. Biomater. 6 (1995) 109–116. doi:10.1002/jab.770060205.

[48] B.F. Boyce, J. Byars, S. McWilliams, M.Z. Mocan, H.Y. Elder, I.T. Boyle, B.J.R. Junor, Histological and electron microprobe studies of mineralisation in aluminium-related osteomalacia, J. Clin. Pathol. (1992). doi:10.1136/jcp.45.6.502.

[49] J.L. Domingo, Vanadium and Tungsten Derivatives as Antidiabetic Agents, Biol. Trace Elem. Res. (2002). doi:10.1385/bter:88:2:097.

[50] A. Mishra, J. Davidson, R. Poggie, P. Kovacs, T. FitzGerald, Mechanical and Tribological Properties and Biocompatibility of Diffusion Hardened Ti-13Nb-13Zr — A New Titanium Alloy for Surgical Implants, in: Med. Appl. Titan. Its Alloy. Mater. Biol. Issues, 2009. doi:10.1520/stp16073s.

[51] K. Wang, L. Gustavson, J. Dumbleton, Microstructure and Properties of a New Beta Titanium Alloy, Ti-12Mo-6Zr-2Fe, Developed for Surgical Implants, in: Med. Appl. Titan. Its Alloy. Mater. Biol. Issues, 2009. doi:10.1520/stp16071s.

[52] V.R. Jablokov, M.J. Nutt, M.E. Richelsoph, H.L. Freese, The application of Ti-15Mo beta titanium alloy in high strength structural orthopaedic applications, J. ASTM Int. (2005). doi:10.1520/stp37549s.

[53] K. Wang, The use of titanium for medical applications in the USA, Mater. Sci. Eng. A. 213 (1996) 134–137. doi:10.1016/0921-5093(96)10243-4.

[54] D. Kuroda, M. Niinomi, M. Morinaga, Y. Kato, T. Yashiro, Design and mechanical properties of new β type titanium alloys for implant materials, Mater. Sci. Eng. A. 243 (1998) 244–249. doi:10.1016/S0921-5093(97)00808-3.

[55] M. Niinomi, T. Hattori, K. Morikawa, T. Kasuga, A. Suzuki, H. Fukui, S. Niwa, Development of low rigidity β-type titanium alloy for biomedical applications, Mater. Trans. (2002). doi:10.2320/matertrans.43.2970.

[56] M. Niinomi, Fatigue performance and cyto-toxicity of low rigidity titanium alloy, Ti-29Nb-13Ta-4.6Zr, Biomaterials. (2003). doi:10.1016/S0142-9612(03)00069-3.

[57] N. Sumitomo, K. Noritake, T. Hattori, K. Morikawa, S. Niwa, K. Sato, M. Niinomi, Experiment study on fracture fixation with low rigidity titanium alloy: Plate

fixation of tibia fracture model in rabbit, in: J. Mater. Sci. Mater. Med., 2008: pp. 1581–1586. doi:10.1007/s10856-008-3372-y.

[58] M. Niinomi, Y. Liu, M. Nakai, H. Liu, H. Li, Biomedical titanium alloys with Young's moduli close to that of cortical bone, Regen. Biomater. 3 (2016) 173–185. doi:10.1093/rb/rbw016.

[59] M. Niinomi, Recent research and development in titanium alloys for biomedical applications and healthcare goods, Sci. Technol. Adv. Mater. 4 (2003) 445–454. doi:10.1016/j.stam.2003.09.002.

[60] Y. Okazaki, T. Tateishi, Y. Ito, Corrosion Resistance of Implant Alloys in Pseudo Physiological Solution and Role of Alloying Elements in Passive Films, Mater. Trans. JIM. 38 (1997) 78–84. doi:10.2320/matertrans1989.38.78.

[61] M. Niinomi, Y. Liu, M. Nakai, H. Liu, H. Li, Biomedical titanium alloys with Young's moduli close to that of cortical bone, Regen. Biomater. 3 (2016) 173–185. doi:10.1093/RB/RBW016.

[62] B. Cantor, I.T.H. Chang, P. Knight, A.J.B. Vincent, Microstructural development in equiatomic multicomponent alloys, Mater. Sci. Eng. A. 375–377 (2004) 213–218. doi:10.1016/j.msea.2003.10.257.

[63] J.-W. Yeh, S.-K. Chen, S.-J. Lin, J.-Y. Gan, T.-S. Chin, T.-T. Shun, C.-H. Tsau, S.-Y. Chang, Nanostructured High-Entropy Alloys with Multiple Principal Elements: Novel Alloy Design Concepts and Outcomes, Adv. Eng. Mater. 6 (2004) 299–303. doi:10.1002/adem.200300567.

[64] M.-H. Tsai, J.-W. Yeh, High-Entropy Alloys: A Critical Review, Mater. Res. Lett. 2 (2014) 107–123. doi:10.1080/21663831.2014.912690.

[65] J.W. Yeh, Recent progress in high-entropy alloys, Ann. Chim. Sci. Des Mater. (2006). doi:10.3166/acsm.31.633-648.

[66] W. Zhang, P.K. Liaw, Y. Zhang, Science and technology in high-entropy alloys, Sci. China Mater. 61 (2018) 2–22. doi:10.1007/s40843-017-9195-8.

[67] M.-H. Tsai, J.-W. Yeh, High-Entropy Alloys: A Critical Review, Mater. Res. Lett. 2 (2014) 107–123. doi:10.1080/21663831.2014.912690.

[68] Y. Zhang, T.T. Zuo, Z. Tang, M.C. Gao, K.A. Dahmen, P.K. Liaw, Z.P. Lu, Microstructures and properties of high-entropy alloys, Prog. Mater. Sci. 61 (2014) 1–93. doi:10.1016/j.pmatsci.2013.10.001.

[69] Y. Zhang, X. Yang, P.K. Liaw, Alloy Design and Properties Optimization of High-Entropy Alloys, JOM. 64 (2012) 830–838. doi:10.1007/s11837-012-0366-5.

[70] L. Vinet, A. Zhedanov, A 'missing' family of classical orthogonal polynomials, J. Phys. A Math. Theor. 44 (2011) 085201. doi:10.1088/1751-8113/44/8/085201.

[71] X.W. Qiu, Y.P. Zhang, L. He, C.G. Liu, Microstructure and corrosion resistance of AlCrFeCuCo high entropy alloy, J. Alloys Compd. 549 (2013) 195–199. doi:10.1016/j.jallcom.2012.09.091.

[72] C. Li, J.C. Li, M. Zhao, Q. Jiang, Effect of aluminum contents on microstructure and properties of AlxCoCrFeNi alloys, J. Alloys Compd. 504 (2010) S515–S518. doi:10.1016/j.jallcom.2010.03.111.

[73] T.-T. Shun, L.-Y. Chang, M.-H. Shiu, Microstructures and mechanical properties of multiprincipal component CoCrFeNiTix alloys, Mater. Sci. Eng. A. 556 (2012) 170–174. doi:10.1016/j.msea.2012.06.075.

[74] O.N. Senkov, J.M. Scott, S.V. Senkova, D.B. Miracle, C.F. Woodward, Microstructure and room temperature properties of a high-entropy TaNbHfZrTi alloy, J. Alloys Compd. 509 (2011) 6043–6048. doi:10.1016/j.jallcom.2011.02.171.

[75] X.F. Wang, Y. Zhang, Y. Qiao, G.L. Chen, Novel microstructure and properties of multicomponent CoCrCuFeNiTix alloys, Intermetallics. 15 (2007) 357–362. doi:10.1016/j.intermet.2006.08.005.

[76] O.N. Senkov, G.B. Wilks, D.B. Miracle, C.P. Chuang, P.K. Liaw, Refractory high-entropy alloys, Intermetallics. 18 (2010) 1758–1765. doi:10.1016/j.intermet.2010.05.014.

[77] Y. Qiu, S. Thomas, M.A. Gibson, H.L. Fraser, N. Birbilis, Corrosion of high entropy alloys, Npj Mater. Degrad. 1 (2017) 15. doi:10.1038/s41529-017-0009-y.

[78] Y. Zou, H. Ma, R. Spolenak, Ultrastrong ductile and stable high-entropy alloys at small scales, Nat. Commun. (2015). doi:10.1038/ncomms8748.

[79] R.B. Nair, H.S. Arora, S. Mukherjee, S. Singh, H. Singh, H.S. Grewal, Exceptionally high cavitation erosion and corrosion resistance of a high entropy alloy, Ultrason. Sonochem. 41 (2018) 252–260. doi:10.1016/j.ultsonch.2017.09.044.

[80] A. Rodriguez, J.H. Tylczak, M. Ziomek-Moroz, Corrosion behavior of CoCrFeMnNi high-entropy alloys (HEAs) under acidic aqueous conditions, ECS Trans. 77 (2017) 741–752. doi:10.1149/07711.0741ecst.

[81] C.C. Juan, M.H. Tsai, C.W. Tsai, C.M. Lin, W.R. Wang, C.C. Yang, S.K. Chen, S.J. Lin, J.W. Yeh, Enhanced mechanical properties of HfMoTaTiZr and HfMoNbTaTiZr refractory high-entropy alloys, Intermetallics. 62 (2015) 76–83. doi:10.1016/j.intermet.2015.03.013.

[82] S.Y. Chen, Y. Tong, K.-K. Tseng, J.-W. Yeh, J.D. Poplawsky, J.G. Wen, M.C. Gao, G. Kim, W. Chen, Y. Ren, R. Feng, W.D. Li, P.K. Liaw, Phase transformations of HfNbTaTiZr high-entropy alloy at intermediate temperatures, Scr. Mater. 158 (2019) 50–56. doi:10.1016/j.scriptamat.2018.08.032.

[83] Y. Zhang, Y. Liu, Y. Li, X. Chen, H. Zhang, Microstructure and mechanical properties of a refractory HfNbTiVSi0.5 high-entropy alloy composite, Mater. Lett. 174 (2016) 82–85. doi:10.1016/j.matlet.2016.03.092.

[84] O.N. Senkov, J.M. Scott, S. V. Senkova, F. Meisenkothen, D.B. Miracle, C.F. Woodward, Microstructure and elevated temperature properties of a refractory TaNbHfZrTi alloy, J. Mater. Sci. (2012). doi:10.1007/s10853-012-6260-2.

[85] D.B. Miracle, O.N. Senkov, A critical review of high entropy alloys and related concepts, Acta Mater. 122 (2017) 448–511. doi:10.1016/j.actamat.2016.08.081.

[86] B. Ghiban, G. Popescu, C. Lazar, L. Rosu, I. Constantin, M. Olaru, B. Carlan, Corrosion Behaviour in Human Stimulation Media of a High Entropy Titan-Based Alloy, IOP Conf. Ser. Mater. Sci. Eng. 374 (2018) 012004. doi:10.1088/1757-899X/374/1/012004.

[87] T. Nagase, M. Todai, T. Hori, T. Nakano, Microstructure of equiatomic and non-equiatomic Ti-Nb-Ta-Zr-Mo high-entropy alloys for metallic biomaterials, J. Alloys Compd. 753 (2018) 412–421. doi:10.1016/j.jallcom.2018.04.082.

[88] A. Motallebzadeh, N.S. Peighambardoust, S. Sheikh, H. Murakami, S. Guo, D. Canadinc, Microstructural, mechanical and electrochemical characterization of TiZrTaHfNb and Ti1.5ZrTa0.5Hf0.5Nb0.5 refractory high-entropy alloys for biomedical applications, Intermetallics. 113 (2019) 106572. doi:10.1016/j.intermet.2019.106572.

[89] B. Gludovatz, A. Hohenwarter, D. Catoor, E.H. Chang, E.P. George, R.O. Ritchie, A fracture-resistant high-entropy alloy for cryogenic applications, Science (80-.). (2014). doi:10.1126/science.1254581.

[90] W. Li, P.K. Liaw, Y. Gao, Fracture resistance of high entropy alloys: A review, Intermetallics. 99 (2018) 69–83. doi:10.1016/j.intermet.2018.05.013.

[91] U. Roy, H. Roy, H. Daoud, U. Glatzel, K.K. Ray, Fracture toughness and fracture micromechanism in a cast AlCoCrCuFeNi high entropy alloy system, Mater. Lett. 132 (2014) 186–189. doi:10.1016/j.matlet.2014.06.067.

Chapter 2:

CORROSION BEHAVIOR OF NOVEL TITANIUM-BASED HIGH ENTROPY ALLOYS DESIGNED FOR MEDICAL IMPLANTS

2.1 Introduction

Discovery of the least chemically active, non-irritating and non-toxic materials that can interact with target tissue has made a significant contribution to the development of biomaterials [1,2]. Among metallic, ceramic and polymeric biomaterials [3,4], metallic alloys emerge as more suitable candidates for applications aimed at repairing and supporting damaged bone tissue [5,6]. Therefore, metals are commonly preferred in orthopedic implants and orthodontic practices to support failed tissue as temporary and permanent implants [7,8]. Specifically, stainless steels, CoCr alloys, and Ti-based alloys constitute the primary choices of metallic biomaterials owing to their enhanced mechanical properties, which are beneficial for implantation applications of hard tissue such as knee joint, hip joint and dental implants [6,9,10]. Nevertheless, problems, such as toxic ion release, wear, or elastic modulus mismatch between an implant and human tissue can bring about important setbacks, especially in long-term applications [5,11–13]. For instance, two commonly utilized metallic implant materials, stainless steel and NiTi shape memory alloy, exhibit a substantial amount of Ni ion release into the bloodstream or the tissue they are in contact with, leading to adverse side effects [7,10,14,15]. Another popular metallic biomaterial, namely the Ti-6Al-4V alloy, poses a health risk in long-term usage owing to V and Al ion release with potential to harm to the nervous system, in addition to possible tissue loss, implant loosening, and failure of prostheses facilitated by stress shielding effect due to modulus mismatch [5,10,16–22]. Consequently, these problems compel researchers to seek alternative metallic biomaterials with excellent corrosion resistance in aggressive environments [23,24].

Recently, a class of alloys with high corrosion resistance, namely the high entropy alloys (HEAs), have attracted significant attention owing to their superior mechanical properties [25–31], which is a result of their higher configurational entropy and ability to form a single solid phase [23,26,32]. HEAs have quickly become strong candidates for various engineering applications owing to their high strength and hardness

[26,27,33–41], high thermal stability [33,41,42], and high fracture toughness [43,44], in addition to their excellent corrosion resistance [23,41,45]. This unique combination of superior mechanical properties is present even at cryogenic temperatures since the high configurational entropy stabilizes disarranged solid phases into a single-phase [26,28,38,46]. Recent studies mainly concentrated on understanding the mechanical behavior of HEAs, as well as their microstructural properties [36,47–50].

In general, the utility of metals in biomedical applications has primarily negative effects on biocompatibility owing to their corrosion tendency, which can damage both the implant and the surrounding tissue and organs [51]. Nevertheless, it is the excellent corrosion resistance exhibited by HEAs that makes them attractive for biomedical applications [51]. Thus, some scientific work has already been undertaken in order to evaluate the corrosion resistance of the HEAs under conditions that simulate the aggressive environment provided by the human body [23,30,34,45,52–55]. The current work aims to contribute to this line of research and focuses on the investigation of corrosion behavior of HEAs in physiological media simulating blood (i.e. simulated body fluid (SBF)) and oral cavity (i.e. artificial saliva (AS)).

Notably, different elemental compositions of HEAs have been improved with the addition of Ti due to its high biocompatibility and high strength. For instance, some studies on the corrosion behavior of Ti-based HEAs showed superior resistance exhibited by these alloys as compared to traditionally used biomaterials, such as Ti-6Al-4V [52], against aggressive environments such as phosphate buffer saline (PBS), NaCl infusion solution, and simulated body solution [52–54]. Specifically, the Ti-Ta-Hf alloy system was modified by the addition of non-toxic late transition elements such as Nb, Zr, Mo [6,10,16,22,54,56–59] to provide enhanced biocompatibility and TiTaHfNb, TiTaHfNbZr and TiTaHfMoZr HEAs were prepared and studied in this work. To the best of the authors' knowledge, the current work constitutes the first study focusing on the corrosion response of these HEA systems to assess their potential use in cardiovascular or oral implants in their bulk form.

Recent studies on one of Ti-Ta-Hf based alloys, namely TiTaHfNbZr alloy, showed that TiTaHfNbZr serves as an effective coating material when deposited on NiTi and Ti-6Al-4V substrates [14,60,61]. In particular, TiTaHfNbZr coating provided superior wear and corrosion resistance in aggressive physiological environments, encouraging further assessment of this particular HEA and its derivatives as

biomaterials. The current study focuses on the TiTaHfNb, TiTaHfNbZr and TiTaHfMoZr HEAs in their as-cast form in order to evaluate their corrosion behavior in bulk form rather than as a coating on another metal substrate, such that their utility as an independent biomaterial can be assessed. For this purpose, bulk TiTaHfNb, TiTaHfNbZr and TiTaHfMoZr samples were subjected to static biocompatibility experiments in SBF and AS, and both samples and the immersion fluids underwent a thorough experimental examination in order to reveal the corrosion behavior of these materials. The key finding is that TiTaHfNbZr alloy exhibited superior corrosion resistance in both SBF and AS, while TiTaHfMoZr sustained the most corrosion damage among all three alloys, and the TiTaHfNb alloy could not tolerate the SBF environment well. Overall, the findings presented and detailed in the remainder of this paper demonstrate the considerable corrosion resistance of these three HEAs, yet also warrant further investigation to uncover their potential use as biomaterials.

2.2 Experimental Procedures

The HEAs studied in this work were synthesized by arc melting with a purity of 99.9%: the TiTaHfNb HEA was composed of 50 wt.% Ti, 16.67 wt.% Ta, 16.67 wt.% Hf and 16.67 wt.% Nb, whereas the TiTaHfNbZr and TiTaHfMoZr compositions were equimolar. The disc-shaped multi-component alloys with a diameter of 50.1 mm and a thickness of 6.1 mm were cut by electrical discharge machining (EDM) to extract 10 mm x 5 mm x 1 mm bulk samples. Contaminations and EDM residue on the bulk sample surfaces were eliminated by mechanical polishing (without any change or with only negligible change) in thickness of the samples. SiC emery papers with various grain sizes ranging from 106 to 2.5 μm were used, followed by polishing with 0.30 μm alumina slurry until the sample surfaces had mirror-like appearance. The bulk samples were cleaned with ethanol and rinsed with de-ionized water. After the cleaning procedure, the bulk samples were immersed into SBF (pH=7.4) and AS (pH=2.3) for 1, 7, 14 and 28 days. The solutions were kept at a constant temperature of 37 ^{0}C throughout the immersion with the aid of an electronically controlled water bath.

The composition of AS and SBF are provided in Table 2-1 [62]. Each HEA sample was deposited separately in a sealed tube, and the tubes were filled with the solutions, where a volume per surface area ratio of 20 mL/cm2 was arranged [63]. The mass of

each bulk sample was recorded before and after the immersion test to detect mass gain or loss by corrosion. Crystallographic identification of the alloys was accomplished by X-ray diffraction (XRD) method on a Bruker D2 Advanced X-ray diffractometer with a Cu-Kα radiation source operated at 30 kV and 10 mA. The incidence angle was about 5° and the acquisition angle ranged from 5° to 90°, where each step was processed with a 0.02° increment. The surface morphology of both untested and tested samples was investigated by a Zeiss Ultra Plus field emission scanning electron microscope (SEM). Ion release from the bulk samples into the immersion fluids was monitored using an Agilent 7700x inductively coupled plasma mass spectrometer (ICP-MS). A Thermo-Scientific K-Alpha X-Ray Photoelectron Spectrometer (XPS) were utilized to obtain chemical content information of from the surface of the samples after immersion tests.

Table 2-1: Composition of the AS and SBF utilized in the static immersion experiments.

Solution	**Ingredients**	**Amount (g/L)**	**pH**
AS	NaCl	0.4	2.3
	KCl	0.4	
	$CaCl_2 . 2H_2o$	0.906	
	$NaH_2PO_4.2H_2O$	0.69	
	$Na_2S.9H_2O$	0.005	
	Urea	1	
SBF	NaCl	8.036	7.4
	$NaHCO_3$	0.352	
	KCL	0.225	
	$K_2HPO_4.3H_2O$	0.23	
	$MgCl_2.6H_2O$	0.311	
	1M HCL	40 mL	
	$CaCl_2 . 2H_2o$	0.293	
	Na_2SO_4	0.072	
	TRIS	6.063	
	1M HCL	0.2 ml	

2.3 Results and Discussion

Surface morphology of the bulk HEAs before the immersion experiments were analyzed by SEM, revealing that TiTaHfNb, TiTaHfNbZr and TiTaHfMoZr had a smooth surface prior to immersion test (Figure 2-1). Some stains were observed on the TiTaHfNb surfaces prior to immersion tests despite the additional polishing process that had been applied to eliminate them from the surface. EDX analysis revealed that the stains are composed of Si and C (Figure 2-2), which stem from SiC emery papers used in the polishing procedure. This implies that the TiTaHfNb surface is not rigid enough, and this mild surface of TiTaHfNb may facilitate the penetration of the immersion solutions into the material, such that the surface establishes a suitable ground for unintended attacks. As can be seen in Figure 2-3 (a), (c) and (d), the SEM micrographs of the TiTaHfNb demonstrate a highly deformed surface following 28 days immersion in SBF. Figure 2-3(a) shows that TiTaHfNb was negatively affected from the SBF environment and the locally intense corrosion behavior leads to enlargement of the corrosion through the thickness as indicated in Figures 2-3 (c) and (d), which may result in pitting corrosion in long term applications. Indeed, several studies support the idea that sulphate and chloride ions have significant effects on the corrosion behavior of metallic materials [53,64–68]. Specifically, existence of chloride ions could accelerate corrosion with the condition of delicate passivation layer. During corrosion process chloride ions can easily penetrate through the thin layer, giving way to pitting corrosion [53,64]. Besides, on TiTaHfNb sample surfaces, the vertically advancing corrosion behavior created ditch like structures and holes that contain particles (Figures 2-3 (c) and (d)). The accumulated particles around and in the holes signify initiation of conceivable crystallization process: NaCl crystals (in Figure 2-3 (c) and (d)) have been revealed by XPS (Figure 2-4), where NaCl formation evidences penetration of chloride ions into the material. Therefore, it can be argued that the chloride ions facilitate pitting corrosion, and sulphate ions further worsen the corrosion by expanding the pits [68]. Therefore, NaCl precipitates seen in Figure 2-3 (c) and (d) can be attributed to pitting corrosion induced by SBF. Consequently, TiTaHfNb cannot tolerate SBF environment since the experimental findings clearly indicate pitting corrosion, and the relatively mild surface of TiTaHfNb may accelerate the corrosion behavior. On the other hand, AS provides a more suitable environment for TiTaHfNb alloy, as evident from the lack of a

substantially deformed surface that formed when immersed in SBF. This significant difference between the surfaces of TiTaHfNb substrates immersed in SBF and AS can be clearly seen in Figures 2-3 (a) and (b). The smoother surface seen in (b) suggests higher corrosion resistance of TiTaHfNb against AS. After all, better surface response to AS was observed in TiTaHfNb despite the lower pH degree of AS.

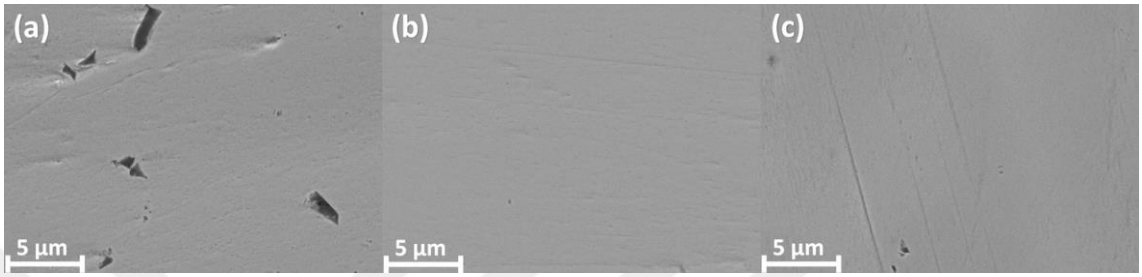

Figure 2-1: The SEM images of the untested (a) TiTaHfNb, (b) TiTaHfNbZr and (c) TiTaHfMoZr sample surfaces following polishing.

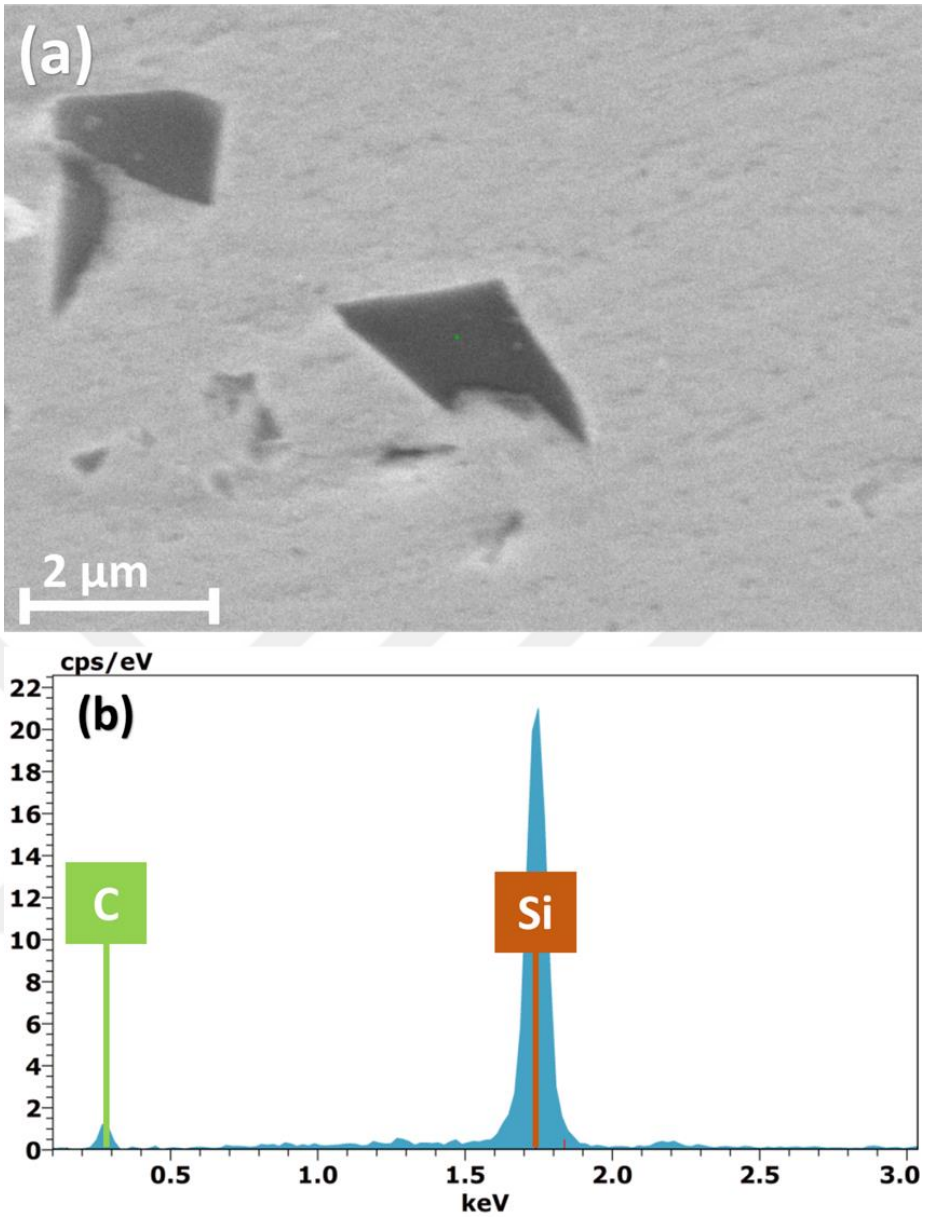

Figure 2-2: (a) Stains on the as-received TiTaHfNb, and (b) EDX analysis of elemental composition of the stains observed on TiTaHfNb surfaces.

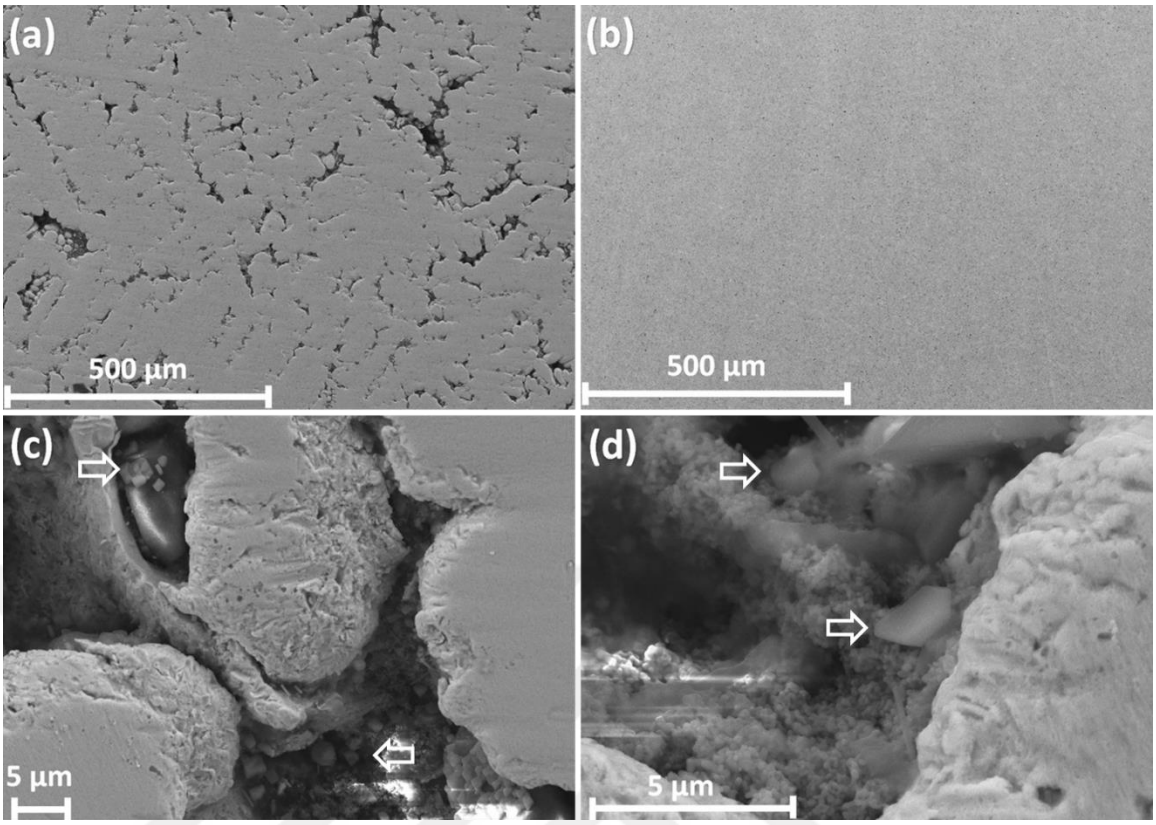

Figure 2-3: SEM micrographs of the bulk TiTaHfNb sample surfaces following immersion for 28 days - (a), (c), (d): SBF, and (b): AS. Arrows at (c) and (d) represent the crystal structures forming on the TiTaHfNb surface after being immersed in SBF for 28 days.

As compared to the TiTaHfNb alloy, TiTaHfNbZr HEA exhibited a more stable behavior in both SBF and AS: as shown in Figure 2-5, there is no significant corrosion on the surface of TiTaHfNbZr following immersion in SBF and AS, and the material highly resists to both these aggressive environments with negligible amount of corrosion. In contrast to TiTaHfNbZr, non-homogeneous degradation prevailed on the surface of TiTaHfMoZr due to significant amount of Mo ion release. Two distinct regions were recognized prior to immersion and following 28 days of immersion in SBF and AS as evident from the SEM images presented in Figure 6. These two regions were analysed by EDX (Figures 2.7 and 2.8), which coexist as a consequence of nonhomogeneous distribution of the components during solidification process that lead to dendritic structures [30]. As illustrated in Figure 2-7 (a) and (b), and 2.8 (a) and (b), dendrites indicate Ta-rich areas with a higher melting point, leading to earlier crystallization [69], and Zr-rich areas dominated the inter-dendrite regions. This inhomogeneous elemental distribution was brought about by the addition of Mo during

manufacturing process. On the other hand, TiTaHfMoZr showed better corrosion resistance in SBF environment. The difference between corroded surfaces induced by SBF and AS are apparent from Figures 2-4 (a) and (c), such that AS induced more damage to the surface of TiTaHfMoZr. Thus, one can conclude that TiTaHfMoZr performs better in SBF than in AS.

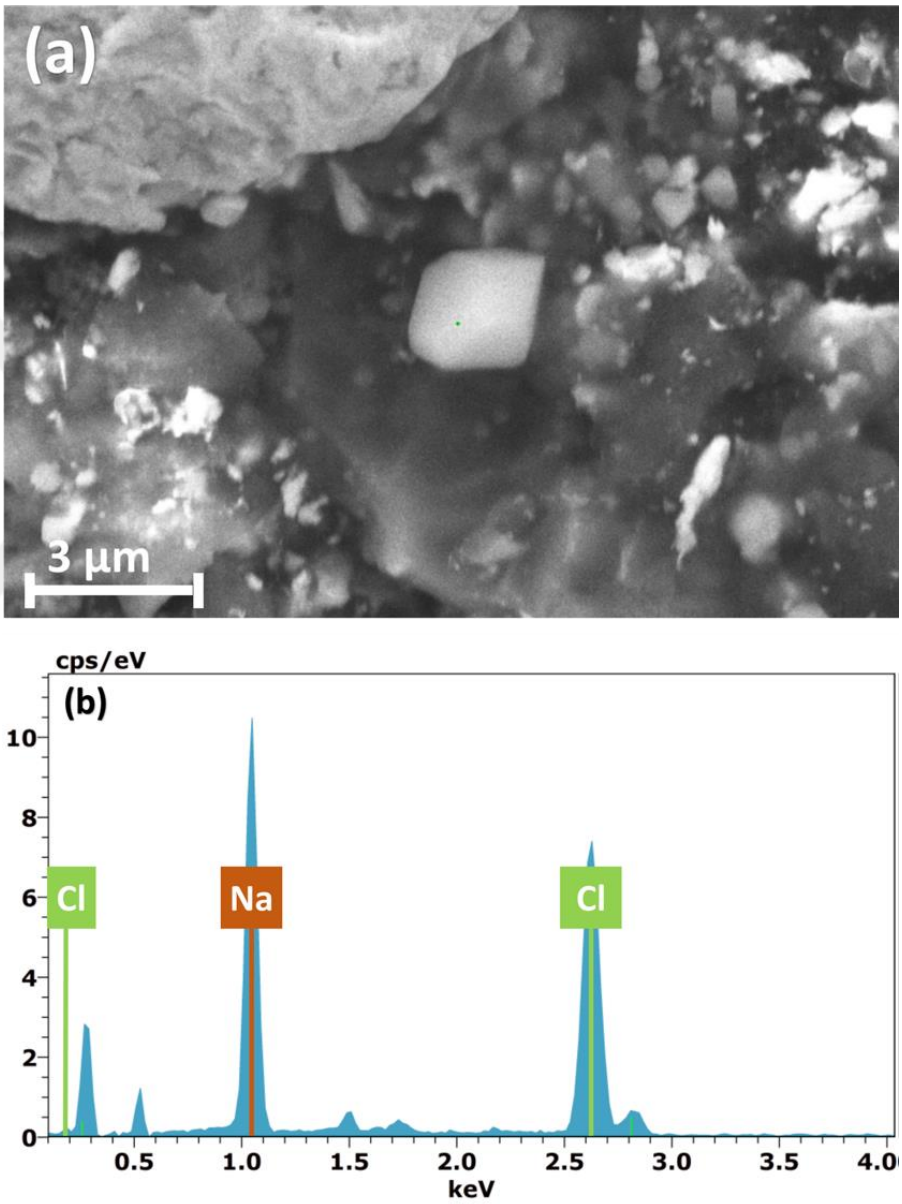

Figure 2-4: (a) A NaCl crystal on TiTaHfNb surface, and (b) EDX analysis of NaCl crystal in (a).

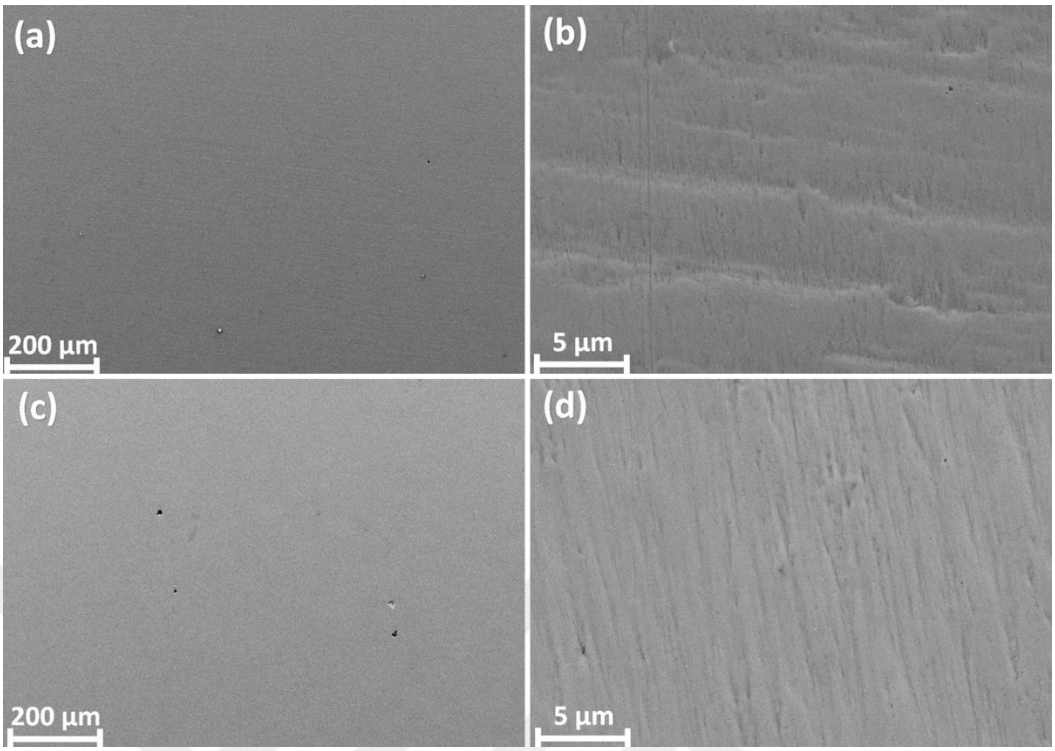

Figure 2-5: SEM micrographs of the bulk TiTaHfNbZr sample surfaces following immersion for 28 days – (a), (b): SBF; (c) and (d): AS.

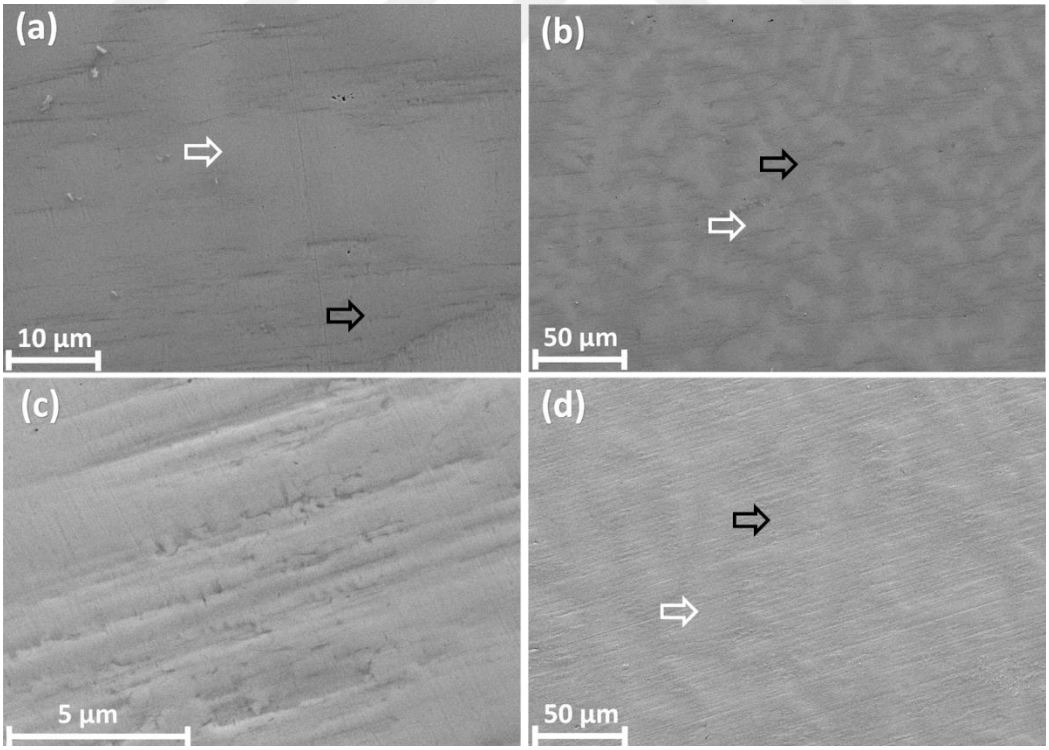

Figure 2-6: SEM micrographs of the bulk TiTaHfMoZr sample surfaces following immersion for 28 days – (a), (b): SBF; (c) and (d): AS. Black arrows at (a), (b) and (d) indicate darker regions; white arrows indicate brighter regions.

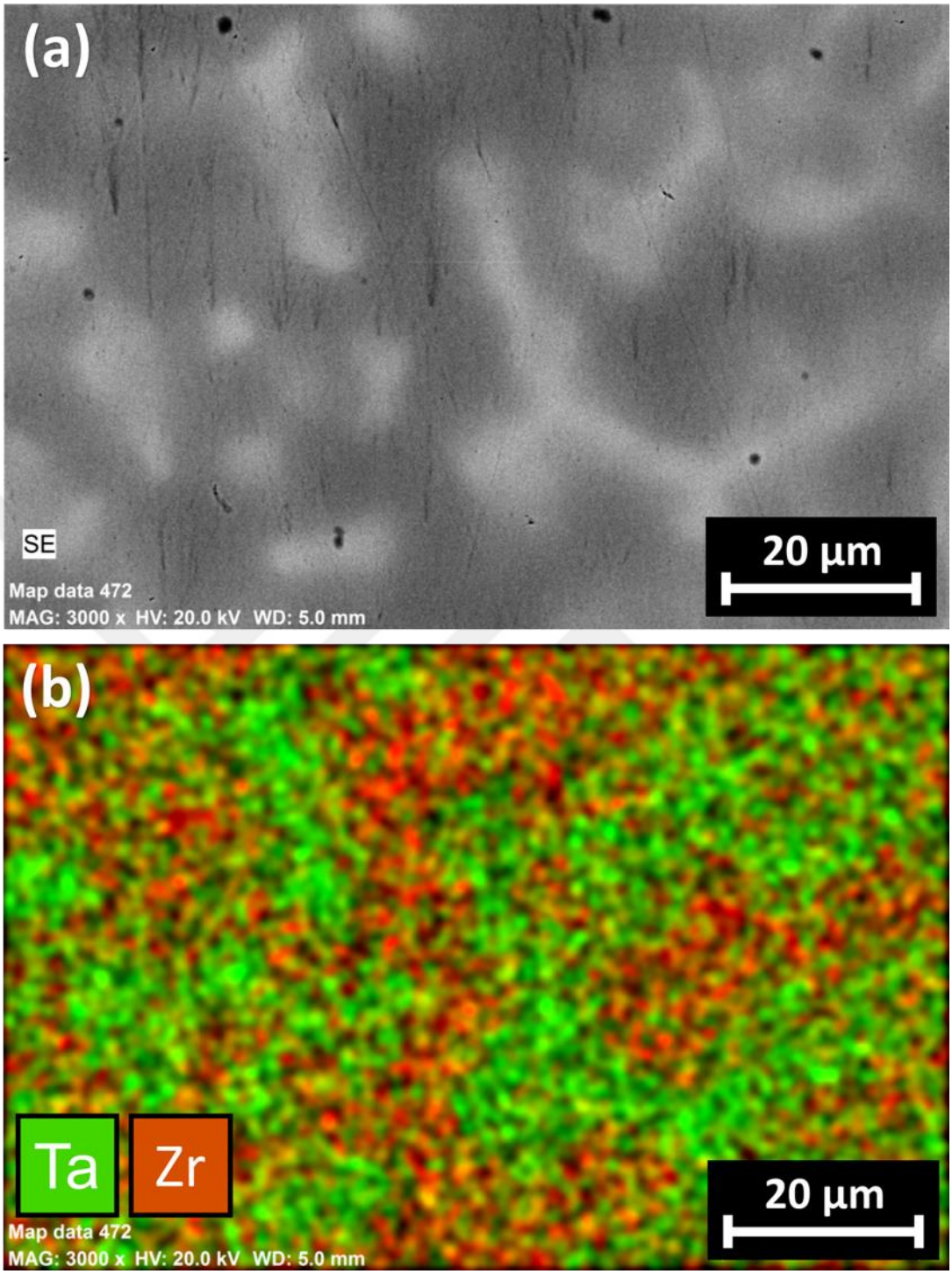

Figure 2-7: EDX analysis results of the as-received TiTaHfMoZr sample: (a) nonhomogenous surface of TiTaHfMoZr, (b) EDX of TiTaHfMoZr surface. Green regions represent Ta-rich areas, and red regions represent Zr-rich areas.

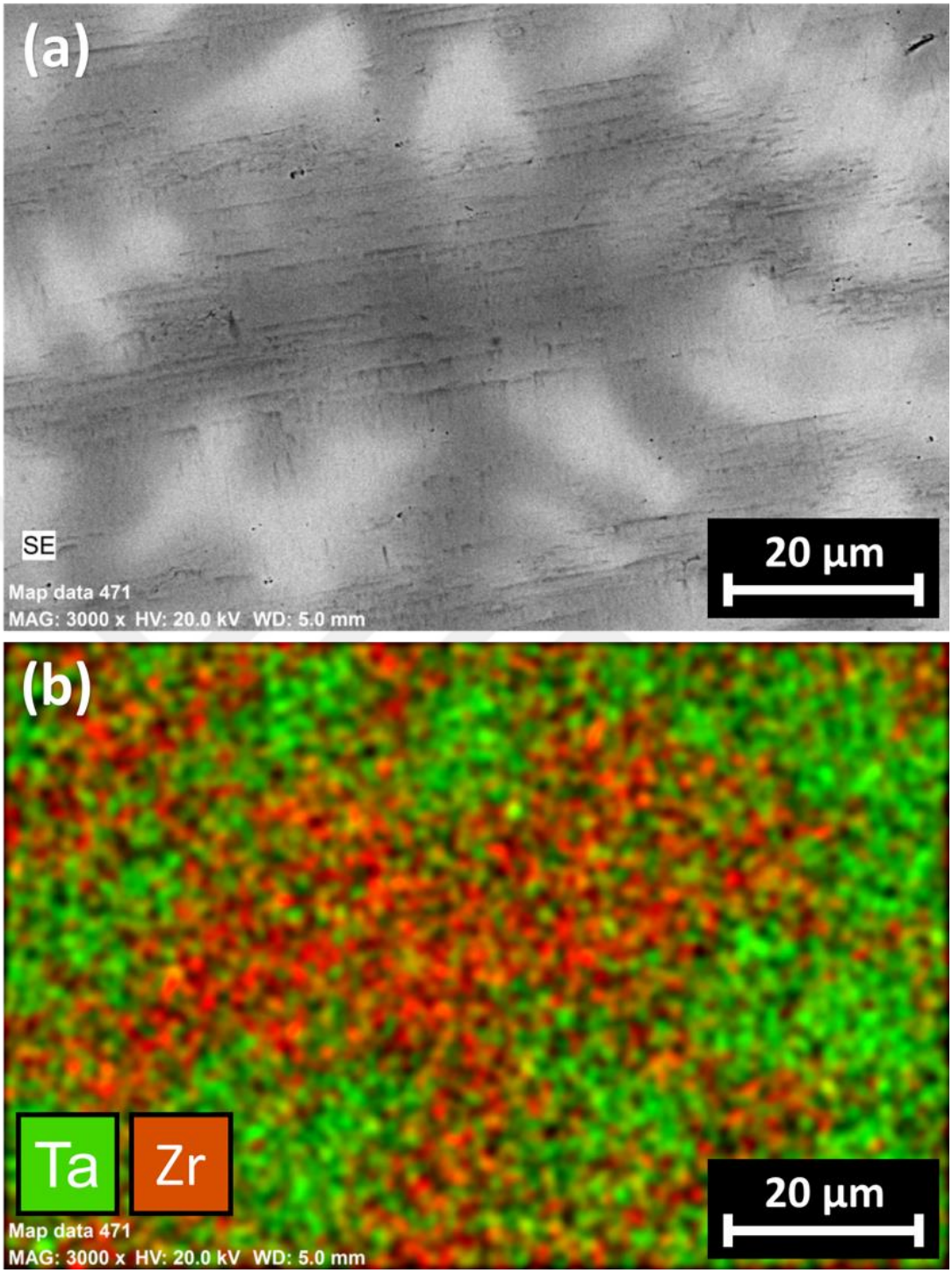

Figure 2-8: EDX analysis results of the TiTaHfMoZr sample following 28 days of immersion in SBF: (a) nonhomogenous surface of TiTaHfMoZr, (b) EDX of TiTaHfMoZr surface; Green regions represent Ta-rich areas, and red regions represent Zr-rich areas.

It should be noted that the low pH value of AS has a significant ionization effect on all three HEAs as evidenced by the surface degradation. SEM micrographs (Figures 2.5 and 2.6) demonstrate the aggressive nature of AS and the corresponding corrosion damage it causes, while supporting data from the ICP-MS experiments (Figure 2.9) demonstrate the negative impact of AS on the ion release behavior of the studied HEAs: the amount of total ion release form all three HEAs was much higher in AS at the end of the 28th day as compared to the SBF.

As illustrated in Figure 2-5, SBF and AS contain very similar levels of ion concentrations after immersion of TiTaHfNb and TiTaHfNbZr substrates, however; addition of Zr enhances corrosion resistance, such that TiTaHfNbZr shows better protection against ion release, as evidenced by the less total ion release from TiTaHfNbZr (as compared to TiTaHfNb) following the 1st week of immersion in both media. The highest total released ion concentrations in SBF and AS were obtained from the immersion tests of TiTaHfMoZr (Figure 2-9). TiTaHfMoZr showed almost 5 and 3 times more ion release into the SBF and AS, respectively, while relatively small quantity of ions was released from the TiTaHfNb and TiTaHfNbZr. This significantly enhanced ion release behavior from the former HEA, is attributed to Mo replacing Nb in the other two materials. Apparently, Nb acts as a stabilizer and restricts the quantity of released ions from the bulk [54,70,71].

An important finding is that the HEA substrates gained mass following immersion tests despite the ion release. For instance, even though a greater amount of ion release was observed in AS for all three HEAs (Figure 2-9), this was accompanied by an increase in mass of the immersed samples as demonstrated in Figure 2-10. The increase in mass following the immersion experiments despite the apparent corrosion is an indication of new formations on the surface: the ions attached to the metallic surface can facilitate the formation of passive oxide layer that initiates osseointegration process [20,72,73], which is very beneficial for biomedical applications. Indeed, a significant mass loss would be expected in the samples due to high ionization from their surfaces. However, the continuously increasing ion release from TiTaHfNb and TiTaHfNbZr (Figure 2.9), as well as the corresponding mass gain patterns presented in Figure 2-10 indicate this protective layer formation.

In the case of TiTaHfMoZr, Mo ion concentrations in SBF and AS started to decrease following the 1st week of immersion (through days 7-14, Figure 2-9) despite

the fact that the mass increased (SBF) or only slightly decreased (AS) (Figure 2-10), implying ions attaching onto TiTaHfMoZr surface or new compounds forming in the immersion solutions. Even though TiTaHfMoZr has the highest amount of ion release among TiTaHfNb and TiTaHfNbZr, there is no significant mass loss in TiTaHfMoZr that indicates a passive layer formation. On the other hand, cyclically repeated elemental release implies a passive layer formation and dissolution over specific time periods [74,75]. Specifically, the total ion release from TiTaHfMoZr increased within the first 7 days, and then decreased until the 14th day, followed by an increased ion concentration up until the end of the 28th day (Figure 2-9). Despite this significant ion release from the TiTaHfMoZr HEA, especially within the first 7 days upon immersion in AS, the nearly constant remaining mass within this period (Figure 2-10) strongly suggests beginning of surface film formation. Therefore, increase in the mass of TiTaHfMoZr during the ion reduction in SBF and AS can be attributed to passive layer on the surface. Consequently, the observed trend between the total ion release (Figure 2-9) and mass change (Figure 2-10) is remarkable and clearly evidences the formation-dissolution cycle of a passive surface layer.

The mass increase in TiTaHfNb (Figure 2-10 (a)) may have been due to NaCl precipitates (Figure 2-3 (c), (d) and Figure 2-4). On the other hand, no new crystal structures were observed on the surfaces of TiTaHfNbZr and TiTaHfMoZr HEAs by SEM (Figure 2-5 and 2-6), and the mass increase in these two materials suggests a passive oxide layer formation. In order to clarify this ambiguity, samples expected to form a passive oxide layer were analyzed with XPS. TiTaHfNbZr and TiTaHfMoZr were significantly exposed to corrosion in AS without reduction in their masses, such that the results of ICP-MS and the observed mass gain led to the investigation of the possibility of a passive oxide layer formation. Therefore, elemental compositions of TiTaHfNbZr and TiTaHfMoZr samples following 28 days of immersion in AS were analyzed by XPS. The samples were initially etched for 60 s to eliminate organic impurities, then the etching process was continued until 3000 s for the TiTaHfNbZr and TiTaHfMoZr samples. XPS analysis results proved that TiTaHfNbZr and TiTaHfMoZr formed a passive oxide layer on their surfaces following a 28-day immersion test in AS, and oxides of Ti,Ta,Hf,Nb,Mo and Zr were found on the surfaces of the HEAs during the post-mortem investigation. It should be noted that the XPS analysis focused on Zr and its oxides, mainly because Zr has ability to form a strong and adherent passive layer

on a material surface [76,77]. As illustrated in Figure 2-11, while both materials have oxygen on their surface, the amount of oxygen decreases and the amount of metal increases concomitant with the distance from the surface. As etching moves from the surface to deeper layers, oxygen is replaced by metal oxide, which is eventually replaced by pure metal elements.

Even though TiTaHfNbZr and TiTaHfMoZr HEAs exhibited higher ion release in AS (pH=2.4) than in SBF (Figure 2-9), a healthier (smoother) surface appearance was noted following the immersion tests in AS with negligible surface degradations as evidenced from SEM images (Figure 2-5 (c) and (d); Figure 2-6 (c) and (d)). This is attributed to the surface layer formation, such that passive layer forming on the surface covers the surface deteriorations initially induced by the corrosion. Examination of the XPS results for these two HEAs (Figure 2-11 (a) and (b)) reveals that oxygen and Zr-oxides predominantly exist on the surface up to 300 s etch time, and Zr-metal appears with further etching. The XPS spectra of the O 1s and Zr 3d peaks are indicated in Figure 2-11 for the 28-day immersed TiTaHfNbZr and TiTaHfMoZr in AS to observe layer properties on the bulk surfaces. The peak of the O 1s profile as shown in Figure 2-11 (c) is located at 530.6 eV binding energy (BE) for TiTaHfNbZr, and 530.9 eV and 530.6 eV BE are the peaks for 0 s etch time and 900 s etch time of TiTaHfMoZr, respectively (Figure 2-11(d)). The O 1s peak locations agree well with the depth profiles (Figure 2-11 (a) and (b)), such that oxygen content prevails on the surface of both HEAs, and the content decreases going from the surface to deeper into the bulk. The Zr 3d spectra shown in Figure 2-11 have doublet peaks of 3d5/2 and 3d3/2 due to spin-orbit-split [78], and the energy difference between the doublets is 2.4 eV [79]. Four doublets (the couples of Zr3d3/2 and Zr3d5/2) have been obtained from the XPS results that can be attributed to four different types of BE of Zr-metal, Zr-oxide and Zr-sub oxides as illustrated in Figure 2-11 (e)) [79,80]. The peaks at 178.2 eV and 180.6 eV binding energy corresponding to Zr 3d5/2 and Zr 3d3/2, respectively, indicate the presence of metallic Zr (Figure 2-11 (e)), as these peaks are consistent with previously reported binding energies of metallic Zr are 178.8 eV [81,82] and 177.93 eV [83] for Zr 3d5/2; and 180.33 eV [83] for Zr 3d3/2. On the other hand, 184.0 eV (Zr 3d5/2) and 181.6 eV (Zr 3d3/2) peaks (Figure 2-11 (e)) strongly point out to the existence of oxide layer formation on the TiTaHfNbZr surface following 28 days immersion in AS. These peaks are close to the binding energy of ZrO_2 that has been reported as 184.3 eV and

181.9 eV corresponding to Zr 3d5/2 and Zr 3d3/2, respectively [84]; and 183.7 eV and 181.3 eV for Zr-oxide (Zr^{+2}) [79], and 186.60 eV [85,86] for ZrO_2.

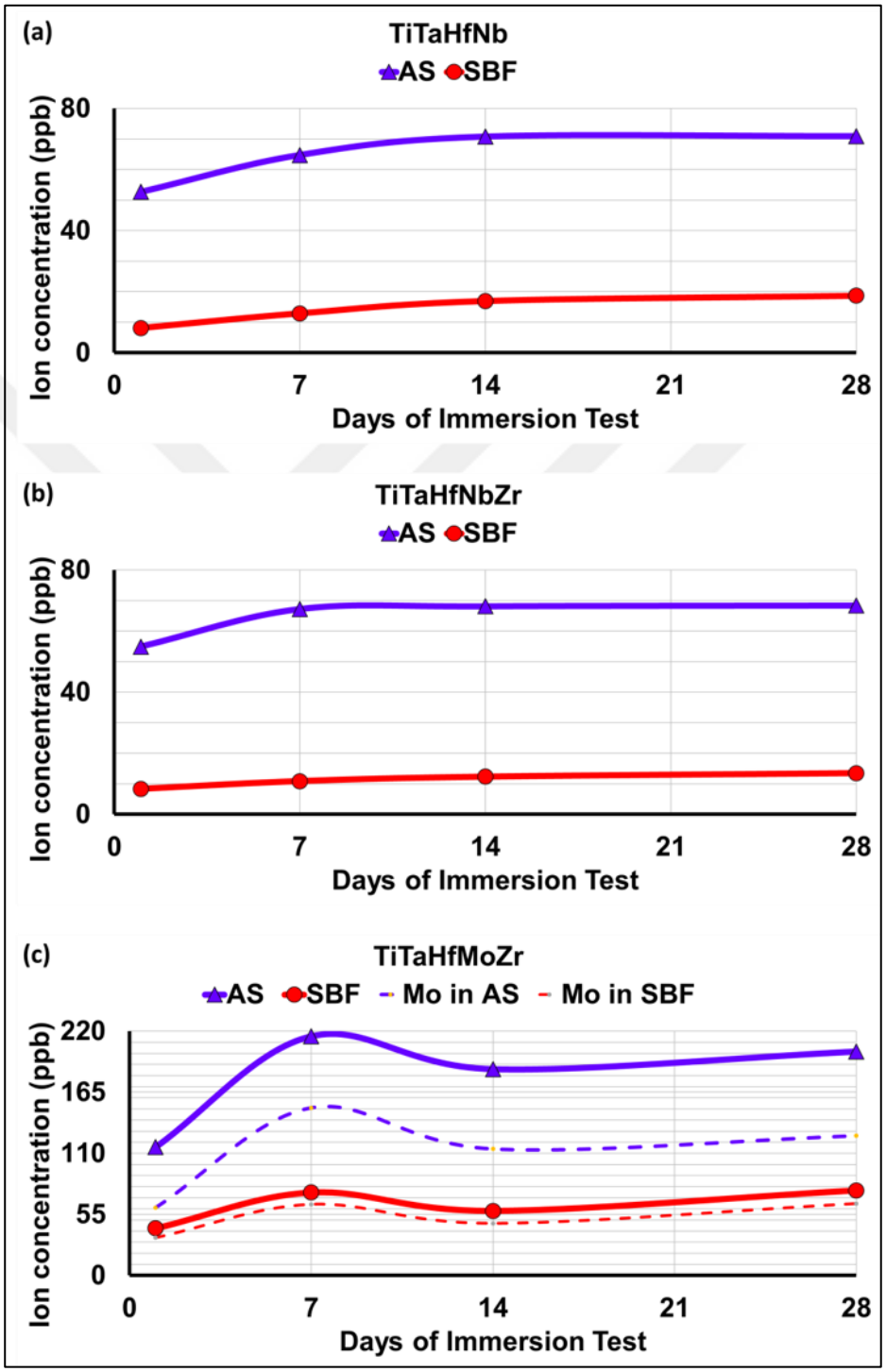

Figure 2-9: Total ion concentrations of TiTaHfNb, TiTaHfNbZr and TiTaHfMoZr in SBF and AS following 1, 7, 14 and 28 days of immersion. Note that the total ion concentration does not include Hf concentration due to its insignificant amount.

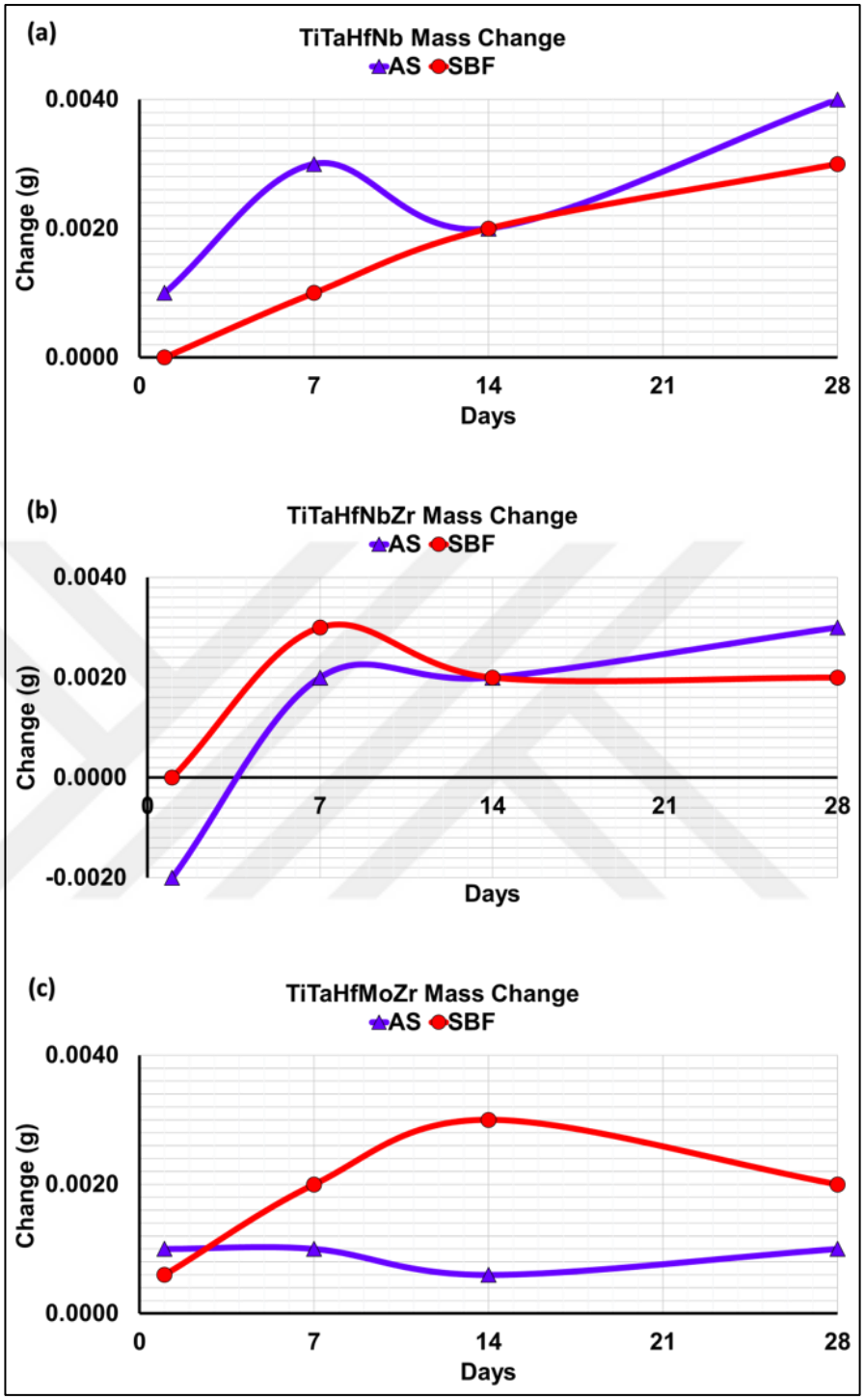

Figure 2-10: Mass change in TiTaHfNb, TiTaHfNbZr, and TiTaHfMoZr samples following 28 days of immersion in AS and SBF.

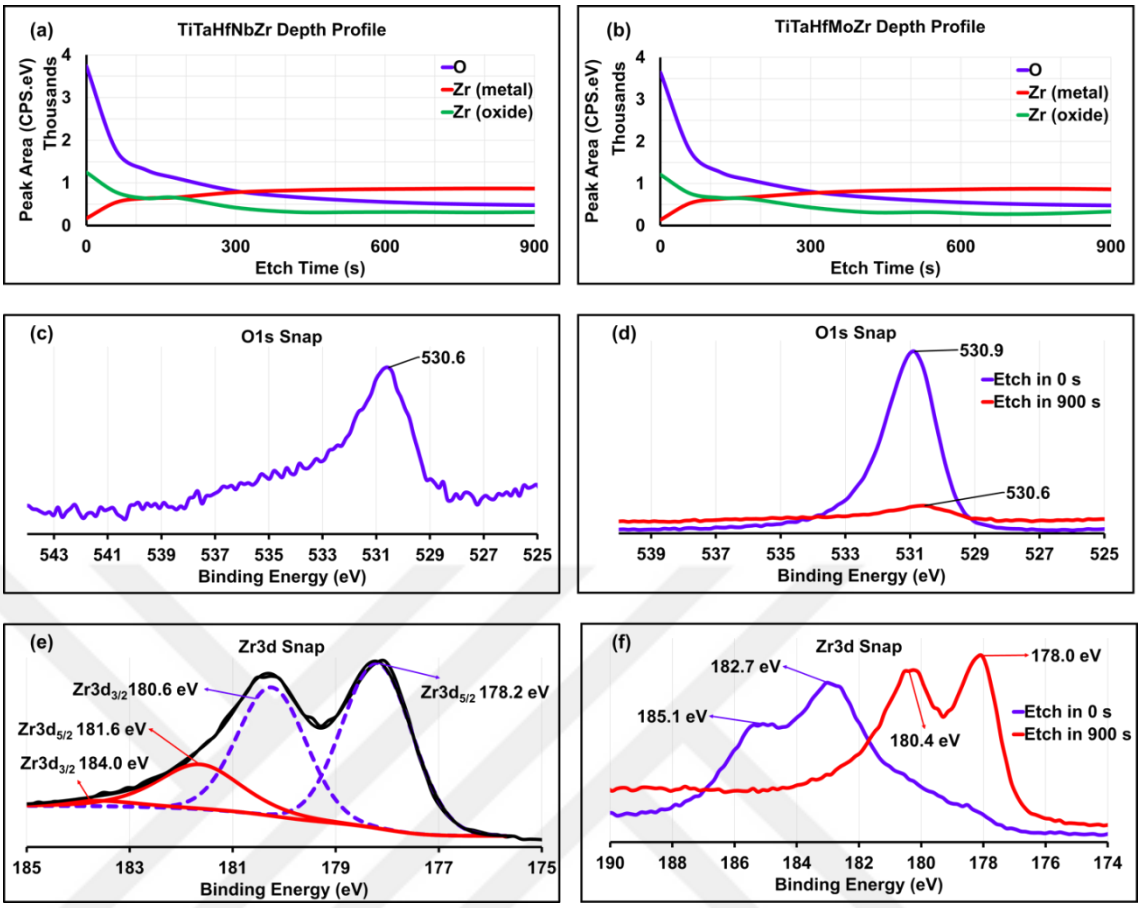

Figure 2-11: XPS depth profiles of (a) TiTaHfNbZr and (b)TiTaHfMoZr; oxygen peaks of (c) TiTaHfNbZr and (d) TiTaHfMoZr; Zr and ZrO2 peaks of (e) TiTaHfNbZr and (f) TiTaHfMoZr.

The relationship between etch time and surface layer properties is presented in Figure 2-11 (f). The peaks are centered at 182.7 eV BE and 185.1 eV BE that agree with the oxide layer formation on TiTaHfMoZr surface following 28 days of immersion in AS, and these peaks are close to the binding energies reported in literature: some studies reported peak values of Zr-oxide (Zr^{3+}) as 182.6 eV and 185.0 eV [79]; and 182.66 eV and 185.06 eV [83], corresponding to Zr 3d5/2 and Zr 3d3/2, respectively. Consequently, the XPS results confirmed the existence of Zr-oxide film on the surface of the HEAs. Similarly, TiTaHfNbZr and TiTaHfMoZr may maintain the same behavior in SBF, because there was a mass increase in the materials along with corrosion following immersion in SBF.

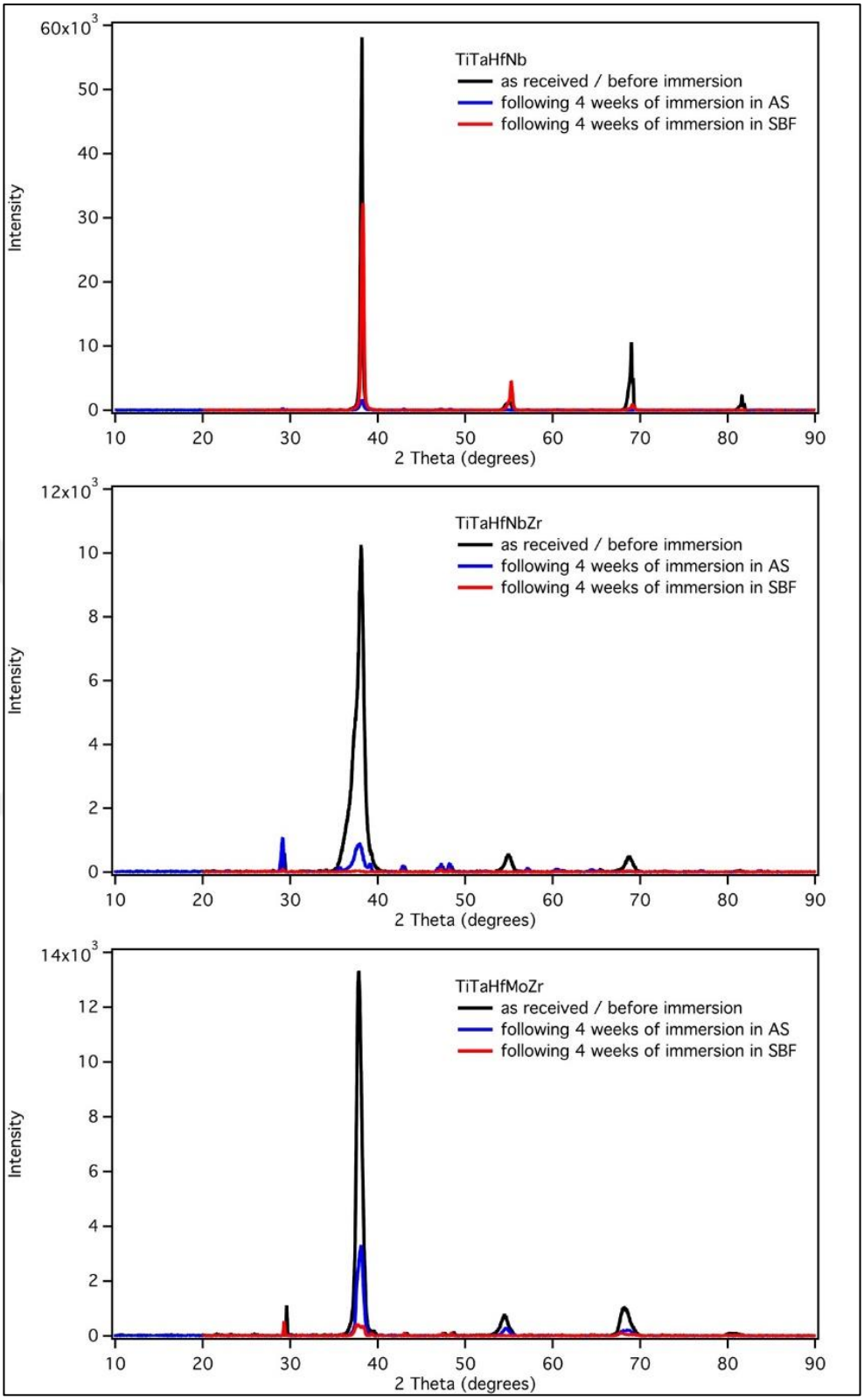

Figure 2-12: XRD scans of TiTaHfNb, TiTaHfNbZr and TiTaHfMoZr prior to and following the immersion experiments.

This passive film formation is supported by XPS results presented in Figure 2.11, as well as the XRD results provided in Figure 2-12. In particular, the XRD data suggests that a crystallization process takes place on the sample surfaces upon static immersion tests. For instance, formation of NaCl crystal structures on TiTaHfNb sample surfaces upon immersion in SBF were clearly observed in SEM (Figures 2.3 (c) and (d)) and EDX (Figure 2-4), and the pointed peaks present in Figure 2-12 indicate that these are new crystal structures that formed on TiTaHfNb. On the other hand, the TiTaHfNbZr shows lower intensity peaks (Figure 2-12): the Zr addition to TiTaHfNb accelerates the formation of a passive layer, leading to an amorphous layer. As for the TiTaHfMoZr HEA, it exhibited higher peak intensity than the TiTaHfNbZr alloy, which can be attributed to possible Mo precipitation and nonhomogeneous structure of TiTaHfMoZr (Figures 2-6, 2.7 and 2.8). This passive layer formation on TiTaHfNb, TiTaHfNbZr and TiTaHfMoZr supported by the current SEM micrographs, ICP-MS results, reported mass changes, XPS results and the XRD data suggests that these TiTaHf-based HEAs can sustain long-term corrosion resistance, which, however; should be studied in detail before drawing any conclusions regarding their biomedical utility.

2.4 Conclusions

Corrosion response of three TiTaHf-based HEAs, namely TiTaHfNb, TiTaHfNbZr and TiTaHfMoZr, was inspected employing static immersion experiments in simulated body fluid (SBF) and artificial saliva (AS) in order to assess the potential biomedical utility of these alloys. As a result of immersion experiments that were carried out for periods of 1, 7, 14 and 28 days, the TiTaHfNb HEA was observed to suffer from pitting corrosion in SBF, while it exhibited a healthier surface following immersion in AS. The presence of Zr and Nb in the substrates was observed to enhance corrosion performance with reduced ion release and better surface properties as evidenced by the results of the TiTaHfNbZr test results. On the contrary, Mo addition resulted in an inhomogeneous microstructure (TiTaHfMoZr), leading to dendrite structures and a significant amount of ion release upon immersion in both media. In addition, XPS and XRD results along with the ICP-MS ion release trends showed that a passive layer formation or crystallization was present on all HEA surfaces, implying that corrosion resistance can be sustained in long-term applications. Overall, the set of

findings presented herein demonstrate the potential of the TiTaHf-based HEAs to be utilized as implant materials, but also warrant a more detailed analysis of these materials before drawing any conclusions.

2.5 Acknowledgments

This work was supported by the BAGEP Award of the Science Academy.

2.6 References

[1] D.F. Williams, On the mechanisms of biocompatibility, Biomaterials. 29 (2008) 2941–2953. doi:10.1016/j.biomaterials.2008.04.023.

[2] D.F. Williams, On the nature of biomaterials, Biomaterials. 30 (2009) 5897–5909. doi:10.1016/j.biomaterials.2009.07.027.

[3] W. Jin, P.K. Chu, Orthopedic Implants, in: Encycl. Biomed. Eng., Elsevier, 2019: pp. 425–439. doi:10.1016/B978-0-12-801238-3.10999-7.

[4] M. Geetha, A.K. Singh, R. Asokamani, A.K. Gogia, Ti based biomaterials, the ultimate choice for orthopaedic implants – A review, Prog. Mater. Sci. 54 (2009) 397–425. doi:10.1016/j.pmatsci.2008.06.004.

[5] M.P. Staiger, A.M. Pietak, J. Huadmai, G. Dias, Magnesium and its alloys as orthopedic biomaterials: A review, Biomaterials. 27 (2006) 1728–1734. doi:10.1016/j.biomaterials.2005.10.003.

[6] M. Niinomi, Recent metallic materials for biomedical applications, Metall. Mater. Trans. A. 33 (2002) 477–486. doi:10.1007/s11661-002-0109-2.

[7] Q. Chen, G.A. Thouas, Metallic implant biomaterials, Mater. Sci. Eng. R Reports. 87 (2015) 1–57. doi:10.1016/j.mser.2014.10.001.

[8] F. Rupp, J. Geis-Gerstorfer, K.E. Geckeler, Dental implant materials: Surface modification and interface phenomena, Adv. Mater. 8 (1996) 254–257. doi:10.1002/adma.19960080316.

[9] U. Kamachimudali, T.M. Sridhar, B. Raj, Corrosion of bio implants, Sadhana. 28 (2003) 601–637. doi:10.1007/BF02706450.

[10] M. Niinomi, M. Nakai, J. Hieda, Development of new metallic alloys for biomedical applications, Acta Biomater. 8 (2012) 3888–3903. doi:10.1016/j.actbio.2012.06.037.

[11] D.A. Puleo, W.W. Huh, Acute toxicity of metal ions in cultures of osteogenic cells derived from bone marrow stromal cells, J. Appl. Biomater. 6 (1995) 109–116. doi:10.1002/jab.770060205.

[12] C. Lhotka, T. Szekeres, I. Steffan, K. Zhuber, K. Zweymüller, Four-year study of cobalt and chromium blood levels in patients managed with two different metal-on-metal total hip replacements, J. Orthop. Res. 21 (2003) 189–195. doi:10.1016/S0736-0266(02)00152-3.

[13] Y. Song, D.S. Xu, R. Yang, D. Li, W.T. Wu, Z.X. Guo, Theoretical study of the effects of alloying elements on the strength and modulus of β-type bio-titanium alloys, Mater. Sci. Eng. A. 260 (1999) 269–274. doi:10.1016/S0921-5093(98)00886-7.

[14] C.B. Aksoy, D. Canadinc, M.B. Yagci, Assessment of Ni ion release from TiTaHfNbZr high entropy alloy coated NiTi shape memory substrates in artificial saliva and gastric fluid, Mater. Chem. Phys. 236 (2019) 121802. doi:10.1016/j.matchemphys.2019.121802.

[15] C.-C. Shih, S.-J. Lin, Y.-L. Chen, Y.-Y. Su, S.-T. Lai, G.J. Wu, C.-F. Kwok, K.-H. Chung, The cytotoxicity of corrosion products of nitinol stent wire on cultured smooth muscle cells, J. Biomed. Mater. Res. 52 (2000) 395–403. doi:10.1002/1097-4636(200011)52:2<395::AID-JBM21>3.0.CO;2-B.

[16] Y. Yuan, Y. Wu, Z. Yang, X. Liang, Z. Lei, H. Huang, H. Wang, X. Liu, K. An, W. Wu, Z. Lu, Formation, structure and properties of biocompatible TiZrHfNbTa high-entropy alloys, Mater. Res. Lett. 7 (2019) 225–231. doi:10.1080/21663831.2019.1584592.

[17] C. Oldani, A. Dominguez, Titanium as a Biomaterial for Implants, in: Recent Adv. Arthroplast., InTech, 2012. doi:10.5772/27413.

[18] S. Rajendran, J. Paulraj, P. Rengan, J. Jeyasundari, M. Manivannan, Corrosion behaviour of metals in artificial saliva in presence of spirulina powder, J. Dent. 1 (2009) 1–8.

[19] S. Rao, T. Ushida, T. Tateishi, Y. Okazaki, S. Asao, Effect of Ti, Al, and V ions on the relative growth rate of fibroblasts (L929) and osteoblasts (MC3T3-E1) cells., Biomed. Mater. Eng. 6 (1996) 79–86. http://www.ncbi.nlm.nih.gov/pubmed/8761518.

[20] S.G. Steinemann, Metal implants and surface reactions, Injury. 27 (1996) S/C16-S/C22. doi:10.1016/0020-1383(96)89027-9.

[21] R. Van Noort, Titanium: The implant material of today, J. Mater. Sci. 22 (1987) 3801–3811. doi:10.1007/BF01133326.

[22] L.N. Miotto, L.M.G. Fais, A.L.R. Ribeiro, L.G. Vaz, Surface properties of Ti-35Nb-7Zr-5Ta, J. Prosthet. Dent. 116 (2016) 102–111. doi:10.1016/j.prosdent.2015.10.024.

[23] Z. Tang, L. Huang, W. He, P. Liaw, Alloying and Processing Effects on the Aqueous Corrosion Behavior of High-Entropy Alloys, Entropy. 16 (2014) 895–911. doi:10.3390/e16020895.

[24] S.D. Cramer, B.S. Covino, eds., Corrosion: Fundamentals, Testing, and Protection, ASM International, 2003. doi:10.31399/asm.hb.v13a.9781627081825.

[25] B. Cantor, I.T.H. Chang, P. Knight, A.J.B. Vincent, Microstructural development in equiatomic multicomponent alloys, Mater. Sci. Eng. A. 375–377 (2004) 213–218. doi:10.1016/j.msea.2003.10.257.

[26] L. Vinet, A. Zhedanov, A 'missing' family of classical orthogonal polynomials, J. Phys. A Math. Theor. 44 (2011) 085201. doi:10.1088/1751-8113/44/8/085201.

[27] Y. Zhang, X. Yang, P.K. Liaw, Alloy Design and Properties Optimization of High-Entropy Alloys, JOM. 64 (2012) 830–838. doi:10.1007/s11837-012-0366-5.

[28] J.-W. Yeh, Alloy Design Strategies and Future Trends in High-Entropy Alloys, JOM. 65 (2013) 1759–1771. doi:10.1007/s11837-013-0761-6.

[29] Y.F. Ye, Q. Wang, J. Lu, C.T. Liu, Y. Yang, Design of high entropy alloys: A single-parameter thermodynamic rule, Scr. Mater. 104 (2015) 53–55. doi:10.1016/j.scriptamat.2015.03.023.

[30] M. Todai, T. Nagase, T. Hori, A. Matsugaki, A. Sekita, T. Nakano, Novel TiNbTaZrMo high-entropy alloys for metallic biomaterials, Scr. Mater. 129 (2017) 65–68. doi:10.1016/j.scriptamat.2016.10.028.

[31] J.-W. Yeh, S.-K. Chen, S.-J. Lin, J.-Y. Gan, T.-S. Chin, T.-T. Shun, C.-H. Tsau, S.-Y. Chang, Nanostructured High-Entropy Alloys with Multiple Principal Elements: Novel Alloy Design Concepts and Outcomes, Adv. Eng. Mater. 6 (2004) 299–303. doi:10.1002/adem.200300567.

[32] W. Zhang, P.K. Liaw, Y. Zhang, Science and technology in high-entropy alloys, Sci. China Mater. 61 (2018) 2–22. doi:10.1007/s40843-017-9195-8.

[33] Y. Qiu, S. Thomas, M.A. Gibson, H.L. Fraser, N. Birbilis, Corrosion of high entropy alloys, Npj Mater. Degrad. 1 (2017) 15. doi:10.1038/s41529-017-0009-y.

[34] X.W. Qiu, Y.P. Zhang, L. He, C.G. Liu, Microstructure and corrosion resistance of AlCrFeCuCo high entropy alloy, J. Alloys Compd. 549 (2013) 195–199. doi:10.1016/j.jallcom.2012.09.091.

[35] C. Li, J.C. Li, M. Zhao, Q. Jiang, Effect of aluminum contents on microstructure and properties of AlxCoCrFeNi alloys, J. Alloys Compd. 504 (2010) S515–S518. doi:10.1016/j.jallcom.2010.03.111.

[36] Z.D. Han, H.W. Luan, X. Liu, N. Chen, X.Y. Li, Y. Shao, K.F. Yao, Microstructures and mechanical properties of Ti NbMoTaW refractory high-entropy alloys, Mater. Sci. Eng. A. 712 (2018) 380–385. doi:10.1016/j.msea.2017.12.004.

[37] T.-T. Shun, L.-Y. Chang, M.-H. Shiu, Microstructures and mechanical properties of multiprincipal component CoCrFeNiTix alloys, Mater. Sci. Eng. A. 556 (2012) 170–174. doi:10.1016/j.msea.2012.06.075.

[38] O.N. Senkov, J.M. Scott, S.V. Senkova, D.B. Miracle, C.F. Woodward, Microstructure and room temperature properties of a high-entropy TaNbHfZrTi alloy, J. Alloys Compd. 509 (2011) 6043–6048. doi:10.1016/j.jallcom.2011.02.171.

[39] X.F. Wang, Y. Zhang, Y. Qiao, G.L. Chen, Novel microstructure and properties of multicomponent CoCrCuFeNiTix alloys, Intermetallics. 15 (2007) 357–362. doi:10.1016/j.intermet.2006.08.005.

[40] O.N. Senkov, G.B. Wilks, D.B. Miracle, C.P. Chuang, P.K. Liaw, Refractory high-entropy alloys, Intermetallics. 18 (2010) 1758–1765. doi:10.1016/j.intermet.2010.05.014.

[41] Y. Qiu, M.A. Gibson, H.L. Fraser, N. Birbilis, Corrosion characteristics of high entropy alloys, Mater. Sci. Technol. 31 (2015) 1235–1243. doi:10.1179/1743284715Y.0000000026.

[42] R. Sriharitha, B.S. Murty, R.S. Kottada, Alloying, thermal stability and strengthening in spark plasma sintered AlxCoCrCuFeNi high entropy alloys, J. Alloys Compd. 583 (2014) 419–426. doi:10.1016/j.jallcom.2013.08.176.

[43] B. Gludovatz, A. Hohenwarter, D. Catoor, E.H. Chang, E.P. George, R.O. Ritchie, ChemInform Abstract: A Fracture-Resistant High-Entropy Alloy for Cryogenic Applications., ChemInform. 45 (2014) no-no. doi:10.1002/chin.201447007.

[44] Z. Zhang, M.M. Mao, J. Wang, B. Gludovatz, Z. Zhang, S.X. Mao, E.P. George, Q. Yu, R.O. Ritchie, Nanoscale origins of the damage tolerance of the high-entropy alloy CrMnFeCoNi, Nat. Commun. 6 (2015) 10143. doi:10.1038/ncomms10143.

[45] Y.-J. Hsu, W.-C. Chiang, J.-K. Wu, Corrosion behavior of FeCoNiCrCux high-entropy alloys in 3.5% sodium chloride solution, Mater. Chem. Phys. 92 (2005) 112–117. doi:10.1016/j.matchemphys.2005.01.001.

[46] M.-H. Tsai, J.-W. Yeh, High-Entropy Alloys: A Critical Review, Mater. Res. Lett. 2 (2014) 107–123. doi:10.1080/21663831.2014.912690.

[47] C.-J. Tong, M.-R. Chen, J.-W. Yeh, S.-J. Lin, S.-K. Chen, T.-T. Shun, S.-Y. Chang, Mechanical performance of the Al x CoCrCuFeNi high-entropy alloy system with multiprincipal elements, Metall. Mater. Trans. A. 36 (2005) 1263–1271. doi:10.1007/s11661-005-0218-9.

[48] N.N. Guo, L. Wang, L.S. Luo, X.Z. Li, Y.Q. Su, J.J. Guo, H.Z. Fu, Microstructure and mechanical properties of refractory MoNbHfZrTi high-entropy alloy, Mater. Des. 81 (2015) 87–94. doi:10.1016/j.matdes.2015.05.019.

[49] Y. Zhang, Y. Liu, Y.X. Li, X. Chen, H.W. Zhang, Microstructure and Mechanical Properties of a New Refractory HfNbSi0.5TiVZr High Entropy Alloy, Mater. Sci. Forum. 849 (2016) 76–84. doi:10.4028/www.scientific.net/MSF.849.76.

[50] C.-C. Juan, M.-H. Tsai, C.-W. Tsai, C.-M. Lin, W.-R. Wang, C.-C. Yang, S.-K. Chen, S.-J. Lin, J.-W. Yeh, Enhanced mechanical properties of HfMoTaTiZr and HfMoNbTaTiZr refractory high-entropy alloys, Intermetallics. 62 (2015) 76–83. doi:10.1016/j.intermet.2015.03.013.

[51] I. Gurappa, Characterization of different materials for corrosion resistance under simulated body fluid conditions, Mater. Charact. 49 (2002) 73–79. doi:10.1016/S1044-5803(02)00320-0.

[52] G. Popescu, B. Ghiban, C.A. Popescu, L. Rosu, R. Truscă, I. Carcea, V. Soare, D. Dumitrescu, I. Constantin, M.T. Olaru, B.A. Carlan, New TiZrNbTaFe high entropy alloy used for medical applications, IOP Conf. Ser. Mater. Sci. Eng. 400 (2018) 022049. doi:10.1088/1757-899X/400/2/022049.

[53] J. Li, X. Yang, R. Zhu, Y. Zhang, Corrosion and Serration Behaviors of TiZr0.5NbCr0.5VxMoy High Entropy Alloys in Aqueous Environments, Metals (Basel). 4 (2014) 597–608. doi:10.3390/met4040597.

[54] B. Ghiban, G. Popescu, C. Lazar, L. Rosu, I. Constantin, M. Olaru, B. Carlan, Corrosion Behaviour in Human Stimulation Media of a High Entropy Titan-Based Alloy, IOP Conf. Ser. Mater. Sci. Eng. 374 (2018) 012004. doi:10.1088/1757-899X/374/1/012004.

[55] A. Motallebzadeh, N.S. Peighambardoust, S. Sheikh, H. Murakami, S. Guo, D. Canadinc, Microstructural, mechanical and electrochemical characterization of TiZrTaHfNb and Ti1.5ZrTa0.5Hf0.5Nb0.5 refractory high-entropy alloys for biomedical applications, Intermetallics. 113 (2019) 106572. doi:10.1016/j.intermet.2019.106572.

[56] S.-P. Wang, J. Xu, (TiZrNbTa)-Mo high-entropy alloys: Dependence of microstructure and mechanical properties on Mo concentration and modeling of solid solution strengthening, Intermetallics. 95 (2018) 59–72. doi:10.1016/j.intermet.2018.01.017.

[57] K. Wang, The use of titanium for medical applications in the USA, Mater. Sci. Eng. A. 213 (1996) 134–137. doi:10.1016/0921-5093(96)10243-4.

[58] Y.-L. Zhou, M. Niinomi, T. Akahori, Changes in mechanical properties of Ti alloys in relation to alloying additions of Ta and Hf, Mater. Sci. Eng. A. 483–484 (2008) 153–156. doi:10.1016/j.msea.2006.09.173.

[59] P.L. Ferrandini, F.F. Cardoso, S.A. Souza, C.R. Afonso, R. Caram, Aging response of the Ti–35Nb–7Zr–5Ta and Ti–35Nb–7Ta alloys, J. Alloys Compd. 433 (2007) 207–210. doi:10.1016/j.jallcom.2006.06.094.

[60] N. Tüten, D. Canadinc, A. Motallebzadeh, B. Bal, Microstructure and tribological properties of TiTaHfNbZr high entropy alloy coatings deposited on Ti 6Al 4V substrates, Intermetallics. 105 (2019) 99–106. doi:10.1016/j.intermet.2018.11.015.

[61] A. Motallebzadeh, M.B. Yagci, E. Bedir, C.B. Aksoy, D. Canadinc, Mechanical Properties of TiTaHfNbZr High-Entropy Alloy Coatings Deposited on NiTi Shape Memory Alloy Substrates, Metall. Mater. Trans. A. 49 (2018) 1992–1997. doi:10.1007/s11661-018-4605-4.

[62] T. Kokubo, H. Takadama, How useful is SBF in predicting in vivo bone bioactivity?, Biomaterials. 27 (2006) 2907–15. doi:10.1016/j.biomaterials.2006.01.017.

[63] I. ASTM, ASTM G31-72: Standard Practice for Laboratory Immersion Corrosion Testing of Metals, Annu. B. ASTM Stand. (2004).

[64] Y. Shi, B. Yang, P. Liaw, Corrosion-Resistant High-Entropy Alloys: A Review, Metals (Basel). 7 (2017) 43. doi:10.3390/met7020043.

[65] Y.L. Chou, Y.C. Wang, J.W. Yeh, H.C. Shih, Pitting corrosion of the high-entropy alloy Co1.5CrFeNi1.5Ti0.5Mo0.1 in chloride-containing sulphate solutions, Corros. Sci. 52 (2010) 3481–3491. doi:10.1016/j.corsci.2010.06.025.

[66] P.C. Pistorius, G.T. Burstein, Growth of corrosion pits on stainless steel in chloride solution containing dilute sulphate, Inf. Manag. 23 (1992) 1885–1897.

[67] Y.Y. Chen, T. Duval, U.D. Hung, J.W. Yeh, H.C. Shih, Microstructure and electrochemical properties of high entropy alloys—a comparison with type-304 stainless steel, Corros. Sci. 47 (2005) 2257–2279. doi:10.1016/j.corsci.2004.11.008.

[68] B. Deng, Y. Jiang, J. Liao, Y. Hao, C. Zhong, J. Li, Dependence of critical pitting temperature on the concentration of sulphate ion in chloride-containing solutions, Appl. Surf. Sci. 253 (2007) 7369–7375. doi:10.1016/j.apsusc.2007.03.034.

[69] K.-K. Tseng, C.-C. Juan, S. Tso, H.-C. Chen, C.-W. Tsai, J.-W. Yeh, Effects of Mo, Nb, Ta, Ti, and Zr on Mechanical Properties of Equiatomic Hf-Mo-Nb-Ta-Ti-Zr Alloys, Entropy. 21 (2018) 15. doi:10.3390/e21010015.

[70] L. Lilensten, J.P. Couzinié, J. Bourgon, L. Perrière, G. Dirras, F. Prima, I. Guillot, Design and tensile properties of a bcc Ti-rich high-entropy alloy with transformation-induced plasticity, Mater. Res. Lett. 5 (2017) 110–116. doi:10.1080/21663831.2016.1221861.

[71] T. Niendorf, D. Canadinc, H.J. Maier, I. Karaman, G.G. Yapici, Microstructure–mechanical property relationships in ultrafine-grained NbZr, Acta Mater. 55 (2007) 6596–6605. doi:10.1016/j.actamat.2007.08.015.

[72] S. Tamilselvi, V. Raman, N. Rajendran, Corrosion behaviour of Ti–6Al–7Nb and Ti–6Al–4V ELI alloys in the simulated body fluid solution by electrochemical impedance spectroscopy, Electrochim. Acta. 52 (2006) 839–846. doi:10.1016/j.electacta.2006.06.018.

[73] F. Toumelin-Chemla, F. Rouelle, G. Burdairon, Corrosive properties of fluoride-containing odontologic gels against titanium, J. Dent. 24 (1996) 109–115. doi:10.1016/0300-5712(95)00033-X.

[74] B. Uzer, O. Birer, D. Canadinc, Investigation of the Dissolution–Reformation Cycle of the Passive Oxide Layer on NiTi Orthodontic Archwires, Shape Mem. Superelasticity. 3 (2017) 264–273. doi:10.1007/s40830-017-0114-3.

[75] S.M. Toker, D. Canadinc, Evaluation of the biocompatibility of NiTi dental wires: A comparison of laboratory experiments and clinical conditions, Mater. Sci. Eng. C. 40 (2014) 142–147. doi:10.1016/j.msec.2014.03.060.

[76] C.L. Qin, W. Zhang, Q.S. Zhang, K. Asami, A. Inoue, Chemical characteristics of the passive surface films formed on newly developed Cu–Zr–Ag–Al bulk metallic glasses, J. Mater. Res. 23 (2008) 2091–2098. doi:10.1557/JMR.2008.0284.

[77] M. V. Popa, E. Vasilescu, P. Drob, C. Vasilescu, S.I. Drob, D. Mareci, J.C.M. Rosca, Corrosion resistance improvement of titanium base alloys, Quim. Nova. 33 (2010) 1892–1896. doi:10.1590/S0100-40422010000900014.

[78] J.F. Watts, J. Wolstenholme, Electron Spectroscopy: Some Basic Concepts, in: An Introd. to Surf. Anal. by XPS AES, John Wiley & Sons, Ltd, Chichester, UK, 2005: pp. 1–15. doi:10.1002/0470867930.ch1.

[79] J. Jayaraj, D. Nanda Gopala Krishna, C. Mallika, U. Kamachi Mudali, Electrochemical Studies and XPS Analysis of the Surface of Zirconium-702 in Concentrated Nitric Acid With and Without Fluoride Ions, Trans. Indian Inst. Met. 71 (2018) 521–531. doi:10.1007/s12666-017-1165-z.

[80] C. Morant, J.M. Sanz, L. Galán, L. Soriano, F. Rueda, An XPS study of the interaction of oxygen with zirconium, Surf. Sci. 218 (1989) 331–345. doi:10.1016/0039-6028(89)90156-8.

[81] H.J.M. Bosman, A.P. Pijpers, A.W.M.A. Jaspers, An X-Ray Photoelectron Spectroscopy Study of the Acidity of SiO2–ZrO2Mixed Oxides, J. Catal. 161 (1996) 551–559. doi:10.1006/jcat.1996.0217.

[82] D.A. Stephenson, N.J. Binkowski, X-ray photoelectron spectroscopy of silica in theory and experiment, J. Non. Cryst. Solids. 22 (1976) 399–421. doi:10.1016/0022-3093(76)90069-7.

[83] M.S. Amrutha, M.T. Rao, S. Ramanathan, Mechanistic Analysis of Anodic Dissolution of Zr in Acidic Fluoride Media, J. Electrochem. Soc. 165 (2018) C162–C170. doi:10.1149/2.0851803jes.

[84] D. Majumdar, D. Chatterjee, X-ray photoelectron spectroscopic studies on yttria, zirconia, and yttria-stabilized zirconia, J. Appl. Phys. 70 (1991) 988–992. doi:10.1063/1.349611.

[85] Z. Li, Y. Liu, W. Kwapinski, J.J. Leahy, ZrO2-modified TiO2 nanorod composite: Hydrothermal synthesis, characterization and application in esterification of organic acid, Mater. Chem. Phys. 145 (2014) 82–89. doi:10.1016/j.matchemphys.2014.01.037.

[86] A. Juma, I. Oja Acik, A.T. Oluwabi, A. Mere, V. Mikli, M. Danilson, M. Krunks, Zirconium doped TiO 2 thin films deposited by chemical spray pyrolysis, Appl. Surf. Sci. 387 (2016) 539–545. doi:10.1016/j.apsusc.2016.06.093.

Chapter 3:

CORROSION BEHAVIOR OF COCRMO MEDIUM ENTROPY ALLOYS DESIGNED FOR MEDICAL IMPLANTS

3.1 Introduction

Metals are widely preferred materials for the use of implants to repair or support damaged bone tissue due to their high strength and toughness compared to ceramics and polymers, and their high elastic modulus with ductility increases the load-bearing capacity [1–3]. On the other hand, the highly corrosive environment of the human body deteriorates the metallic implants over time and causes the release of metallic ions into the body environment. Therefore, corrosion is one of the main problems in metallic materials since the ion release from an implant into a body environment can cause adverse biological responses and implant failures [2–5].

Titanium and its alloys, stainless steel and CoCrMo alloys have wide applications as biomedical implants for orthodontic and orthopedic purposes such as dental skeletal structures, screws, hip and knee implants [6]. However, the metallic implantable materials include metals such as Ni, V, Cr, which can cause cytotoxic effects on the host body. On the other hand, their ability to form a passive layer facilitates corrosion resistance against the body environment and reduces the amount of ion release into the body [6]. Therefore, the biocompatibility of a metallic material is mainly established by the passive oxide layer formation on the metallic surface [7].

However, the protective layer exposed to corrosion deteriorates over time, mainly based on the degree of corrosion which is affected by some factors such as the thickness of the passive layer, the composition of an implant, mechanical stresses, and chemical composition of the surrounding environment [6,7]. Thus, corrosion exists with ion release from the implantable material to the human body, and it is a significant point that a passive layer on the implant surface can reduce or eliminate ion release from the implant by acting as a barrier between the implant and an abrasive body environment [8].

Moreover, the chemical composition of the surrounding environment influences the quantity of ion release such that the changes in pH strongly relate to the amount of ion release from the implant [9]. Throughout the life of the patient, the pH value of

biological environments can change for various causes such as an infection, surgery, healing process, and metabolic activities [10,11]. In particular, the pH of oral environment may vary easily as bacterial activity in dental plaques lowers pH and alkaline or acidic food consumption negatively affects on pH of oral environment [9,11], and in a particular case, that pathological diseases can lead extremely acidic environment with pH = 2.0-3.0 in oral cavity [7,12].

CoCrMo alloys have popular applications as orthopedic and orthodontic implant materials, such as screws and pins, owing to their high biocompatibility, high strength, high creep resistance, and lower elastic modulus with addition to high corrosion resistance [2,4,8,14–16]. Specifically, CoCrMo alloys are known for their excellent corrosion resistance and biocompatibility properties making them advantageous in biomedical applications. Co, Cr, and Mo oxides spontaneously form a passive layer on the CoCrMo surface, and the passive layer formation protects the implant against the corrosive environment and facilitates biocompatibility of the implant [13,14].

The previous studies on the passivation behavior and corrosion resistance of CoCrMo under different simulated body conditions have mainly showed that passive layer formation on CoCrMo alloy establishes excellent corrosion resistance [2,6,13,14,17]. However, it has been observed that the pH of the environment has significant effects on corrosion behavior, such that low pH values increase the corrosion rate as well as passivation layer solubility [2,9].

Besides, many studies confirm that the amount of released ion from CoCrMo is based on a complex system that does not depend on the weight percentage of the constituents[2,13,15]. Primarily, Co-release has been observed in higher amounts due to the selective dissolution of Co from CoCrMo [15,18]. In addition, the least amount of ions released from CoCrMo was observed to be Cr, such that the chemical composition of the passive layer on CoCrMo mainly composed of Cr oxides [2,18]. The chromium-like passivity eliminates high Cr release from the implant, and therefore Cr concentration in a body maintains stable or with a negligible amount of ion compared to Co and Mo release into the body [2,13,15].

Consequently, CoCrMo alloys have attracted attention as implantable materials due to their excellent corrosion resistance and passivation behavior, which can reduce the effects of corrosion, which is the main problem in metallic biomaterials. This study investigates on the corrosion behavior of CoCrMo against an extremely acidic oral

environment (pH=2.3) and simulated body fluid conditions (pH=7.4) at 37˚C in order to evaluate the biocompatibility of CoCrMo under the corrosive body environment.

3.2 Experimental Procedures

The study was performed with CoCrMo alloy with a chemical composition of 27 wt.% Cr, 6 wt.% Mo, and balance Co (wt.%), with 99.9 wt.% purity. The disc-shaped CoCrMo alloy has a diameter of 50.1 mm and a thickness of 6.1 mm, and the disc-shaped alloy was cut by electrical discharge machining (EDM) to obtain 10 mm x 5 mm x 1 mm bulk samples. The sample surfaces were mechanically ground using SiC emery papers with grain sizes ranging from 106 to 2.5 μm to eliminate any contaminations on the samples (with only negligible change in the thickness of the samples). The samples were polished with 0.30 μm alumina slurry until the surfaces reach to mirror-like appearance, then the samples were cleaned in an ultrasonic water bath with ethanol and rinsed with de-ionized water. After the sample preparation, the bulk samples were statically immersed into AS (pH=2.3) and SBF (pH=7.4) for 1, 7, 14 and 28 days, and the elemental composition of SBF and AS was shown in Table 3-1 [19]. The immersion test was carried out at a constant temperature of 37 ^{0}C in an electronically controlled water bath to simulate body temperature. The bulk samples were transferred to sealed tubes which were filled with AS and SBF according to a volume per surface area ratio of 20 mL/cm^2 [20]. Mass change in each sample was recorded to observe mass gain or loss after the immersion test. Microstructural characterization of CoCrMo alloy was done by X-ray diffraction (XRD) method on a Bruker D2 Advanced X-ray diffractometer. The incidence angle was kept at about 5° with a Cu-Kα radiation source which was operated at 30 kV and 10 mA, and the acquisition angle ranged from 5° to 90° with 0.02° increment.

The surface morphology of the bulk samples has been analyzed by a Zeiss Ultra Plus field emission scanning electron microscope (SEM) before and after the immersion test. Elemental compositions of the immersion solutions after the immersion test were detected by an Agilent 7700x inductively coupled plasma mass spectrometer (ICP-MS) to observe ion release from the immersed samples for the following 1,7,14,28 days.

Table 3-1: Composition of the AS and SBF utilized in the static immersion experiments.

Solution	Ingredients	Amount (g/L)	pH
AS	NaCl	0.4	2.3
	KCl	0.4	
	$CaCl_2 . 2H_2o$	0.906	
	$NaH_2PO_4.2H_2O$	0.69	
	$Na_2S.9H_2O$	0.005	
	Urea	1	
SBF	NaCl	8.036	7.4
	$NaHCO_3$	0.352	
	KCL	0.225	
	$K_2HPO_4.3H_2O$	0.23	
	$MgCl_2.6H_2O$	0.311	
	1M HCL	40 mL	
	$CaCl_2 . 2H_2o$	0.293	
	Na_2SO_4	0.072	
	TRIS	6.063	
	1M HCL	0.2 ml	

3.3 Results and Discussion

The surface characteristics of the bulk CoCrMo alloys were investigated before and after the immersion test by SEM in order to observe degradations on the surfaces following their immersion in AS and SBF for 1, 7, 14, 28 days. As illustrated in Figure 3-1, there is no significant difference in the surface appearance of CoCrMo samples before and after the immersion tests that CoCrMo had a smooth surface and no localized corrosion in both of AS and SBF after 28 days immersion. On the other hand, ICP-MS results indicate a significant amount of ionization from the CoCrMo samples during the immersion tests in AS and SBF. According to ICP-MS results that are shown in Figure 3-2, the rate of increase in ion release is higher in the early stages of the immersion

tests. As illustrated in Figure 3-2, the highest amount of Co, Cr, and Mo release was observed at the end of the first day in AS and SBF, and the quantity of released Co, Cr and Mo increases with a slower rate after the 7^{th} day in AS and SBF.

Particularly, as illustrated in Figure 3-2 the quantity of released Co ions from CoCrMo is the highest in AS and SBF while the lowest quantity of released ions is Cr after the immersion tests in AS and SBF that can be attributed to the higher solubility of an oxide layer of Co [2]. Besides, negligible change in the amount of Cr release from CoCrMo has been observed during the immersion tests in AS and SBF (Figure 3-2 (b)). The negligible change in the amount of Cr release from CoCrMo to AS and SBF in the following days suggests chromium-like passivity on CoCrMo surface that the oxide film of Cr governs the total ion release in AS and SBF [2]. On the other hand, as can be seen in Figure 3-2 that the less amount of Cr release has occurred in SBF than AS, which can be attributed to the higher passivation ability of CoCrMo in SBF. Moreover, according to ICP-MS results (Figure 3-2), CoCrMo alloy exhibits complex ionization systems without depending on the quantity of elemental composition. To illustrate, Cr is the second most plentiful constituent in CoCrMo, however, Cr dissolved from CoCrMo in the least amount. Consequently, Co preferentially released from CoCrMo and the mechanism behind the amount of ion release is controlled by a more complex system [2,13,15,21,22].

Moreover, the amount of ion release has been affected by the pH of the solution. According to ICP-MS results (Figure 3-2), the total ion release is much higher in AS than in SBF owing to the low pH of AS (Figure 3-2 (a)(b)(c)). Illustrated in Figure 3-2 that Co and Cr have almost 4 and 32 times more ion release in AS than SBF, while the amount of Mo release in AS (pH=2.3) and SBF (pH=7.4) has a slight difference. The amount of Mo ion release is not significantly affected by low pH as opposite to Co and Cr since Mo oxides are more stable in acidic solutions as discussed in the literature [2,23].

On the other hand, some white particles have been observed on the bulk surface of CoCrMo after 28 days in SBF (in Figure 3-1 (d)). The white particles were analyzed by EDX as can be seen in Figure 3-3 that CaO precipitates were detected on the CoCrMo surface after 28 days in SBF. Besides, Ca^{2+} incorporation on the bulk CoCrMo surface supports bone-like hydroxyapatite formation and osseointegration process by facilitating the interaction between the implant and bone tissue [24–26]. Addition to Ca^{2+}

concentration of SBF, some ions in SBF such as HPO_4^{2-} and CO_3^{2-} enhance apatite deposition on CoCrMo [24,27,28].

Moreover, hydroxyapatite formation has been observed by the results obtained from the XPS analysis. As can be seen in Figure 3-4, the XPS results indicate to hydroxyapatite depositions and oxide layer formation on the CoCrMo bulk samples after the immersion tests in AS and SBF for the following 28 days. The XPS spectrum of O1 s shows OH^-, O^{2-} and H_2O formations on the CoCrMo samples in AS and SBF after 28-days (Figure 3-4(a)(b)). Besides, it is illustrated in Figure 3-4 (c)(d) that hydroxyapatite formation on CoCrMo has been supported by the peaks of Ca 2p3/2 and 2p1/2, and 350.5 eV binding energy of $CaCO_3$, and P 2d peaks that are located at the average of 133.5 eV binding energy as obtained by the XPS results [29].

Moreover, Figure 3-5 illustrates the peaks of Cr 2d that are located at 573.5 eV, 574.6 eV, 576.8 eV for AS; and Figure 3-6 shows 573.7 eV, 574.6 eV, 576.2 eV binding energies for SBF, that the binding energies represent metallic Cr, carbide-like formations (C-Cr) and Cr^{3+} oxide respectively [13,22,30,31] for AS and SBF. Moreover, XPS results revealed that the passive layer on CoCrMo consists of Mo oxides in AS and SBF (Figure 3-5 and Figure 3-6). The peaks of Mo^0 and Mo^{4+} oxides are located at 227.3 eV, 230.8eV and 230.0 eV binding energies respectively for AS (Figure 3-5(b)) , and Mo^0 with 227.2 eV, Mo^{4+} with 230.2 eV, Mo^{6+} with 233.2 eV binding energies exist for the CoCrMo in SBF (Figure 3-6 (c)) [13,22,30]. On the other hand, Co-oxides have been observed for the samples immersed in SBF as illustrated in Figure 3-6 (c).

In other words, AS and SBF create a convenient environment for hosting both the CoCrMo implant and the human tissue with facilitating the osseointegration process by bone-like apatite formation and passive oxide layer. Moreover, the mass of the CoCrMo samples increases with time despite the loss of ions from CoCrMo as illustrated in Figure 3-4. Therefore, it can be said that the passive layer and hydroxyapatite formations cause mass gain after the immersion tests in AS and SBF.

Overall, CoCrMo alloy exhibits high biocompatibility and shows promising results in order to use in dental and orthopedic applications. The passive layer with bone-like appetite formations on CoCrMo protects the CoCrMo alloy against the corrosive environment, even in the extremely acidic environment of AS without significant degradation. It is noteworthy that hydroxyapatite formation was detected after 28 days

of immersion in AS and SBF, such that CoCrMo alloy can able to enhance the binding between CoCrMo implant and a human tissue by osseointegration process. The findings indicate the high potential of CoCrMo which provides excellent corrosion resistance and biocompatibility.

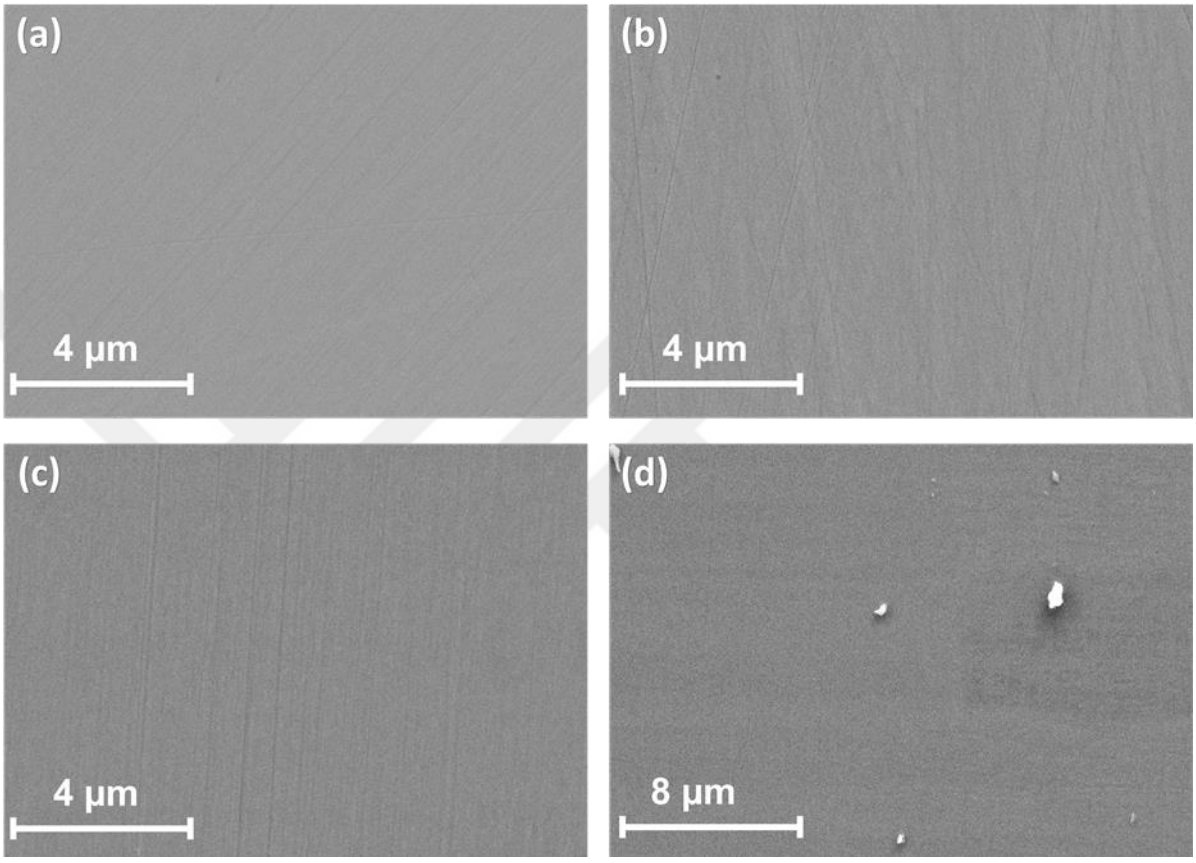

Figure 3-1: The SEM images of (a) the untested CoCrMo, (b) the bulk CoCrMo sample surface following immersion in AS for 28 days, (c) (d) the bulk CoCrMo sample surfaces following immersion in SBF for 28 days

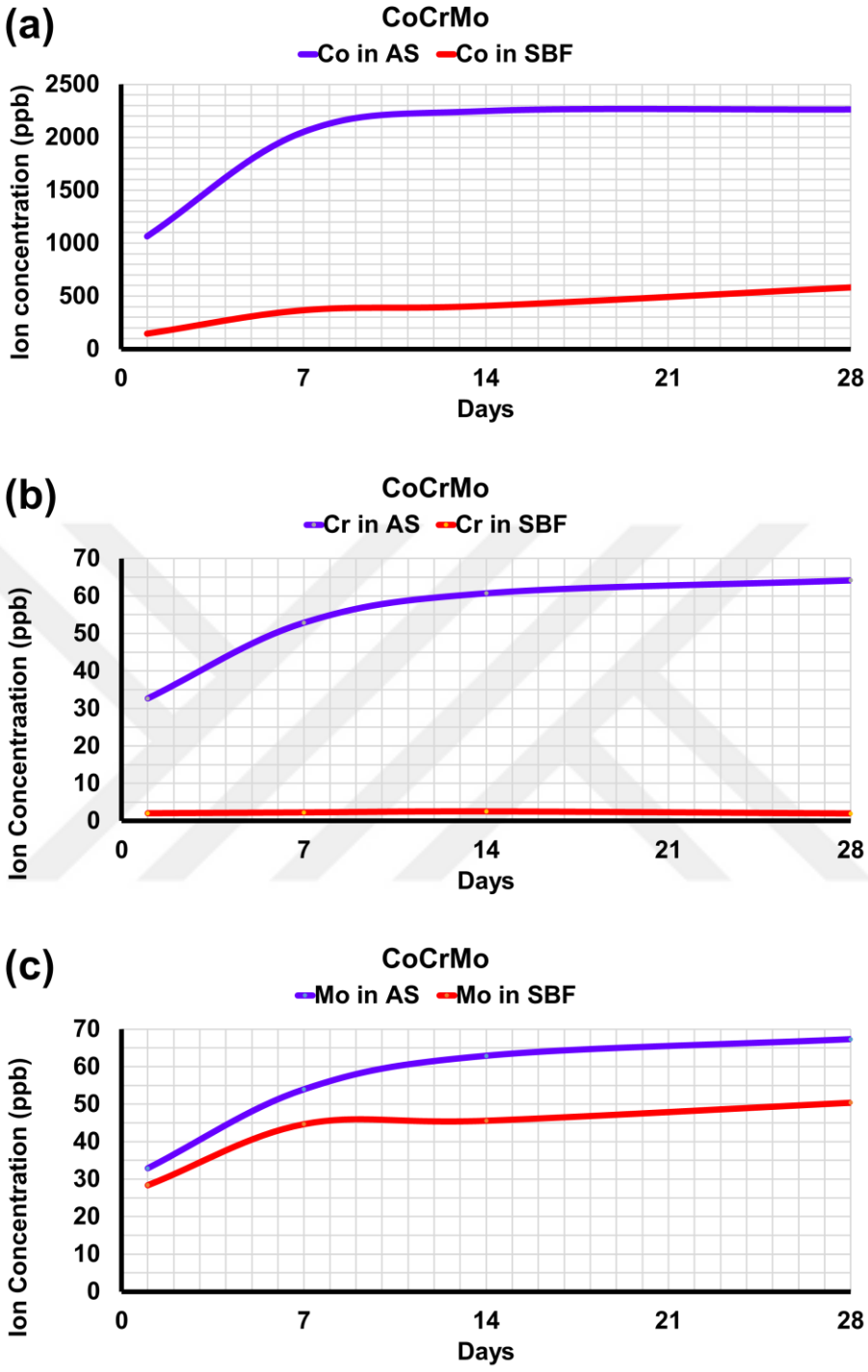

Figure 3-2: (a) The quantity of released Co ions from CoCrMo, (b) The quantity of released Cr ions from CoCrMo, (c) The quantity of released Mo ions from CoCrMo

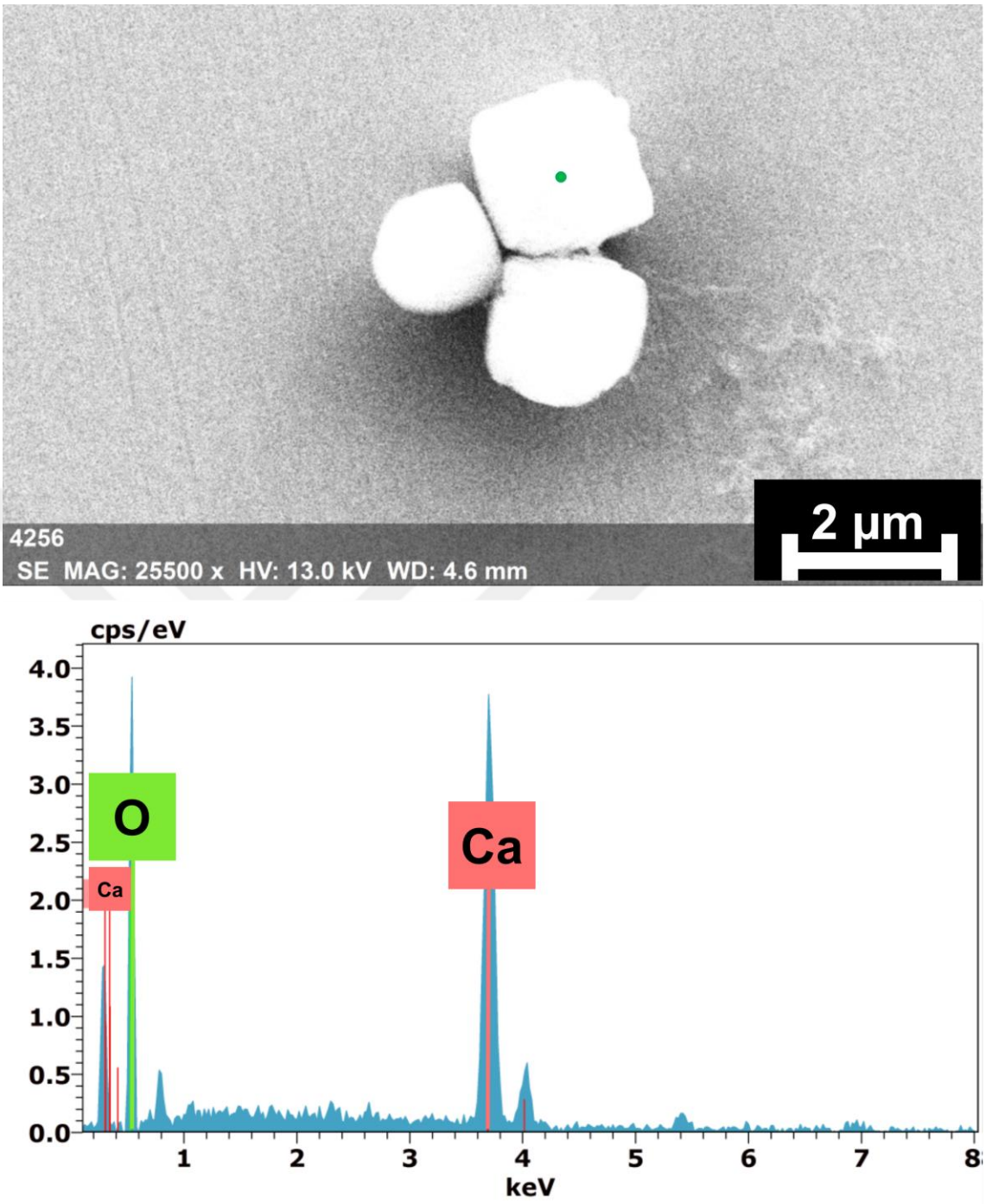

Figure 3-3:(a) CaO on CoCrMo surface, and (b) EDX analysis of CaO in (a).

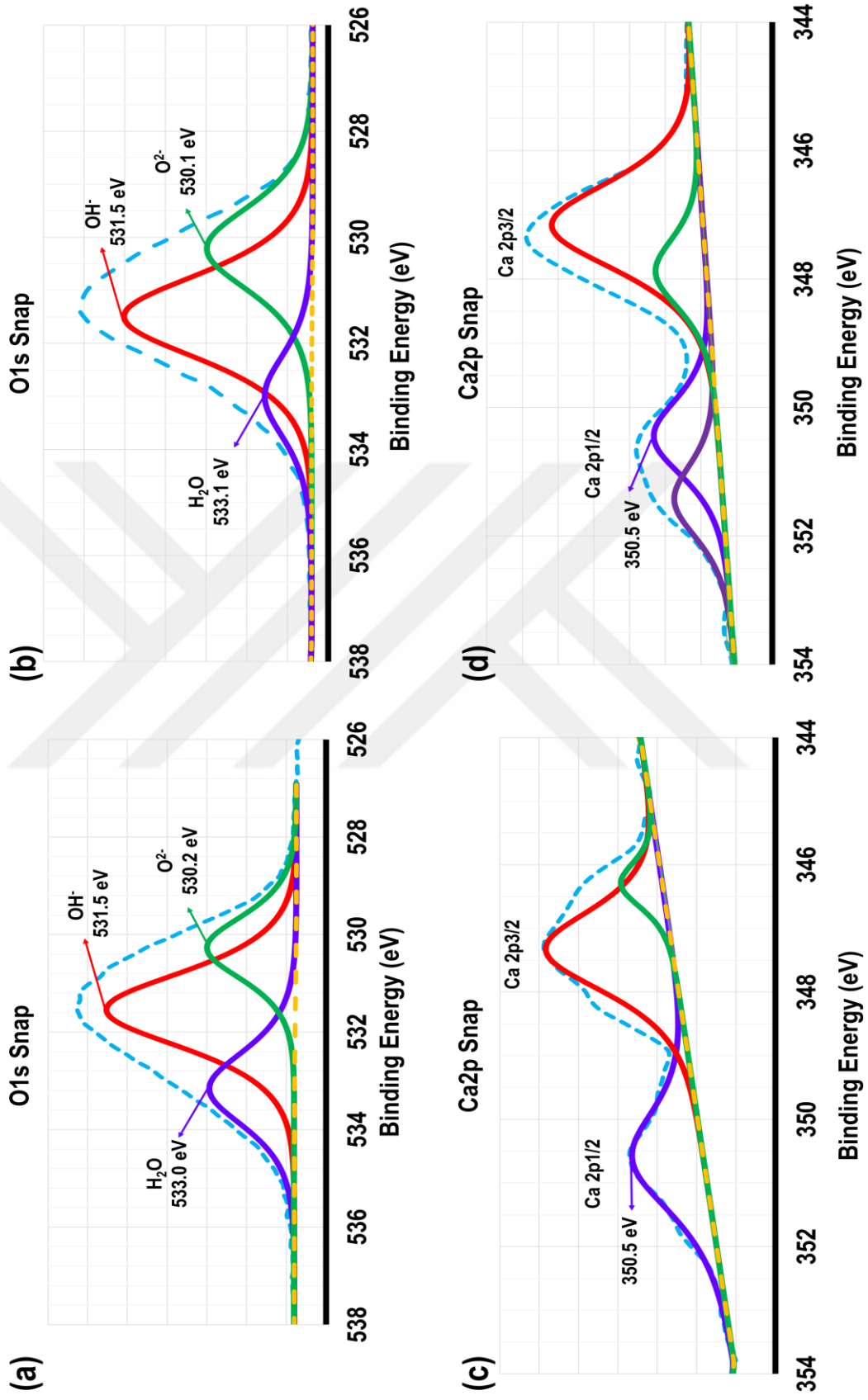

Figure 3-4 XPS depth profiles of; (a)(c) CoCrMo in AS for following 28-day immersion, (b) (c) CoCrMo in SBF for following 28-day immersion

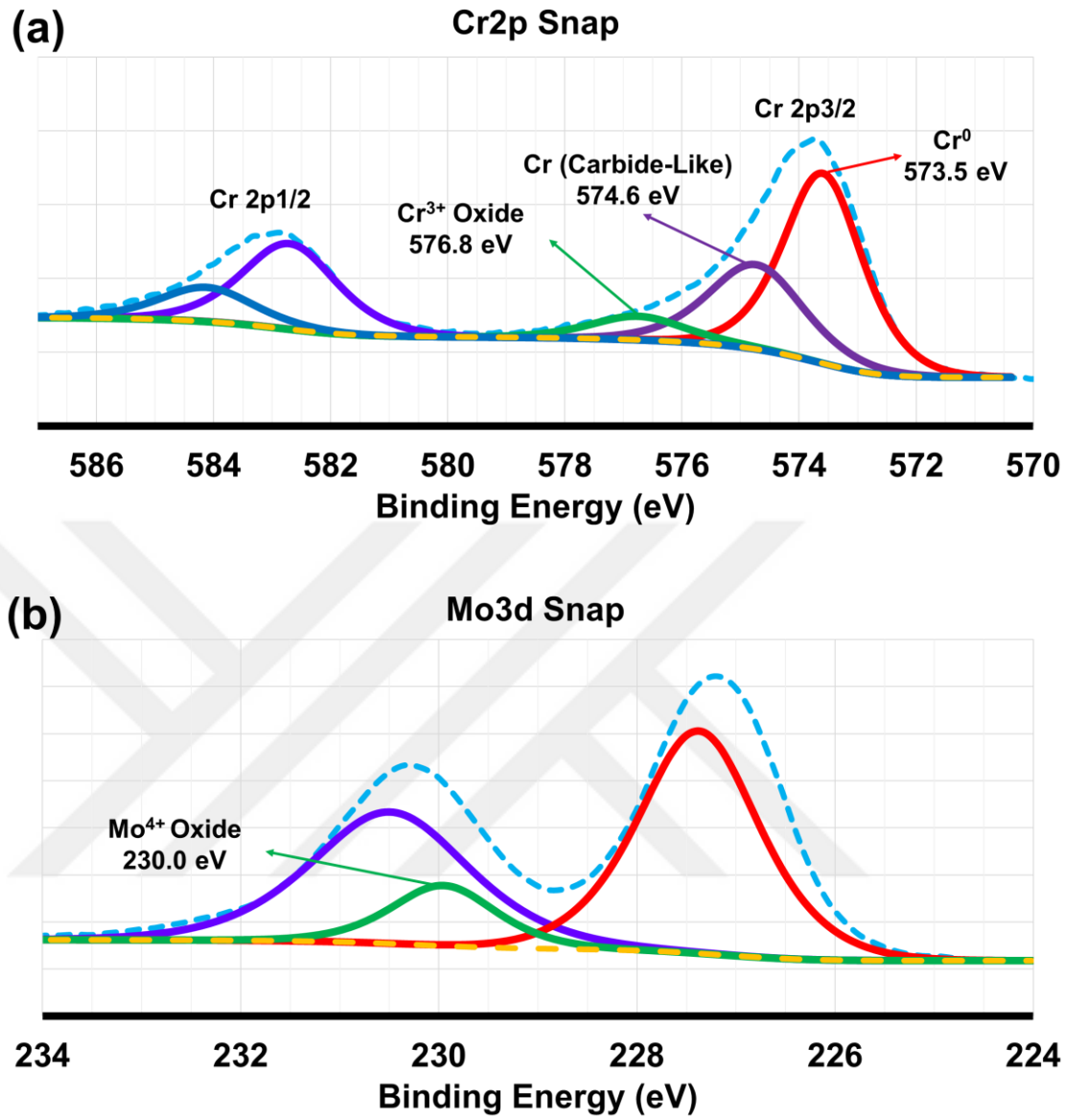

Figure 3-5: XPS depth profile of CoCrMo in AS after 28-days immersion test; (a) Cr2p Profile, (b) Mo3d Profile

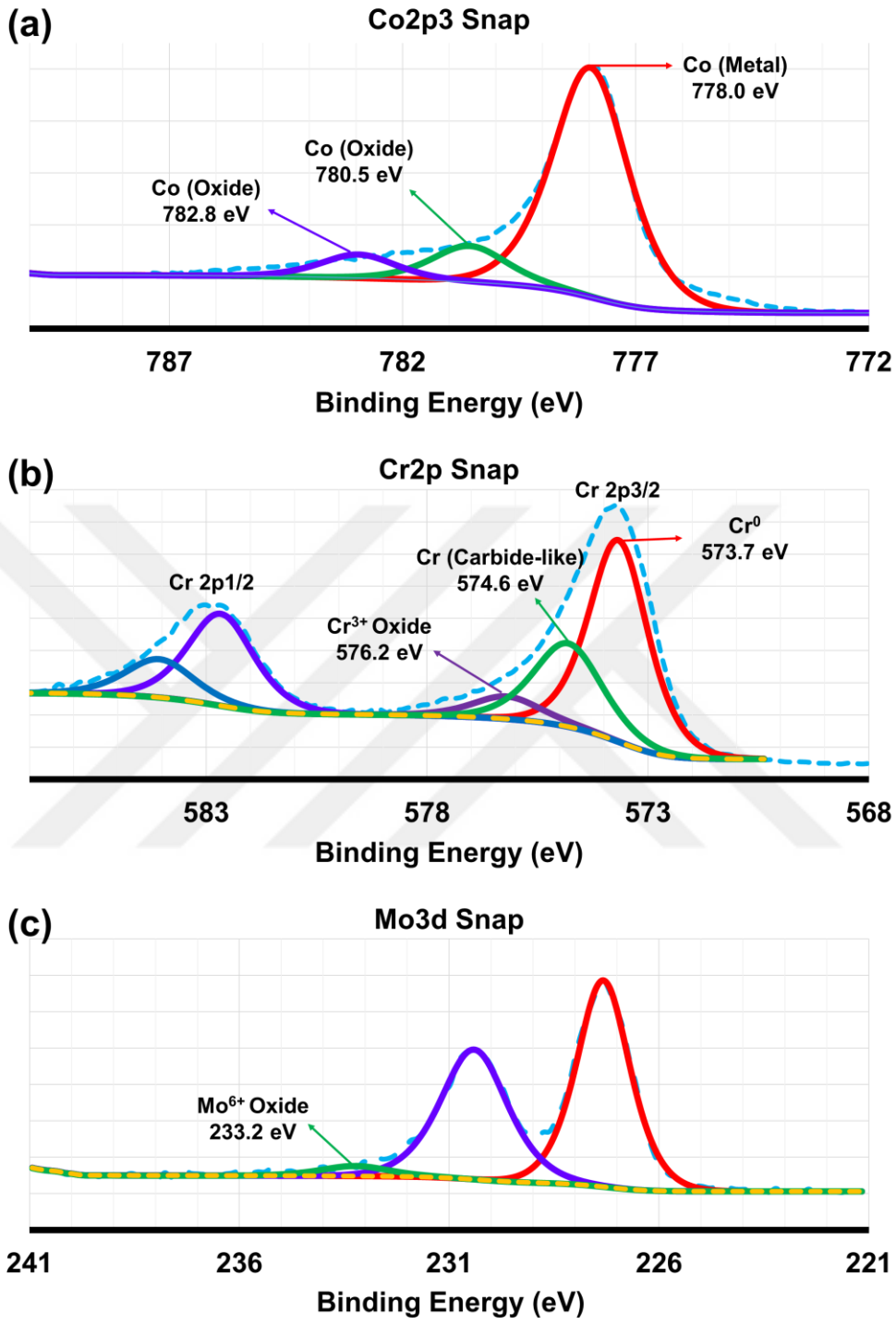

Figure 3-6: XPS depth profile of CoCrMo in SBF after 28-days immersion test; (a) Co2p3 Profile, (b) Cr2p Profile , (c) Mo3d Profile

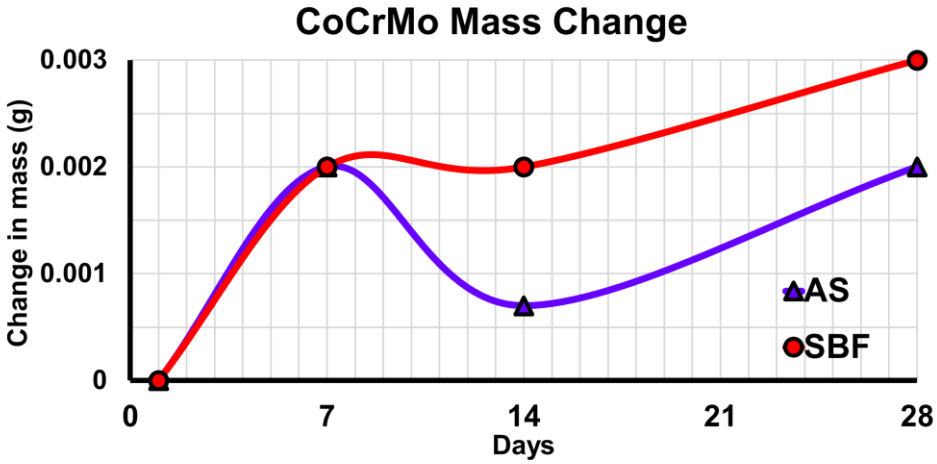

Figure 3-7: Mass Change in CoCrMo during the immersion tests in AS and SBF

3.4 Conclusions

The corrosion behavior of CoCrMo alloy was studied by static immersion experiments in artificial saliva (AS) and simulated body fluid (SBF) at 37˚C for 1, 7, 14 and 28 days. Overall, CoCrMo shows excellent biocompatibility in both AS and SBF. On the other hand, CoCrMo alloy showed better corrosion resistance in SBF, such that the lower quantity of ion release was observed, and the low pH of AS increases the amount of ion release. Besides, it can be concluded that the chromium-like passivation layer on CoCrMo protects the implant from the corrosive environment of AS and SBF, and less ionization from SBF can be attributed to higher pH and thicker chromium-like passivation layer than that on AS.

Consequently, CoCrMo alloy is an advantageous metallic material in biomedical applications due to excellent corrosion resistance and the ability to form a passive layer and hydroxyapatites. However, ionization from CoCrMo alloy in very acidic environments (pH=2.0-3.0) is so high, therefore the corrosion resistance of CoCrMo in low pH solutions should be improved in further studies.

3.5 References

[1] M.P. Staiger, A.M. Pietak, J. Huadmai, G. Dias, Magnesium and its alloys as orthopedic biomaterials: A review, Biomaterials. 27 (2006) 1728–1734. doi:10.1016/j.biomaterials.2005.10.003.

[2] M. Metikoš-Huković, Z. Pilić, R. Babić, D. Omanović, Influence of alloying elements on the corrosion stability of CoCrMo implant alloy in Hank's solution, Acta Biomater. 2 (2006) 693–700. doi:10.1016/j.actbio.2006.06.002.

[3] U. Kamachimudali, T.M. Sridhar, B. Raj, Corrosion of bio implants, Sadhana. 28 (2003) 601–637. doi:10.1007/BF02706450.

[4] M.Z. Ibrahim, A.A.D. Sarhan, F. Yusuf, M. Hamdi, Biomedical materials and techniques to improve the tribological, mechanical and biomedical properties of orthopedic implants – A review article, J. Alloys Compd. 714 (2017) 636–667. doi:10.1016/j.jallcom.2017.04.231.

[5] Y. Okazaki, E. Gotoh, Comparison of metal release from various metallic biomaterials in vitro, Biomaterials. 26 (2005) 11–21. doi:10.1016/j.biomaterials.2004.02.005.

[6] N. Espallargas, C. Torres, A.I. Muñoz, A metal ion release study of CoCrMo exposed to corrosion and tribocorrosion conditions in simulated body fluids, Wear. 332–333 (2015) 669–678. doi:10.1016/j.wear.2014.12.030.

[7] I.D. Dimić, I.L. Cvijović-Alagić, I.T. Kostić, A.A. Perić-Grujić, M.P. Rakin, S.S. Putić, B.M. Bugarski, OtpuŠtanje metalnih jona iz biokompatibilne legure kobalta, Chem. Ind. Chem. Eng. Q. 20 (2014) 571–577. doi:10.2298/CICEQ130813039D.

[8] U. Türkan, O. Öztürk, A.E. Eroğlu, Metal ion release from TiN coated CoCrMo orthopedic implant material, Surf. Coatings Technol. 200 (2006) 5020–5027. doi:10.1016/j.surfcoat.2005.05.005.

[9] N. Rinčić, I. Baučić, S. Miko, M. Papić, E. Prohić, Corrosion behaviour of the Co-Cr-Mo dental alloy in solutions of different composition and different pH values, Coll. Antropol. 27 (2003) 99–106.

[10] C. Valero Vidal, A. Igual Muñoz, Effect of physico-chemical properties of simulated body fluids on the electrochemical behaviour of CoCrMo alloy, Electrochim. Acta. 56 (2011) 8239–8248. doi:10.1016/j.electacta.2011.06.068.

[11] I. Mutlu, E. Oktay, Characterization of 17-4 PH stainless steel foam for biomedical applications in simulated body fluid and artificial saliva environments, Mater. Sci. Eng. C. 33 (2013) 1125–1131. doi:10.1016/j.msec.2012.12.004.

[12] M. Hurlbutt, B. Novy, D. Young, Dental caries: A pH-mediated disease., J Calif Dent Hyg Assoc. 25 (2010) 9–15.

[13] A.W.E. Hodgson, S. Kurz, S. Virtanen, V. Fervel, C.-O.A. Olsson, S. Mischler, Passive and transpassive behaviour of CoCrMo in simulated biological solutions, Electrochim. Acta. 49 (2004) 2167–2178. doi:10.1016/j.electacta.2003.12.043.

[14] F. Contu, B. Elsener, H. Böhni, Corrosion behaviour of CoCrMo implant alloy during fretting in bovine serum, Corros. Sci. 47 (2005) 1863–1875. doi:10.1016/j.corsci.2004.09.003.

[15] Z. Guo, X. Pang, Y. Yan, K. Gao, A.A. Volinsky, T.-Y. Zhang, CoCrMo alloy for orthopedic implant application enhanced corrosion and tribocorrosion properties by nitrogen ion implantation, Appl. Surf. Sci. 347 (2015) 23–34. doi:10.1016/j.apsusc.2015.04.054.

[16] M. Long, H.. Rack, Titanium alloys in total joint replacement—a materials science perspective, Biomaterials. 19 (1998) 1621–1639. doi:10.1016/S0142-9612(97)00146-4.

[17] C. Valero Vidal, A. Igual Muñoz, Effect of physico-chemical properties of simulated body fluids on the electrochemical behaviour of CoCrMo alloy, Electrochim. Acta. 56 (2011) 8239–8248. doi:10.1016/J.ELECTACTA.2011.06.068.

[18] X. Yang, N. Xiang, B. Wei, Effect of fluoride content on ion release from cast and selective laser melting-processed Co-Cr-Mo alloys, J. Prosthet. Dent. 112 (2014) 1212–1216. doi:10.1016/j.prosdent.2013.12.022.

[19] T. Kokubo, H. Takadama, How useful is SBF in predicting in vivo bone bioactivity?, Biomaterials. 27 (2006) 2907–15. doi:10.1016/j.biomaterials.2006.01.017.

[20] I. ASTM, ASTM G31-72: Standard Practice for Laboratory Immersion Corrosion Testing of Metals, Annu. B. ASTM Stand. (2004).

[21] T. Hanawa, Metal ion release from metal implants, Mater. Sci. Eng. C. 24 (2004) 745–752. doi:10.1016/j.msec.2004.08.018.

[22] T. Hanawa, S. Hiromoto, K. Asami, Characterization of the surface oxide film of a Co-Cr-Mo alloy after being located in quasi-biological environments using XPS, Appl. Surf. Sci. 183 (2001) 68–75. doi:10.1016/S0169-4332(01)00551-7.

[23] W.A. Badawy, F.M. Al-Kharafi, Corrosion and passivation behaviors of molybdenum in aqueous solutions of different pH, Electrochim. Acta. (1998). doi:10.1016/S0013-4686(98)00180-7.

[24] T. Miyazaki, H.-M. Kim, T. Kokubo, C. Ohtsuki, H. Kato, T. Nakamura, Mechanism of bonelike apatite formation on bioactive tantalum metal in a simulated body fluid, Biomaterials. 23 (2002) 827–832. doi:10.1016/S0142-9612(01)00188-0.

[25] J.W. Park, K.B. Park, J.Y. Suh, Effects of calcium ion incorporation on bone healing of Ti6Al4V alloy implants in rabbit tibiae, Biomaterials. 28 (2007) 3306–3313. doi:10.1016/j.biomaterials.2007.04.007.

[26] R. Godley, D. Starosvetsky, I. Gotman, Bonelike apatite formation on niobium metal treated in aqueous NaOH, J. Mater. Sci. Mater. Med. 15 (2004) 1073–1077. doi:10.1023/B:JMSM.0000046388.07961.81.

[27] X. Zhang, Z.M. Xiu, X.W. Li, Preparation and Characterization of (HAp/SiO2)/Ti Biocomposites, Adv. Mater. Res. 217–218 (2011) 88–92. doi:10.4028/www.scientific.net/AMR.217-218.88.

[28] Charlena, S.G. Sukaryo, M. Fajar, Hidroxyapatite Coating on CoCrMo Alloy Titanium Nitride Coated Using Biomimetic Method, J. Phys. Conf. Ser. 776 (2016) 012056. doi:10.1088/1742-6596/776/1/012056.

[29] E. Pecheva, L. Pramatarova, A. Toth, T. Hikov, D. Fingarova, S. Stavrev, E. Iacob, L. Vanzetti, Effect of nanodiamond particles incorporation in hydroxyapatite coatings, ECS Trans. 25 (2009) 403–410. doi:10.1149/1.3204431.

[30] S. Karimi, T. Nickchi, A.M. Alfantazi, Long-term corrosion investigation of AISI 316L, Co-28Cr-6Mo, and Ti-6Al-4V alloys in simulated body solutions, Appl. Surf. Sci. 258 (2012) 6087–6096. doi:10.1016/j.apsusc.2012.03.008.

[31] E. Bertero, C. V. Manzano, E. Pellicer, J. Sort, R.M. Ulfig, S. Mischler, J. Michler, L. Philippe, “Green” Cr(III)-glycine electrolyte for the production of FeCrNi coatings: Electrodeposition mechanisms and role of by-products in terms of coating composition and microstructure, RSC Adv. 9 (2019) 25762–25775. doi:10.1039/c9ra04262h.

Chapter 4:

FRACTURE BEHAVIOR OF NOVEL BIOMEDICAL TITAHF-BASED HIGH ENTROPY ALLOYS UNDER IMPACT LOADING

4.1 Introduction

Metallic materials are extensively used in biomedical applications to support failed tissue in orthodontic and orthopedic applications owing to their superior mechanical properties [1–4]. As compared to other biomedical metallic materials, such as stainless steel and Co-based alloys, Ti-based alloys have attracted considerable attention owing to their excellent biocompatibility combined with high strength, good corrosion and wear resistance, and relatively lower elastic modulus [2,5–7]. The Ti-6Al-4V alloy has been used as a common Ti-based biomedical material, however some concerns on toxicity and mechanical biocompatibility have led to the search for alternative materials [8–10]. In particular, Ti-6Al-4V contains V and Al that can damage the nervous system if released into blood stream in long term applications, and elastic modulus mismatch between the bone and the Ti-6Al-4V implant can lead to tissue loss, implant loosening and prostheses failure [3,5,11–17]. Therefore, nontoxic alloys with a low elastic modulus have been developed to obtain enhanced biocompatibility, including Ti-6Al-7Nb, Ti-15Mo-3Nb, Ti-13Nb-13Zr, Ti-15Sn-4Nb-2Ta-0.2Pd, Ti–16Nb–10Hf, and Ti-Nb-Ta-Zr (TNTZ) system alloys, such as Ti–35.3Nb–5.1Ta–7.1Zr and Ti–29Nb–13Ta–4.6Zr [10,18–24]. Among these alloys, the TNTZ alloys stand out since all their constituent elements exhibit biocompatibility individually, and the alloys possess lower elastic modulus as compared to the Ti-6Al-4V alloy, resulting in improved fatigue and fracture characteristics [25–27].

Fracture is an important consideration for implant materials, and it is strongly influenced by the microstructure [28–30]. Main concerns regarding the fracture of the implants revolve around the defects in the design and manufacturing process, non-passive fit of the superstructure leading to unstable forces within implant-bone interfaces, and biomechanical and physiological load factors [28,29,31]. Despite definitely having an influence, material defects such as porosity are not main causes of fracture, yet the loading usually dictates quite significantly [28,29,32]. Therefore, a non-passive fit may create an extra stress on an implant and bone, facilitating implant

fracture [29,33]. Moreover, an adequate prosthesis design is a requirement to eliminate undesirable forces, and obtain effective durability under irregular loading [28,29]. Thus, an implantable material must be ideally ductile to be easily formed according to the desired design of an implant, and at the same time, rigid enough to withstand applied loading. Consequently, implant materials should satisfy specific requirements such as high corrosion resistance, high toughness and fracture resistance to withstand possible degradation in aggressive environments and irregular loading that might be inevitable due to specific movements of the human body [4,6,7].

While numerous studies have been carried to develop conventional biomedical alloys with microstructures to satisfy the aforementioned demands, a new class of metallic materials, namely the high entropy alloys (HEAs), have emerged recently [34,35], some of which also constitute ideal candidates for utility in biomedical applications. The HEAs have exceptional mechanical properties such as high strength and toughness [36–46], excellent corrosion resistance [46–48], high fracture toughness [49,50] and high thermal stability [38,46,51] brought about by their multi-principal elements leading to a high configurational entropy and thereby forming a single stable solid phase [37,47,52]. Indeed, certain HEAs exhibit good biocompatibility owing to their high corrosion resistance and protective oxide layer formation on the surface in aggressive environments [53–58].

In an effort to enhance the mechanical compatibility with the bone tissue, several HEAs with body centered cubic (BCC) structures have been developed containing early transition elements such as Ti, Hf, Nb, Zr, Mo and Ta in order to obtain high strength and ductility, low modulus, improved fracture resistance and hardness, and thereby eliminate problems due to the loss of the bone integrity that can cause sudden failure of an implant, and mechanical insufficiencies during service life [29,30,59–61]. The newly developed HEAs that consist of the early transition elements such as TiNbTaZrMo [26,60,62] showed excellent biocompatibility as compared to pure Ti and the Ti-6Al-4V alloy, and superior mechanical properties such as high strength and high workability have been obtained in HEAs such as TaNbHfZrTi that contain transition elements [43,59,60,63–67]. Moreover, some studies on HfNbTaTiZr, HfMoTaTiZr and HfMoNbTaTiZr systems revealed their high strength and ductility with relatively low elastic modulus [59,68,69] that seem promising due to their non-toxic compositions.

Based on previous promising results reported on HEAs based on early transition elements, we developed three derivatives of TiTaHf-based HEAs, namely TiTaHfNb, TiTaHfNb and TiTaHfMoZr, which contain only non-toxic transition elements. Despite the fact that a few previous studies evaluated TiTaHfNb-based HEAs [62–65,68–70], there is a lack of information about their fracture mechanisms in the case of a sudden failure, such as under impact loading, which is very much relevant to their utility as implants. In order to fill this gap and help evaluating the potential of these selected TiTaHf-based HEAs as implant materials from a mechanics point of view, we focused on the mechanical properties and qualitative evaluations of fracture response of the BCC structured TiTaHfNb, TiTaHfNbZr, and TiTaHfMoZr HEAs at 298 K under impact loading. With this purpose, TiTaHfNb, TiTaHfNbZr and TiTaHfMoZr HEA samples were subjected to Charpy impact and nano-indentation tests, and thorough pre- and post-mortem microstructure analysis was performed utilizing X-ray diffraction and scanning electron microscopy analyses. The findings presented in this paper show that TiTaHfNb, TiTaHfNbZr, and TiTaHfMoZr HEAs have good mechanical properties and significant fracture resistance. Specifically, the TiTaHfNb alloy exhibited superior fracture toughness, and addition of Zr and Mo decreased the energy absorption capacity of the TiTaHf-based HEA system. In addition, while the TiTaHfNb exhibited mostly ductile behavior, the TiTaHfNbZr HEA exhibited brittle and ductile regions evidencing a mixed fracture mode. Overall, the current findings indicate that these three TiTaHf-based HEAs exhibit promising mechanical response for utility in implant applications, warranting further elaboration on their mechanical and biocompatible response.

4.2 Experimental Procedures

In this study, HEAs with a purity of 99.9% were produced by arc melting: the TiTaHfNb HEA was composed of 50 wt.% Ti, 16.67 wt.% Ta, 16.67 wt.% Hf and 16.67 wt.% Nb, whereas TiTaHfNbZr and TiTaHfMoZr compositions were equimolar. The disc-shaped multi-component alloys with a diameter of 50.1 mm and a thickness of 6.1 mm were cut by an electrical discharge machine (EDM) to obtain 10 mm x 5 mm x 1 mm bulk samples, and 45 mm x 6 mm x 3 mm impact test samples with a 1 mm deep notch at the center. It should be noted that dimensions of the V-notch specimens utilized in the impact tests were adjusted to our test equipment in accord with the Charpy Impact

test standards [71]. Charpy impact test, also known as the Charpy V-Notch test (CVN), was performed on the three aforementioned HEAs at 298 K utilizing a TERCO MT3016 Impact Tester with a 30 J capacity, followed by an analysis of fracture surface of the samples carried out on a Zeiss Ultra Plus field emission scanning electron microscope (SEM).

The surfaces of the bulk samples were mechanically ground with SiC emery papers with coarseness ranging from 106 to 2.5 μm, then polished with 0.30 μm alumina slurry to reach mirror-like appearance, and the bulk samples were cleaned ultrasonically with ethanol and rinsed with de-ionized water. Following the polishing/cleaning procedure, crystallographic characterization of the samples was carried out by X-ray diffraction (XRD) method on a Bruker D2 Advanced X-ray diffractometer using a Cu-Kα radiation source. The XRD was operated at 30 kV and 10 mA with an incidence angle of 5°, and the scanning region ranged from 5° to 90° with a 0.02° increment.

Mechanical characterization of the bulk HEAs was accomplished by nano-indentation tests that were carried out on Agilent G200 tester with Berkovich type indenter in load-control mode at a maximum applied load of 300 mN. Each indentation test was performed under a loading/unloading rate of 30 mN with a 10 s hold time at maximum load before unloading.

4.3 Results and Discussion

The initial microstructural characterization of single-phase TiTaHfNb, TiTaHfNbZr and TiTaHfMoZr HEAs was carried out with XRD, where the experimental lattice parameters and the corresponding peak values were calculated using Bragg's Law (Figure 4-1). The results confirmed that the TiTaHfNb, TiTaHfNbZr and TiTaHfMoZr HEAs have a BCC structure, and the lattice parameters are 3.329 Å, 3.340 Å, and 3.362 Å, respectively. These three HEAs are newly developed and there is a very limited number of studies on their properties, however the peak values and the lattice parameters are consistent with the literature [43,59,72–75]. Moreover, Young's moduli of TiTaHfNb, TiTaHfNbZr and TiTaHfMoZr were measured by nano-indentation and determined as 112.2 GPa, 131.6 GPa and 158.9 GPa, respectively. Even though these values are still far from that of the bone which is about 30 GPa [11,76], they are still significantly lower than those of commonly utilized biomaterials such as 316 L stainless

steel and Co-based alloys with elastic moduli within 180-210 GPa range [11], offering an enhancement in terms of mechanical compatibility with the bone.

The corresponding hardnesses were measured as 3.5 GPa for TiTaHfNb, 6.5 GPa for TiTaHfNbZr, and 6.6 GPa for TiTaHfMoZr. In Figure 4-2, stress and strain graphs from nano-indentation tests are provided. Accordingly, the TiTaHfNb HEA exhibits higher plastic strains at fracture, and TiTaHfNbZr and TiTaHfMoZr HEAs demonstrated less ductility. Consequently, it is clear that addition of Mo decreases the hardness and increases the elastic modulus: hardnesses of TiTaHfNbZr and TiTaHfMoZr HEAs are almost twice that of the TiTaHfNb HEA, and the greater difference can be attributed to solid solution strengthening [77].

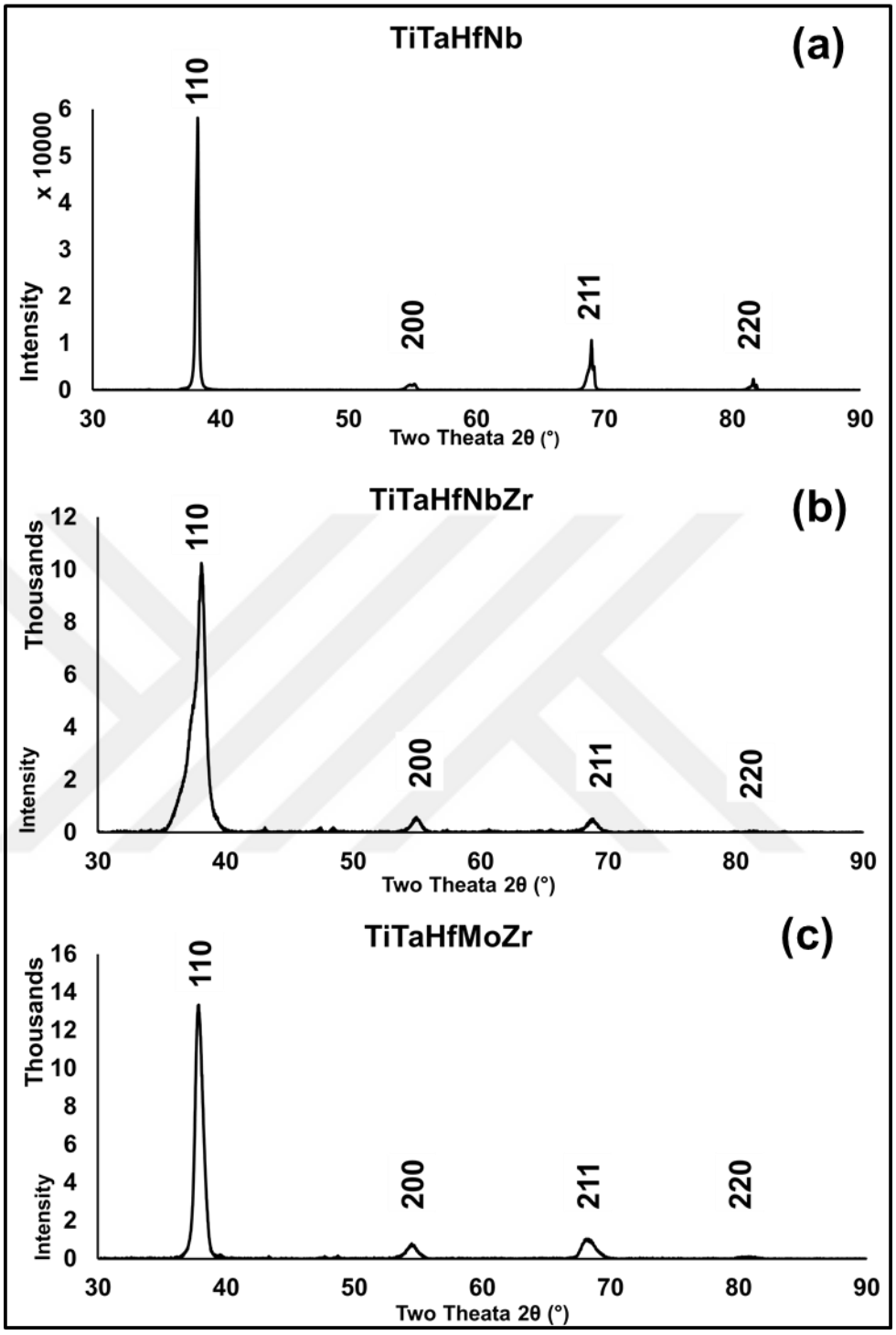

Figure 4-1: XRD results of (a) TiTaHfNb, (b) TiTaHfNbZr, and (c) TiTaHfMoZr HEAs.

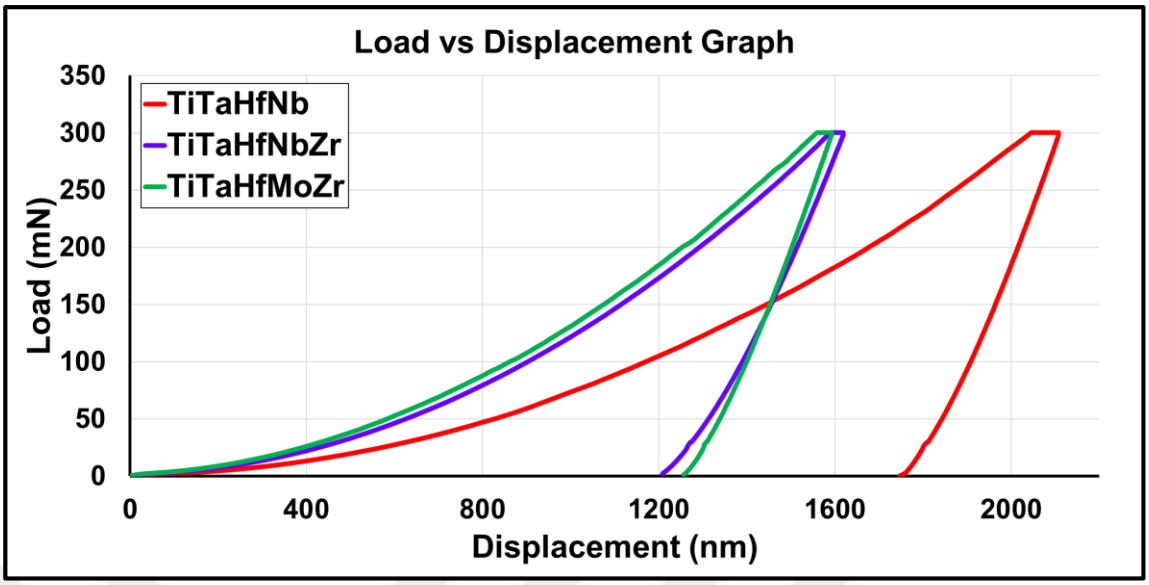

Figure 4-2: Load vs Displacement data for TiTaHfNb, TiTaHfNbZr, TiTaHfMoZr HEAs as obtained by nano-indentation tests.

CVN experiments were performed in order to assess the energy absorption capacities of TiTaHfNb, TiTaHfNbZr and TiTaHfMoZr HEAs. As illustrated in Figure 4-3, contrary to typical behavior, the TiTaHfNb sample was not completely broken into pieces, and the test was repeated to ensure that the observed response was not sample specific. The impact energy was measured as 14.7 J and 14.9 J in these two CVN tests of TiTaHfNb. On the other hand, significantly lower impact energy values were exhibited by TiTaHfNbZr and TiTaHfMoZr HEAs, namely 0.25 J and 0.1 J, respectively. Following the CVN experiments, fracture surfaces of TiTaHfNb, TiTaHfNbZr and TiTaHfMoZr were analyzed with SEM. The corresponding SEM micrographs from the limited inspection area of TiTaHfNb HEA (Figure 4-4(a)) indicate evidence of ductile behavior, namely a significant tearing pattern, and a predominately cup-and-cone type of fracture surface is evident (Figure 4-4(b)). On the other hand, a closer look at the tearing patterns (Figure 4-4(c)) reveals flat surfaces with chevron marks (Figure 4-4(d)) and cleavage facets (Figure 4-4(e)). Consequently, both ductile and brittle fracture modes are active in the TiTaHfNb HEA, as evidence by the coexistence of cup-and-cone structures and shiny fracture zones with cleavage facets.

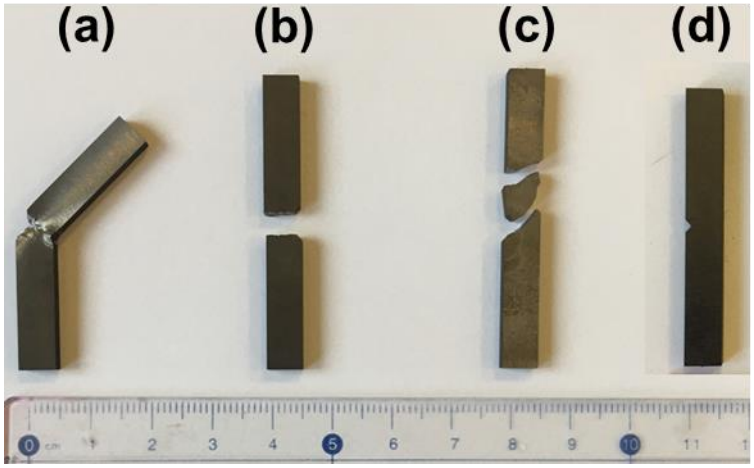

Figure 4-3: The CVN test samples of (a) TiTaHfNb, (b) TiTaHfNbZr, and (c) TiTaHfMoZr HEAs following the experiment; (d) representative untested CVN test sample. The scale provided in the figure is in cm.

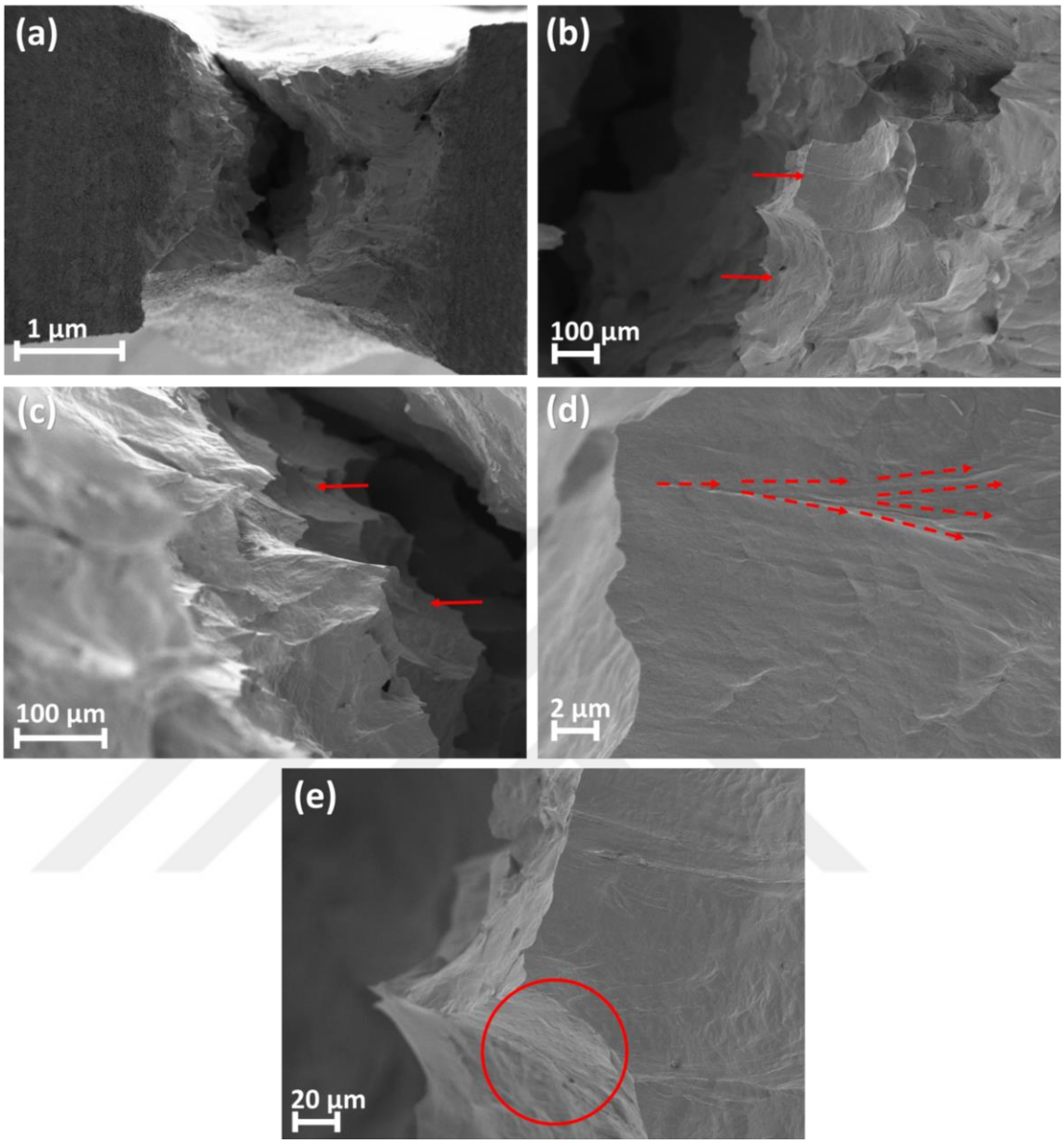

Figure 4-4: SEM micrographs of TiTaHfNb HEA fracture surface: (a) limited inspection area, (b) tearing patterns, and cup-and-cone structures, (c) tearing region, (d) flat surface with Chevron marks (red lines), and (e) overview of cleavage surface (red circle).

In comparison to the TiTaHfNb HEA, the TiTaHfNbZr alloy exhibits a more complicated fracture surface with coexisting slant and flat regions, where both bull and shiny surface zones can be seen (Figure 4-5). In particular, small and shiny angular facets form in a rock-candy like texture (Figure 4-5(a)), which can be attributed to intergranular crack formations along the grain boundaries (Figures 4-5(b) and (c)). Moreover, Chevron marks and river patterns observed on the fracture surface with

cavity formations (Figure 4-5(b)) mainly result from brittle fracture: the red lines in Figure 4-5(b) represent the propagation path of chevron marks that point at the crack origin, and the blue lines highlight the river lines and cleavage surfaces near the region that has elongated dimples. Figure 4-5(c) demonstrates the significant differences in the fracture patterns on TiTaHfNbZr, such that there is a transition zone formation with ladder like structures between the smooth (left) and the non-smooth (right) regions. Indeed, a closer look at the Figure 4-5(d) reveals that while river like patterns and striations can be observed in the transition zone, elongated dimples constitute evidence of shear forces acting on the material during fracture. The fracture surface contains brittle and ductile zones throughout the fracture surface (Figure 4-5(e)), a closer look at the regions reveals tilt and twist formation on the cleavage zone (Figure 4-5 (g)) and small dimples around the grain boundaries (Figure 4-5 (h)), as well as equiaxed dimples (Figure 4-5 (f)). Accordingly, despite the fact that the fracture surface of the TiTaHfNbZr HEA is dominated by cleavage, ductile regions are evident, including elongated dimples due to tearing process and shear forces. Thus, one can conclude that the TiTaHfNbZr HEA also fractures on a mixed fracture mode under impact loading, with brittle mode dominating.

In the case of the TiTaHfMoZr HEA, mainly flat facets with river patterns and chevron marks can be observed on the fracture surface (Figure 4-6). Moreover, both intercrystalline and transcrystalline fracture are facilitated with limited crack propagation (Figures 4-6(a), (b) and (c)). Tongue formation which is a result of small scale height elevations as can be seen in Figure 4-6(b), which can be attributed to twinning mechanism [78], and the twin boundary fracture [79] may lead to the formation of yellow-dashed-line region in Figure 4-6(c). In addition, the ladder-like formations (Figures 4-6(c) and (d)) due to cleavage fracture, and striations that are directed gradually along shear forces (Figure 4-6 (e)) indicate rapid fracture. Therefore, cleavage fracture dominates the fracture surface of the TiTaHfMoZr HEA, and the material exhibits a much more brittle behavior than TiTaHfNb and TiTaHfNbZr with the lowest impact energy of 0.1 J.

The CVN experiments and the corresponding microstructural analyses demonstrated that modifications made to the elemental compositions of TiTaHf-based HEAs significantly influence the fracture behavior. Specifically, addition of Zr to TiTaHfNb significantly decreased the impact energy and enhanced the brittleness,

where the impact energy decreased down to 0.25 J from an average of 14.8 J. Yet the lowest energy absorption capacity was observed in the case of TiTaHfMoZr HEA, namely 0.1 J, and this alloy also exhibited the most brittle response. This can be attributed to multiple phase formations facilitated by Mo addition (Figures 4-7 (a) and (b)). The corresponding EDX analyses revealed that a non-homogenous microstructure with dendritic and interdendritic regions are present, as evidenced by Ta-rich and Zr-rich, compositions, respectively. On the other hand, TiTaHfNbZr HEA exhibits strictly defined fracture regions of brittle and ductile nature, which coexist (Figure 4-5). An EDX analysis revealed that the constituents of TiTaHfNbZr are homogenously dispersed in the microstructure (Figures 4-7 (c) and (d)). Therefore, some dislocation behavior may be the reason behind its mixed fracture mode.

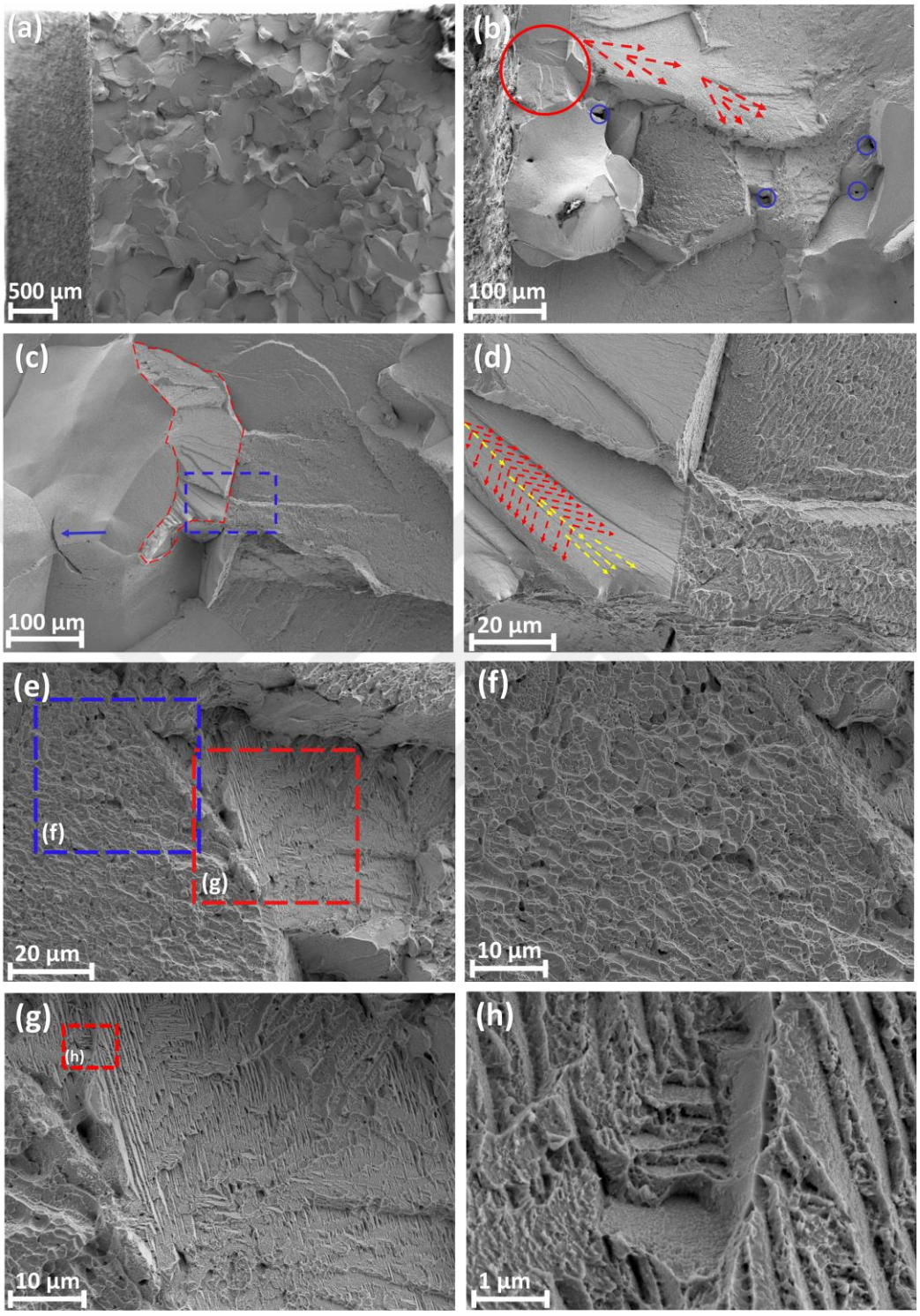

Figure 4-5: SEM micrographs of the fracture surface of TiTaHfNbZr HEA: **(a)** rock-candy like surface, **(b)** inter-crystalline structures, river patterns and ladder like structures, and red lines represent chevron marks propagation, and blue circles indicate cavity formations; **(c)** smooth and rough regions are coexistent where the red boundary represents transition zone; **(d)** close-up view of the transition zone and the rough surface, with river patterns and elongated dimples, respectively, **(e)** coexisting ductile and brittle zones, **(f)** elongated dimples, **(g)** cleavage zone with twist and tilt structures, **(h)** close-up view of dimples along grain boundaries, and nano-pores.

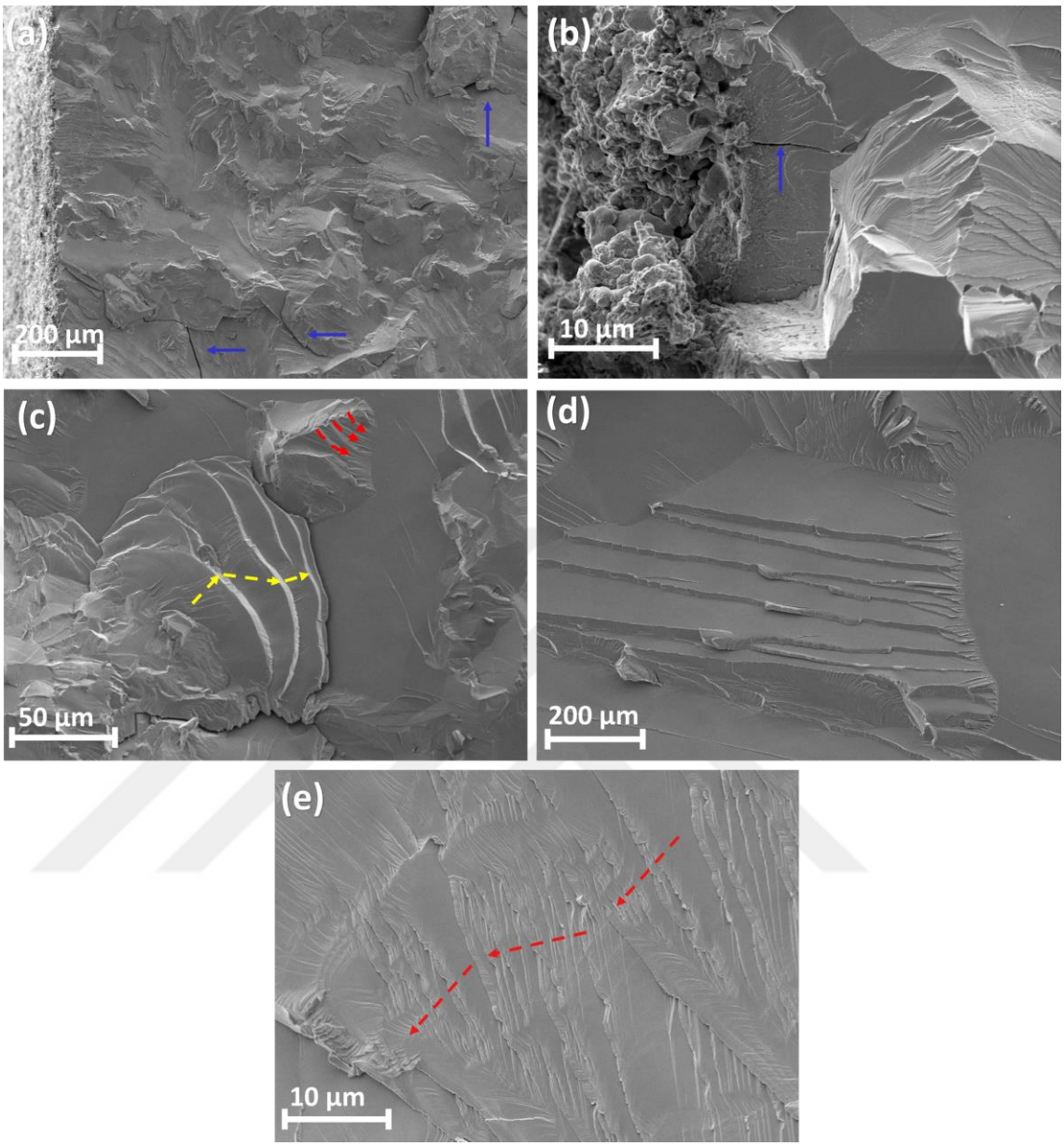

Figure 4-6: SEM micrographs of fracture surface of TiTaHfMoZr HEA: (a) blue arrows indicate intergranular and transgranular fracture, (b) tongues and river patterns, where the blue arrow indicates transgranular fracture, (c) twin boundary fracture, ladder-like structures, and intergranular fracture, (d) cleavage surface, and (e) striations directed along shear.

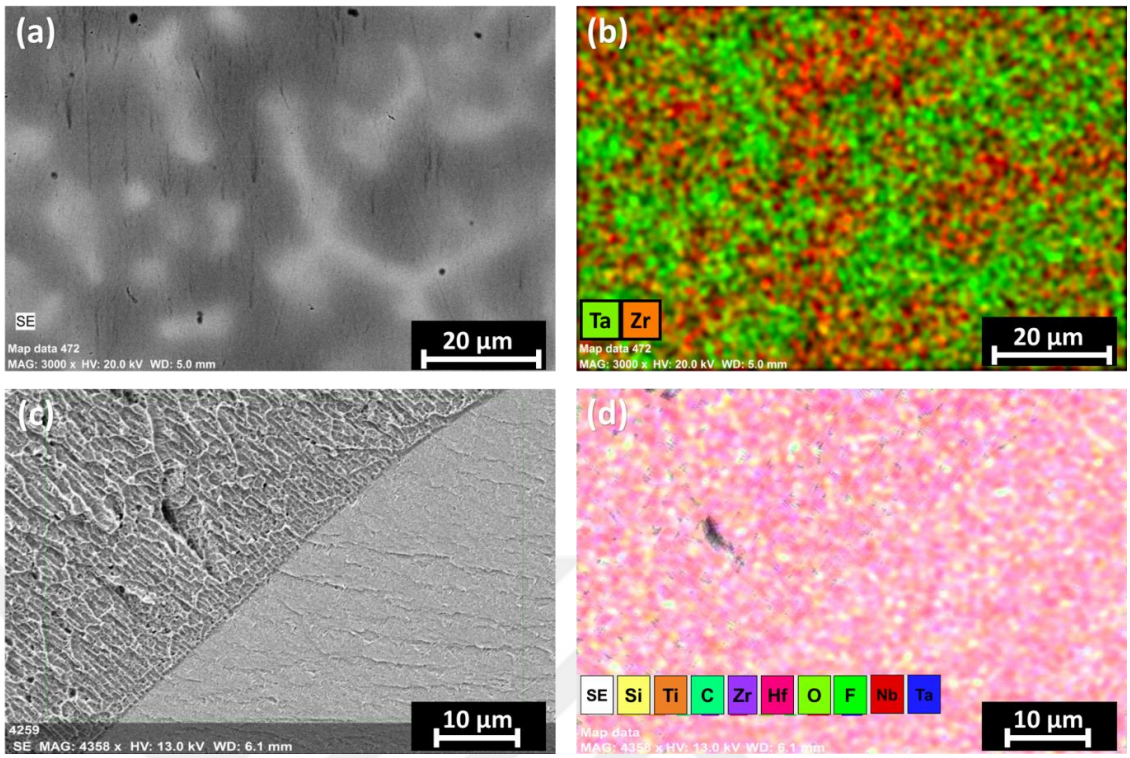

Figure 4-7: EDX results showing (a) nonhomogenous surface of the as-received TiTaHfMoZr, and (b) the corresponding elemental mapping where the green regions represent Ta-rich areas, and red regions represent Zr-rich areas; (c) the as-received homogenous surface of TiTaHfNbZr, and (d) the corresponding elemental mapping.

4.4 Conclusion

Fracture response of three TiTaHf-based high-entropy alloys (HEAs), namely TiTaHfNb, TiTaHfNbZr and TiTaHfMoZr alloys was investigated employing Charpy impact tests at 298 K. The experimental findings revealed that the TiTaHfNb HEA has the highest energy absorption capacity and exhibits a more ductile behavior as compared to the TiTaHfNbZr and TiTaHfMoZr HEAs. The presence of Zr in the substrates led to a decrease in impact energy, and the TiTaHfNbZr showed mixed fracture characteristics with predominantly brittle behavior. Moreover, Mo addition resulted in an inhomogeneous microstructure (TiTaHfMoZr), leading to dendrite formation and significant decrease in energy absorption capacity, and cleavage surfaces and quasi cleavage structures were evident upon brittle fracture of this HEA. Overall, the findings reported herein not only demonstrate the potential of the TiTaHf-based HEAs to be utilized as implant materials, but also warrant further investigation of their mechanical response and biocompatibility prior to their utility in medical applications.

4.5 Acknowledgments

This work was supported by the BAGEP Award of the Science Academy. B. Bal acknowledges the AGU-BAP [grant number FAB-2017-77].

4.6 References

[1] N. Mitsuo, Mechanical properties of biomedical titanium alloys, Mater. Sci. Eng. A. 243 (1998) 231–236. http://www.sciencedirect.com/science/article/pii/S092150939700806X.

[2] M. Niinomi, Recent metallic materials for biomedical applications, Metall. Mater. Trans. A. 33 (2002) 477–486. doi:10.1007/s11661-002-0109-2.

[3] M.P. Staiger, A.M. Pietak, J. Huadmai, G. Dias, Magnesium and its alloys as orthopedic biomaterials: A review, Biomaterials. 27 (2006) 1728–1734. doi:10.1016/j.biomaterials.2005.10.003.

[4] Q. Chen, G.A. Thouas, Metallic implant biomaterials, Mater. Sci. Eng. R Reports. 87 (2015) 1–57. doi:10.1016/j.mser.2014.10.001.

[5]R. Van Noort, Titanium: The implant material of today, J. Mater. Sci. 22 (1987) 3801–3811. doi:10.1007/BF01133326.

[6] T. Akahori, M. Niinomi, Fracture characteristics of fatigued Ti–6Al–4V ELI as an implant material, Mater. Sci. Eng. A. 243 (1998) 237–243. doi:10.1016/S0921-5093(97)00807-1.

[7] S. Sanivarapu, S. Moogla, R. Kuntcham, L. Kolaparthy, Implant fractures: Rare but not exceptional, J. Indian Soc. Periodontol. 20 (2016) 6. doi:10.4103/0972-124X.154190.

[8] C.N. Elias, J.H.C. Lima, R. Valiev, M.A. Meyers, Biomedical applications of titanium and its alloys, JOM. 60 (2008) 46–49. doi:10.1007/s11837-008-0031-1.

[9] Y. Li, C. Yang, H. Zhao, S. Qu, X. Li, Y. Li, New Developments of Ti-Based Alloys for Biomedical Applications, Materials (Basel). 7 (2014) 1709–1800. doi:10.3390/ma7031709.

[10] M.F. López, J.A. Jiménez, A. Gutiérrez, Corrosion study of surface-modified vanadium-free titanium alloys, Electrochim. Acta. (2003). doi:10.1016/S0013-4686(03)00006-9.

[11] M. Niinomi, M. Nakai, J. Hieda, Development of new metallic alloys for biomedical applications, Acta Biomater. 8 (2012) 3888–3903. doi:10.1016/j.actbio.2012.06.037.

[12] Y. Yuan, Y. Wu, Z. Yang, X. Liang, Z. Lei, H. Huang, H. Wang, X. Liu, K. An, W. Wu, Z. Lu, Formation, structure and properties of biocompatible TiZrHfNbTa high-entropy alloys, Mater. Res. Lett. 7 (2019) 225–231. doi:10.1080/21663831.2019.1584592.

[13] C. Oldani, A. Dominguez, Titanium as a Biomaterial for Implants, in: Recent Adv. Arthroplast., InTech, 2012. doi:10.5772/27413.

[14] S. Rajendran, J. Paulraj, P. Rengan, J. Jeyasundari, M. Manivannan, Corrosion behaviour of metals in artificial saliva in presence of spirulina powder, J. Dent. (2009).

[15] S. Rao, T. Ushida, T. Tateishi, Y. Okazaki, S. Asao, Effect of Ti, Al, and V ions on the relative growth rate of fibroblasts (L929) and osteoblasts (MC3T3-E1) cells., Biomed. Mater. Eng. 6 (1996) 79–86. http://www.ncbi.nlm.nih.gov/pubmed/8761518.

[16] S.G. Steinemann, Metal implants and surface reactions, Injury. 27 (1996) S/C16-S/C22. doi:10.1016/0020-1383(96)89027-9.

[17] L.N. Miotto, L.M.G. Fais, A.L.R. Ribeiro, L.G. Vaz, Surface properties of Ti-35Nb-7Zr-5Ta, J. Prosthet. Dent. 116 (2016) 102–111. doi:10.1016/j.prosdent.2015.10.024.

[18] E. Kobayashi, T.J. Wang, H. Doi, T. Yoneyama, H. Hamanaka, Mechanical properties and corrosion resistance of Ti-6Al-7Nb alloy dental castings, J. Mater. Sci. Mater. Med. 9 (1998) 567–574. doi:10.1023/A:1008909408948.

[19] S. Tamilselvi, V. Raman, N. Rajendran, Corrosion behaviour of Ti–6Al–7Nb and Ti–6Al–4V ELI alloys in the simulated body fluid solution by electrochemical impedance spectroscopy, Electrochim. Acta. 52 (2006) 839–846. doi:10.1016/j.electacta.2006.06.018.

[20] M.A. Khan, R.L. Williams, D.F. Williams, The corrosion behaviour of Ti-6Al-4V, Ti-6Al-7Nb and Ti-13Nb-13Zr in protein solutions, Biomaterials. (1999). doi:10.1016/S0142-9612(98)00217-8.

[21] Y. Okazaki, S. Rao, Y. Ito, T. Tateishi, Corrosion resistance, mechanical properties: corrosion fatigue strength and cytocompatibility of new Ti alloys without A1 and V, Biomaterials. (1998). doi:10.1016/S0142-9612(97)00235-4.

[22] Y. Okazaki, T. Tateishi, Y. Ito, Corrosion Resistance of Implant Alloys in Pseudo Physiological Solution and Role of Alloying Elements in Passive Films, Mater. Trans. JIM. 38 (1997) 78–84. doi:10.2320/matertrans1989.38.78.

[23] M. Niinomi, Metallic biomaterials, J. Artif. Organs. 11 (2008) 105–110. doi:10.1007/s10047-008-0422-7.

[24] D. Kuroda, H. Kawasaki, A. Yamamoto, S. Hiromoto, T. Hanawa, Mechanical properties and microstructures of new Ti-Fe-Ta and Ti-Fe-Ta-Zr system alloys, in: Mater. Sci. Eng. C, 2005. doi:10.1016/j.msec.2005.04.004.

[25] D. Raducanu, V.D. Cojocaru, A. Nocivin, I. Cinca, N. Serban, E.M. Cojocaru, Contributions to Mechanical Characteristics Improvement of Some Biomedical TNTZ Alloys by Adding Fe, Si, and O: A Comparative Study, JOM. 71 (2019) 264–271. doi:10.1007/s11837-018-3091-x.

[26] M. Todai, T. Nagase, T. Hori, A. Matsugaki, A. Sekita, T. Nakano, Novel TiNbTaZrMo high-entropy alloys for metallic biomaterials, Scr. Mater. 129 (2017) 65–68. doi:10.1016/j.scriptamat.2016.10.028.

[27] M.T. Mohammed, Z.A. Khan, A.N. Siddiquee, Beta Titanium Alloys: The Lowest Elastic Modulus for Biomedical Applications: A Review Surface Modifications through FSP View project MACHINING View project, Int. J. Chem. Nucl. Metall. Mater. Eng. 8 (2014) 726–731. https://www.researchgate.net/publication/265396160.

[28] C.W. Gealh, V. Mazzo, F. Barbi, E.T. Camarini, Osseointegrated implant fracture: Causes and treatment, J. Oral Implantol. (2011). doi:10.1563/AAID-JOI-D-09-00135.1.

[29] N. Tagger Green, E.E. Machtei, J. Horwitz, M. Peled, Fracture of Dental Implants: Literature Review and Report of a Case, Implant Dent. 11 (2002) 137–143. doi:10.1097/00008505-200204000-00014.

[30] K. Shemtov-Yona, D. Rittel, On the mechanical integrity of retrieved dental implants, J. Mech. Behav. Biomed. Mater. (2015). doi:10.1016/j.jmbbm.2015.05.014.

[31] A. Piattelli, A. Scarano, M. Piattelli, E. Vaia, S. Matarasso, Hollow Implants Retrieved for Fracture: A Light and Scanning Electron Microscope Analysis of 4 Cases, J. Periodontol. 69 (1998) 185–189. doi:10.1902/jop.1998.69.2.185.

[32] A. Piattelli, M. Piattelli, A. Scarano, L. Montesani, Light and scanning electron microscopic report of four fractured implants., Int. J. Oral Maxillofac. Implants. 13 (1998) 561–564.

[33] A.A. Siddiqui, R. Caudill, Proceedings of the fourth International Symposium on Implant Dentistry: Focus on esthetics, J. Prosthet. Dent. (1994). doi:10.1016/0022-3913(94)90295-x.

[34] Y. Zhang, T.T. Zuo, Z. Tang, M.C. Gao, K.A. Dahmen, P.K. Liaw, Z.P. Lu, Microstructures and properties of high-entropy alloys, Prog. Mater. Sci. 61 (2014) 1–93. doi:10.1016/j.pmatsci.2013.10.001.

[35] D.B. Miracle, O.N. Senkov, A critical review of high entropy alloys and related concepts, Acta Mater. 122 (2017) 448–511. doi:10.1016/j.actamat.2016.08.081.

[36] Y. Zhang, X. Yang, P.K. Liaw, Alloy Design and Properties Optimization of High-Entropy Alloys, JOM. 64 (2012) 830–838. doi:10.1007/s11837-012-0366-5.

[37] L. Vinet, A. Zhedanov, A ‘missing’ family of classical orthogonal polynomials, J. Phys. A Math. Theor. 44 (2011) 085201. doi:10.1088/1751-8113/44/8/085201.

[38] Y. Qiu, S. Thomas, M.A. Gibson, H.L. Fraser, N. Birbilis, Corrosion of high entropy alloys, Npj Mater. Degrad. 1 (2017) 15. doi:10.1038/s41529-017-0009-y.

[39] X.W. Qiu, Y.P. Zhang, L. He, C.G. Liu, Microstructure and corrosion resistance of AlCrFeCuCo high entropy alloy, J. Alloys Compd. 549 (2013) 195–199. doi:10.1016/j.jallcom.2012.09.091.

[40] C. Li, J.C. Li, M. Zhao, Q. Jiang, Effect of aluminum contents on microstructure and properties of AlxCoCrFeNi alloys, J. Alloys Compd. 504 (2010) S515–S518. doi:10.1016/j.jallcom.2010.03.111.

[41] Z.D. Han, H.W. Luan, X. Liu, N. Chen, X.Y. Li, Y. Shao, K.F. Yao, Microstructures and mechanical properties of Ti NbMoTaW refractory high-entropy alloys, Mater. Sci. Eng. A. 712 (2018) 380–385. doi:10.1016/j.msea.2017.12.004.

[42] T.-T. Shun, L.-Y. Chang, M.-H. Shiu, Microstructures and mechanical properties of multiprincipal component CoCrFeNiTix alloys, Mater. Sci. Eng. A. 556 (2012) 170–174. doi:10.1016/j.msea.2012.06.075.

[43] O.N. Senkov, J.M. Scott, S.V. Senkova, D.B. Miracle, C.F. Woodward, Microstructure and room temperature properties of a high-entropy TaNbHfZrTi alloy, J. Alloys Compd. 509 (2011) 6043–6048. doi:10.1016/j.jallcom.2011.02.171.

[44] X.F. Wang, Y. Zhang, Y. Qiao, G.L. Chen, Novel microstructure and properties of multicomponent CoCrCuFeNiTix alloys, Intermetallics. 15 (2007) 357–362. doi:10.1016/j.intermet.2006.08.005.

[45] O.N. Senkov, G.B. Wilks, D.B. Miracle, C.P. Chuang, P.K. Liaw, Refractory high-entropy alloys, Intermetallics. 18 (2010) 1758–1765. doi:10.1016/j.intermet.2010.05.014.

[46] Y. Qiu, M.A. Gibson, H.L. Fraser, N. Birbilis, Corrosion characteristics of high entropy alloys, Mater. Sci. Technol. 31 (2015) 1235–1243. doi:10.1179/1743284715Y.0000000026.

[47] Z. Tang, L. Huang, W. He, P. Liaw, Alloying and Processing Effects on the Aqueous Corrosion Behavior of High-Entropy Alloys, Entropy. 16 (2014) 895–911. doi:10.3390/e16020895.

[48] Y.-J. Hsu, W.-C. Chiang, J.-K. Wu, Corrosion behavior of FeCoNiCrCux high-entropy alloys in 3.5% sodium chloride solution, Mater. Chem. Phys. 92 (2005) 112–117. doi:10.1016/j.matchemphys.2005.01.001.

[49] B. Gludovatz, A. Hohenwarter, D. Catoor, E.H. Chang, E.P. George, R.O. Ritchie, ChemInform Abstract: A Fracture-Resistant High-Entropy Alloy for Cryogenic Applications., ChemInform. 45 (2014) no-no. doi:10.1002/chin.201447007.

[50] Z. Zhang, M.M. Mao, J. Wang, B. Gludovatz, Z. Zhang, S.X. Mao, E.P. George, Q. Yu, R.O. Ritchie, Nanoscale origins of the damage tolerance of the high-entropy alloy CrMnFeCoNi, Nat. Commun. 6 (2015) 10143. doi:10.1038/ncomms10143.

[51] R. Sriharitha, B.S. Murty, R.S. Kottada, Alloying, thermal stability and strengthening in spark plasma sintered AlxCoCrCuFeNi high entropy alloys, J. Alloys Compd. 583 (2014) 419–426. doi:10.1016/j.jallcom.2013.08.176.

[52] W. Zhang, P.K. Liaw, Y. Zhang, Science and technology in high-entropy alloys, Sci. China Mater. 61 (2018) 2–22. doi:10.1007/s40843-017-9195-8.

[53] G. Popescu, B. Ghiban, C.A. Popescu, L. Rosu, R. Truscă, I. Carcea, V. Soare, D. Dumitrescu, I. Constantin, M.T. Olaru, B.A. Carlan, New TiZrNbTaFe high entropy alloy used for medical applications, IOP Conf. Ser. Mater. Sci. Eng. 400 (2018) 022049. doi:10.1088/1757-899X/400/2/022049.

[54] V. Braic, M. Balaceanu, M. Braic, A. Vladescu, S. Panseri, A. Russo, Characterization of multi-principal-element (TiZrNbHfTa)N and (TiZrNbHfTa)C coatings for biomedical applications, J. Mech. Behav. Biomed. Mater. 10 (2012) 197–205. doi:10.1016/j.jmbbm.2012.02.020.

[55] B. Ghiban, G. Popescu, C. Lazar, L. Rosu, I. Constantin, M. Olaru, B. Carlan, Corrosion Behaviour in Human Stimulation Media of a High Entropy Titan-Based Alloy, IOP Conf. Ser. Mater. Sci. Eng. 374 (2018) 012004. doi:10.1088/1757-899X/374/1/012004.

[56] C.B. Aksoy, D. Canadinc, M.B. Yagci, Assessment of Ni ion release from TiTaHfNbZr high entropy alloy coated NiTi shape memory substrates in artificial saliva and gastric fluid, Mater. Chem. Phys. 236 (2019) 121802. doi:10.1016/j.matchemphys.2019.121802.

[57] X. Qiu, Corrosion behavior of Al2CrFeCo CuNiTi high-entropy alloy coating in alkaline solution and salt solution, Results Phys. 12 (2019) 1737–1741. doi:10.1016/j.rinp.2019.01.090.

[58] Y. Shi, B. Yang, P. Liaw, Corrosion-Resistant High-Entropy Alloys: A Review, Metals (Basel). 7 (2017) 43. doi:10.3390/met7020043.

[59] C.-C. Juan, M.-H. Tsai, C.-W. Tsai, C.-M. Lin, W.-R. Wang, C.-C. Yang, S.-K. Chen, S.-J. Lin, J.-W. Yeh, Enhanced mechanical properties of HfMoTaTiZr and HfMoNbTaTiZr refractory high-entropy alloys, Intermetallics. 62 (2015) 76–83. doi:10.1016/j.intermet.2015.03.013.

[60] S.-P. Wang, J. Xu, TiZrNbTaMo high-entropy alloy designed for orthopedic implants: As-cast microstructure and mechanical properties, Mater. Sci. Eng. C. 73 (2017) 80–89. doi:10.1016/j.msec.2016.12.057.

[61] K.-K. Tseng, C.-C. Juan, S. Tso, H.-C. Chen, C.-W. Tsai, J.-W. Yeh, Effects of Mo, Nb, Ta, Ti, and Zr on Mechanical Properties of Equiatomic Hf-Mo-Nb-Ta-Ti-Zr Alloys, Entropy. 21 (2018) 15. doi:10.3390/e21010015.

[62] T. Nagase, M. Todai, T. Hori, T. Nakano, Microstructure of equiatomic and non-equiatomic Ti-Nb-Ta-Zr-Mo high-entropy alloys for metallic biomaterials, J. Alloys Compd. 753 (2018) 412–421. doi:10.1016/j.jallcom.2018.04.082.

[63] O.N. Senkov, G.B. Wilks, J.M. Scott, D.B. Miracle, Mechanical properties of Nb25Mo25Ta25W25 and V20Nb20Mo20Ta20W20 refractory high entropy alloys, Intermetallics. 19 (2011) 698–706. doi:10.1016/j.intermet.2011.01.004.

[64] Y.D. Wu, Y.H. Cai, T. Wang, J.J. Si, J. Zhu, Y.D. Wang, X.D. Hui, A refractory Hf25Nb25Ti25Zr25 high-entropy alloy with excellent structural stability and tensile properties, Mater. Lett. 130 (2014) 277–280. doi:10.1016/j.matlet.2014.05.134.

[65] G. Dirras, L. Lilensten, P. Djemia, M. Laurent-Brocq, D. Tingaud, J.-P. Couzinié, L. Perrière, T. Chauveau, I. Guillot, Elastic and plastic properties of as-cast equimolar TiHfZrTaNb high-entropy alloy, Mater. Sci. Eng. A. 654 (2016) 30–38. doi:10.1016/j.msea.2015.12.017.

[66] O.N. Senkov, S.L. Semiatin, Microstructure and properties of a refractory high-entropy alloy after cold working, J. Alloys Compd. 649 (2015) 1110–1123. doi:10.1016/J.JALLCOM.2015.07.209.

[67] H. Huang, Y. Wu, J. He, H. Wang, X. Liu, K. An, W. Wu, Z. Lu, Phase-Transformation Ductilization of Brittle High-Entropy Alloys via Metastability Engineering, Adv. Mater. (2017). doi:10.1002/adma.201701678.

[68] J. Zýka, J. Málek, J. Veselý, F. Lukáč, J. Čížek, J. Kuriplach, O. Melikhova, Microstructure and Room Temperature Mechanical Properties of Different 3 and 4 Element Medium Entropy Alloys from HfNbTaTiZr System, Entropy. 21 (2019) 114. doi:10.3390/e21020114.

[69] A. Motallebzadeh, M.B. Yagci, E. Bedir, C.B. Aksoy, D. Canadinc, Mechanical Properties of TiTaHfNbZr High-Entropy Alloy Coatings Deposited on NiTi Shape Memory Alloy Substrates, Metall. Mater. Trans. A. 49 (2018) 1992–1997. doi:10.1007/s11661-018-4605-4.

[70] C.C. Juan, M.H. Tsai, C.W. Tsai, C.M. Lin, W.R. Wang, C.C. Yang, S.K. Chen, S.J. Lin, J.W. Yeh, Enhanced mechanical properties of HfMoTaTiZr and HfMoNbTaTiZr refractory high-entropy alloys, Intermetallics. 62 (2015) 76–83. doi:10.1016/j.intermet.2015.03.013.

[71] ASTM E 23-12c, Standard Test Methods for Notched Bar Impact Testing of Metallic Materials, Standards. i (2013) 1–25. doi:10.1520/E0023-12C.2.

[72] S.-P. Wang, J. Xu, (TiZrNbTa)-Mo high-entropy alloys: Dependence of microstructure and mechanical properties on Mo concentration and modeling of solid solution strengthening, Intermetallics. 95 (2018) 59–72. doi:10.1016/j.intermet.2018.01.017.

[73] A. Motallebzadeh, N.S. Peighambardoust, S. Sheikh, H. Murakami, S. Guo, D. Canadinc, Microstructural, mechanical and electrochemical characterization of TiZrTaHfNb and Ti1.5ZrTa0.5Hf0.5Nb0.5 refractory high-entropy alloys for biomedical applications, Intermetallics. 113 (2019) 106572. doi:10.1016/j.intermet.2019.106572.

[74] J.-P. Couzinié, G. Dirras, Body-centered cubic high-entropy alloys: From processing to underlying deformation mechanisms, Mater. Charact. 147 (2019) 533–544. doi:10.1016/j.matchar.2018.07.015.

[75] F. Lukáč, M. Dudr, J. Čížek, P. Harcuba, T. Vlasák, M. Janeček, J. Kuriplach, J. Moon, H.S. Kim, J. Zýka, J. Málek, Defects in High Entropy Alloy HfNbTaTiZr Prepared by High Pressure Torsion, Acta Phys. Pol. A. 134 (2018) 891–894. doi:10.12693/APhysPolA.134.891.

[76] I. Kopova, J. Stráský, P. Harcuba, M. Landa, M. Janeček, L. Bačákova, Newly developed Ti–Nb–Zr–Ta–Si–Fe biomedical beta titanium alloys with increased strength and enhanced biocompatibility, Mater. Sci. Eng. C. 60 (2016) 230–238. doi:10.1016/j.msec.2015.11.043.

[77] C.C. Juan, K.K. Tseng, W.L. Hsu, M.H. Tsai, C.W. Tsai, C.M. Lin, S.K. Chen, S.J. Lin, J.W. Yeh, Solution strengthening of ductile refractory HfMoxNbTaTiZr high-entropy alloys, Mater. Lett. 175 (2016) 284–287. doi:10.1016/j.matlet.2016.03.133.

[78] R.W. Hertzberg, Deformation and Fracture Mechanics of Engineering Materials, 1977.

[79] F. Khan, S.K. Panigrahi, Age hardening, fracture behavior and mechanical properties of QE22 Mg alloy, J. Magnes. Alloy. 3 (2015) 210–217. doi:10.1016/j.jma.2015.08.002.

Chapter 5:

FRACTURE BEHAVIOR AND MECHANICAL PROPERTIES OF COCRMO MEDIUM ENTROPY ALLOYS DESIGNED FOR MEDICAL IMPLANTS

5.1 Introduction

CoCrMo alloys have promising biological and mechanical properties that provide advantageous usage in mainly dental applications and hard tissue replacements. While an aggressive environment of human fluids threatens to chemical biocompatibility, mechanical integrity must be considered, such that parafunctional and cyclic loadings exist during the lifetime of an implant.

In this chapter, mechanical properties and fracture behavior of CoCrMo have been investigated under an impact loading. It was mainly observed that CoCrMo has high hardness and high Young's modulus as compared to traditionally used biomaterials. Moreover, CoCrMo showed mainly brittle fracture mode, yet some plastic response has been observed at the last stages of the fracture. Consequently, CoCrMo alloys show good mechanical properties, however, higher Young's modulus than that of bone can lead to stress shielding effect, and loss of prosthesis in long term applications.

5.2 Experimental Procedures

CoCrMo alloy with a chemical composition of 27 wt.% Cr, 6 wt.% Mo, and balance wt.% Co with a purity of 99.9% was produced by arc melting as a disc-shaped alloy with a diameter of 50.1 mm and a thickness of 6.1 mm, and the disc-shaped alloy was cut by an electrical discharge machine (EDM) to extract 10x 5 x 1mm bulk samples for mechanical characterization, and 45mm x 6mm x 3mm sample with a 1mm deep notch at the center for Charpy impact test. Charpy impact energy was measured by employing TERCO MT3016 Impact Tester with a 30 J capacity at 298 K. It is the important point that the size of the impact sample was optimized to the impact tester according to Charpy impact test standards [1].

The contaminations on the bulk surfaces were eliminated by mechanically grinding with SiC emerge papers from 106 to 2.5 µm, consequently polishing with 0.30 µm

alumina slurry in order to obtain surfaces without oxide layer and contaminations. The bulk samples were cleaned with ethanol in an ultrasonic water bath and rinsed with de-ionized water. Mechanical properties of each of the polished samples were evaluated by nano-indentation tests that were performed on Agilent G200 tester with Berkovich type indenter in a load-control mode at a loading/unloading rate of 30 mN with a maximum load of 300 mN, and a 10 s holding time at the maximum load. The fracture surface morphologies were investigated by a Zeiss Ultra Plus field emission scanning electron microscope (SEM), and energy- dispersive spectrometry (EDS).

5.3 Results and Discussion

Charpy impact test was employed to observe energy absorption capacity, and CoCrMo absorbed 6.5 J energy during its fracture. After the impact test, fracture surface properties of the CoCrMo alloy were examined by SEM. Fracture patterns indicate to mixed fracture mode of CoCrMo alloy at 298 K. As illustrated in Figure 5-1 (a) cleavage surface properties with dimple-like regions lead to quasi cleavage regions [1] and mixed-mode fracture. A closer look at the region (b) in Figure 5-1 (a) reveals a rapid fracture surface with dimpled areas and the effects of shear forces as can be evidenced by elongated and shallow dimples (Figure 5-1 (b)). Some of the dimpled regions were shown in Figure 5-1 (a) in red squares, and dimple-like structures take place together with the brittle surface features. Dimpled regions around the brittle regions indicate predominantly brittle behavior with few ductile features in the microstructure.

In Figure 5-1 (c), brittle surface characteristics have been observed with differently oriented striations which were shown with yellow arrows. While the left side of the SEM micrograph in Figure 5-1 (c) mostly exhibits brittle featured surfaces with well-developed river patterns and radial striations, the right side of Figure 5-1 (c) has more ductile features with slant surfaces and dimpled regions.

The red squared region in Figure 5-1 (c) acts as a transition region between the flat and the slant surfaces, and Figure 5-1 (d) shows a closer look at the transition region. A closer look at Figure 5-1 (d) shows chevron marks, radial striations and river patterns that are shown with yellow arrows, and elongated dimples. As illustrated in Figure 5-1 (d), striations predominantly exist as evidence of brittle behavior on the fracture surface.

However, there are some indications on plastic behavior such that the micro-void formations which are illustrated with white arrows in Figure 5-1 (d)(e) (f) have been observed around the dimpled regions, and the micro-voids coalescence occurred by plastic deformation at the last step of the fracture [2]. In addition to microvoids, deeper cavity formations have been observed in dimpled regions, and some cavities occurred around the elongated dimples which are resulted by shear forces (Figure 5-1 (c)(d)(e)). Moreover, secondary crack formations are illustrated in Figure 5-1 (a)(d)(e)(f) by green arrows that can be attributed to excessive plastic deformation which causes crack initiation and nucleation [2].

Moreover, promising plastic deformation has been observed from the nanoindentation results as can be seen in Figure 5-2 (a). According to results, CoCrMo alloy exhibits a high hardness of 5 GPa and Young's modulus of 262.7 GPa than that of traditional alloys, and the findings are compatible with the literature [3,4]. When compared to the CoCrMo alloy to other popular metallic biomaterials such as Ti and Ti-6Al-4V, it can be seen that CoCrMo shows greater plasticity, higher hardness and Young's modulus among them. Besides, the hardness of CoCrMo alloy decreases with deeper penetration into the CoCrMo surface as can be seen in Figure 5-2 (b) that shows the softening behavior of CoCrMo at 298K. The softening behavior of CoCrMo alloy can be advantageous in the machining process in high strain rates.

Consequently, CoCrMo alloy absorbed 6.5 J energy during the impact test, and brittle behavior was observed as the main fracture mode. On the other hand, some ductile properties have been observed by dimpled regions, and some deep cavities were also observed due to tearing and rupture processes. Moreover, the elastic modulus of CoCrMo is much higher than the bone's elastic modulus of approximately 30 GPa, which can lead to implant failures in long term applications due to elastic modulus mismatch [3,5–8].

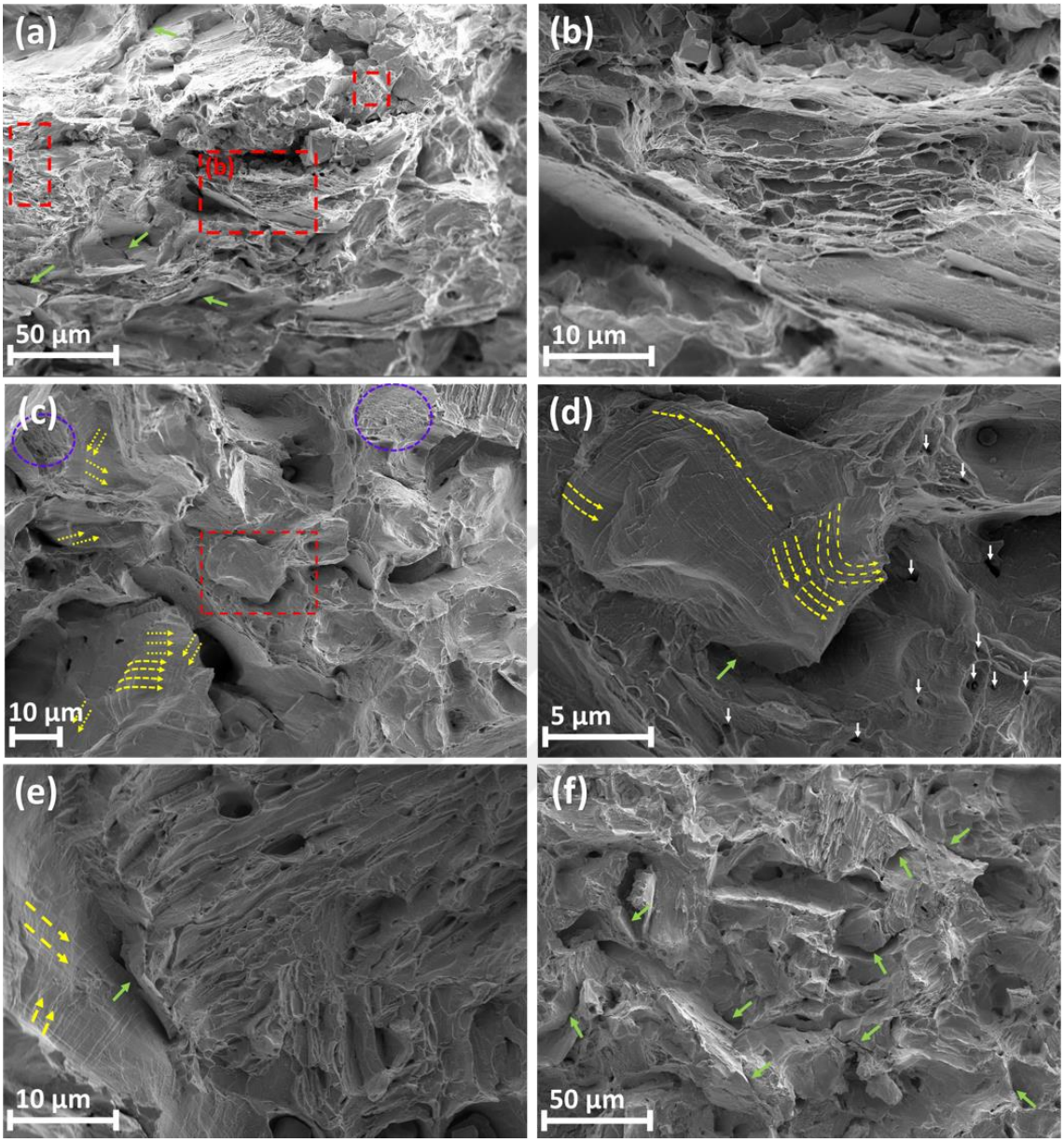

Figure 5-1: SEM micrographs of CoCrMo fracture surface, a) Quasi-cleavage surface, and secondary cracks that are represented by green arrows; b) Elongated dimples and micro dimples; c) Cleavage surfaces with striations that are represented by yellow arrow, and ductile regions that are represented by blue circles, and transition region that is represented by red square; d) Flat surface with chevron marks, and striations (Yellow Lines), dimples, cavity formations, micro-voids that are represented by white arrows, and secondary cracks that are represented by green arrows; e) Elongated dimples, and cage-like striations (yellow arrows), and secondary cracks that are represented by green arrows; f) Quasi cleavage surface with secondary cracks that are represented by green arrows

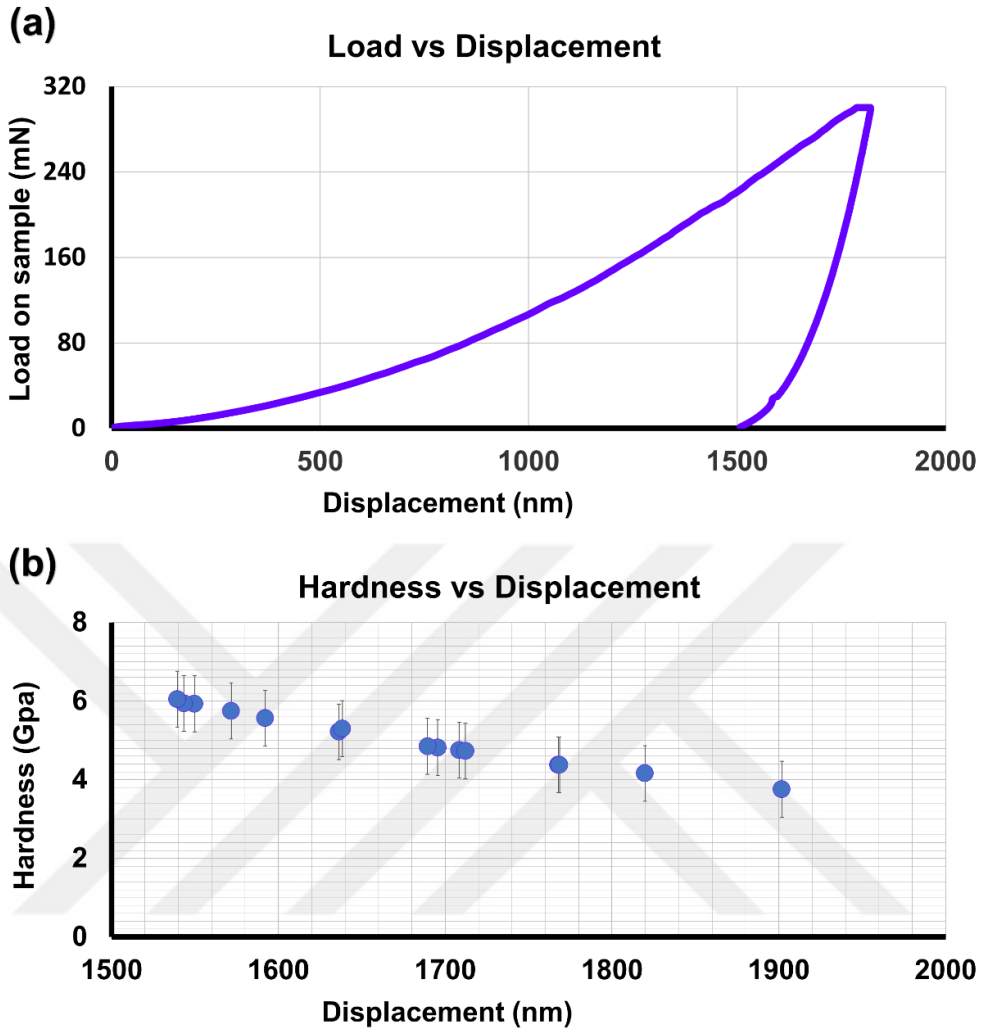

Figure 5-2: Nanoindentation results of CoCrMo tested with a Berkovich Indenter, (a) Load – Displacement curve of CoCrMo with the maximum load of 300 mN, (b) Hardness-Displacement curve of CoCrMo

5.4 Conclusion

The fracture surface of CoCrMo alloy has been examined by Charpy impact test in order to evaluate the fracture behavior of CoCrMo under sudden loading. Cleavage surface properties and dimpled regions were mainly observed together on the fracture surface of CoCrMo, such that quasi-cleavage behavior was indicated. On the other hand, brittle regions were predominantly observed on the fracture surface of CoCrMo with river patterns and chevron marks. In addition to brittle regions, dimples have been observed and they provide ductility to CoCrMo.

Overall, CoCrMo alloy has high hardness and shows mainly brittle fracture behavior under an impact loading with some plasticity at the last stages of fracture. On

the other hand, higher Young's modulus of CoCrMo can lead to mechanical incompatibility. Consequently, CoCrMo shows satisfactory mechanical properties such as high strain capacity to use as an implant however investigations should be continued to obtain low-modulus Co-based alloys.

5.5 References

[1] J. Anburaj, S.S.M. Nazirudeen, R. Narayanan, B. Anandavel, A. Chandrasekar, Ageing of forged superaustenitic stainless steel: Precipitate phases and mechanical properties, Mater. Sci. Eng. A. 535 (2012) 99–107. doi:10.1016/j.msea.2011.12.048.

[2] F.G.L. Pereira, J.M. Lourenço, R.M. do Nascimento, N.A. Castro, Fracture Behavior and Fatigue Performance of Inconel 625, Mater. Res. 21 (2018). doi:10.1590/1980-5373-mr-2017-1089.

[3] S. Saber-Samandari, C.C. Berndt, K.A. Gross, Selection of the implant and coating materials for optimized performance by means of nanoindentation, Acta Biomater. 7 (2011) 874–881. doi:10.1016/j.actbio.2010.09.023.

[4] M. Gradzka-Dahlke, J.R. Dabrowski, B. Dabrowski, Modification of mechanical properties of sintered implant materials on the base of Co-Cr-Mo alloy, J. Mater. Process. Technol. (2008). doi:10.1016/j.jmatprotec.2007.11.034.

[5] M. Niinomi, M. Nakai, J. Hieda, Development of new metallic alloys for biomedical applications, Acta Biomater. 8 (2012) 3888–3903. doi:10.1016/j.actbio.2012.06.037.

[6] L.N. Miotto, L.M.G. Fais, A.L.R. Ribeiro, L.G. Vaz, Surface properties of Ti-35Nb-7Zr-5Ta: Effects of long-term immersion in artificial saliva and fluoride solution, J. Prosthet. Dent. 116 (2016) 102–111. doi:10.1016/j.prosdent.2015.10.024.

[7] Y. Song, D.S. Xu, R. Yang, D. Li, W.T. Wu, Z.X. Guo, Theoretical study of the effects of alloying elements on the strength and modulus of β-type bio-titanium alloys, Mater. Sci. Eng. A. 260 (1999) 269–274. doi:10.1016/S0921-5093(98)00886-7.

[8] I. Kopova, J. Stráský, P. Harcuba, M. Landa, M. Janeček, L. Bačákova, Newly developed Ti–Nb–Zr–Ta–Si–Fe biomedical beta titanium alloys with increased strength and enhanced biocompatibility, Mater. Sci. Eng. C. 60 (2016) 230–238. doi:10.1016/j.msec.2015.11.043.

Chapter 6:
CONCLUSION

Metallic materials have been widely used in biomedical applications due to their properties that are superior to ceramic and polymer materials such as high strength and ductility. Nevertheless, metallic materials suffer from chemical and mechanical degradation over time in applications within the human body. Ions released from an implant may lead to adverse effects on body tissues as well as prosthesis failure in long term applications. Moreover, higher elastic modulus of metallic materials as compared to that of bones is a significant problem in biomedical applications since higher elastic modulus can damage the mechanical integrity between the implant and the bone. Therefore, the biological and mechanical compatibility of an implant must be satisfied in order to eliminate unfavorable results such as toxicity and sudden failure of an implant. In this study, the biological and mechanical compatibility of novel metallic materials has been investigated to evaluate their potential utilization in the biomedical field.

The high entropy alloys of TiTaHfNb, TiTaHfNbZr, TiTaHfMoZr, and the medium entropy alloy CoCrMo were examined under various testing methods in their bulk state in order to independently evaluate their bio-related properties. The results showed that the HEAs and CoCrMo alloys are strong candidates as implant materials. The immersion tests of HEAs and CoCrMo in AS and SBF revealed their excellent corrosion resistance with an oxide layer formation on their surfaces. In addition, the hydroxyapatite layer has been observed on CoCrMo surfaces after 28-day immersion in AS and SBF. The hydroxyapatite formation on CoCrMo alloy facilitates the integration between the implant and the human tissue, and CoCrMo presents great improvements in the repairing and healing process in orthopedic and orthodontic applications.

Addition to excellent biocompatibility, the mechanical properties of the HEAs and CoCrMo alloy are excellent to support to human tissue, and specifically to hard tissues. Particularly, high fracture toughness was obtained by TiTaHfNb, and fracture surface morphology mainly indicates ductile behavior. The addition of the transition elements (Nb, Zr, and Mo) into TiTaHf-based alloy creates a high difference in the impact toughness of the alloys and their fracture behavior. While TiTaHfNb shows high

toughness with mostly ductile behavior, TiTaHfNbZr shows mixed-mode fracture and TiTaHfMoZr shows predominantly brittle behavior. Moreover, CoCrMo alloy exhibits brittle behavior with some ductility, and it showed high strain under an impact loading.

To conclude, the special design of high entropy alloys and medium entropy alloys present excellent biological and mechanical properties that make them strong candidates as new generation of implants.